pH-sensitive TAT-decorated PEGylated liposomal silybin: synthesis, in vitro and in vivo anti-tumor evaluation

Seyedeh Hoda Alavizadeh[1], Fatemeh Gheybi[2], Mahmoud Reza Jaafari[1]

[1]Department of Pharmaceutical Nanotechnology, School of Pharmacy, Mashhad University of Medical Sciences, Mashhad, Iran

[2]Department of Medical Biotechnology and Nanotechnology, Faculty of Medicine, Mashhad University of Medical Sciences, Mashhad, Iran

Mashhad University of Medical Sciences

Introduction

Biological barriers of tumor microenvironment influence the penetration of nanomedicine within the tumor. PEGylation for example hinders efficient nanoparticle cell interaction. PEG-detachable systems could be designed to respond to various tumor specific stimuli.

We used SLB, a polyphenolic flavonoid known for outstanding pharmacological activity which shows low bioavailability and intensive metabolism. Though SLB formulation developed with enhanced oral absorption, few have enabled parenteral application of this compound. We report herein the fabrication of a PEG-detachable silybin (SLB) liposome decorated with TAT-peptide.

Methods

Acyl hydrazide-activated PEG_{2000} was prepared and linked with ketone-derivatized DPPE via an acid labile hydrazone bond to form $mPEG_{2000}$-HZ-PE. TAT peptide was conjugated with a shorter PEG_{1000}-PE spacer and efficacy of coupling was monitored by TLC using silica plates.

TAT peptide conjugated with a shorter PEG1000-PE spacer was post-inserted into PEGylated liposome (DPPC:SPC:Chol). The patent-based method was used to prepare SLB-SPC complex to be incorporated into liposomes. Briefly, SLB in an aprotic solvent, acetone, was mixed with SPC overnight under stirring, the mixture was concentrated in vacuum and diluted with n-hexane and the precipitated pale yellow complex was collected by filtration and dried under vacuum at 40 °C.
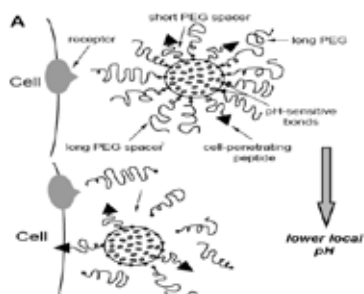

Fig 1. pH sensitive nanoliposomal of Silibinin targeted with TAT peptides

The pH sensitivity investigated using DiI liposome and FACS analysis. Therapeutic efficacy was assessed in 4T1 tumor-bearing BALB/c mice.

Results

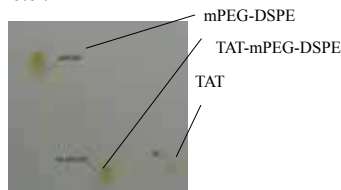The efficacy of TAT coupling was monitored by TLC. Liposomes were around 100 nm in diameter.

Fig 2.
TLC silica plates and mobile phase of chloroform:methanol:water(90:18:2%v/v) and iodine vapor exposure.

Table 1
Size of different SLB liposomal formulation

Formulation	Size By Number (nm)	PDI	Zeta potential (mV)
mPEG-DSPE	78±4	0.23±0.01	-16.5
mPEG-DSPE/TAT-PEG1000	79±4	0.23±0/01	-15.3
mPEG-HZ-PE	123±3	0.20±0.02	-6.83
mPEG-HZ-PE /TAT-PEG1000	124±5	0.14±0.01	-4.97

SLB association within SLB-SPC lipid complex enhanced encapsulation efficiency which stably reached up to 50% (Table 2). $mPEG_{2000}$-HZ-DPPE liposome enhanced cell killing due to the PEG detachment over time in 4T1 cancer.

Table 2
Encapsulation efficiency and IC_{50}

Formulation	Encapsulation (%)	IC50 (μg/ml) 72 h
mPEG-DSPE	50.6	28.36 ± 7.9
mPEG-DSPE/TAT-PEG1000	43.7	21.2 ±4.2
mPEG-HZ-PE	40.6	6.72 ± 3.9
mPEG-HZ-PE /TAT-PEG1000	34.4	6.03 ± 3.6

Flow cytometry indicated pH-sensitivity of DiI labeled SLB liposomes. The presence of TAT in pH-sensitive formulation ($mPEG_{2000}$-HZ-DPPE/TAT-PEG_{1000}) promoted cellular association due to TAT exposure (Fig. 3).

in vivo results were promising with pH-sensitive liposome detaching PEG upon exposure to acidic tumor microenvironment and retarded tumor growth and prolonged the survival of 4T1 tumor-bearing BALB/c mice (Fig 4).
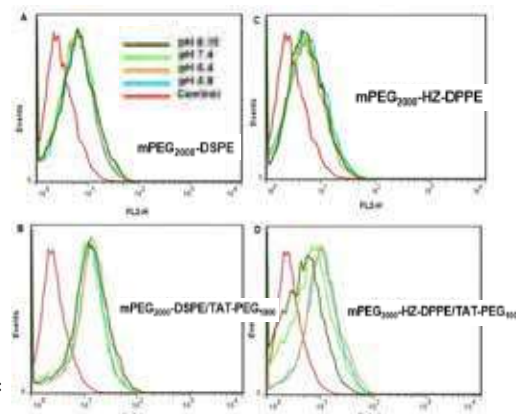

Fig. 3
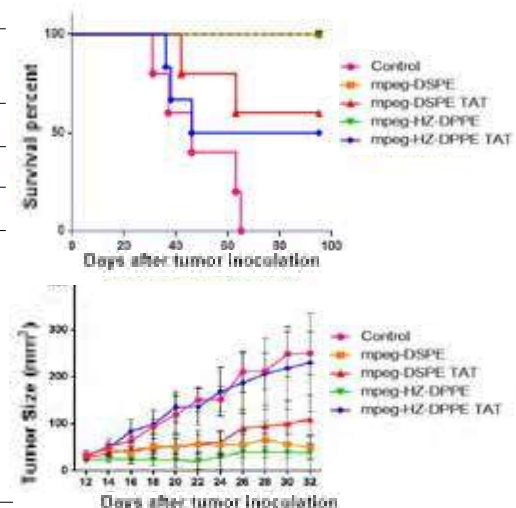Flow cytometry of DiI labeled SLB liposomes in 4T1 cells.

Fig. 4
Therapeutic efficacy in 4T1 tumor-bearing BALB/c mice.

Conclusion

SLB-SPC complex could be efficiently loaded into liposomes to enhance its therapeutic efficacy. Further, the features of tumor environment including the lowered pH could be used to enhance the efficacy of liposome using PEG-detachment. However, the efficacy of TAT is still under question.

References

Kale, A. A. and V. P. Torchilin (2007). Journal of drug targeting 15(7-8): 538-545.

Teymouri, M., A. Badiee, S. Golmohammadzadeh, K. Sadri, J. Akhtari, M. Mellat, A. Nikpoor and M. Jaafari (2016). International journal of pharmaceutics 511(1): 236-244.

Jaafari, M. R., F. Gheybi and S. M. R. Sorkhabadi (2017). Google Patents.

LIPOSOMAL PEPTIDE-BASED VACCINE COMBINED WITH LIPOSOMAL CELECOXIB FOR MELANOMA TREATMENT

Vajiheh Jahani1, Mona Yazdani1, Ali Badiee1,2, MahmouReza Jaafari1,2, Leila Arabi1,2*

1-Nanotechnology Research Center, School of Pharmacy, Mashhad University of Medical Sciences, Mashhad Iran.
2-Department of Pharmaceutical Nanotechnology, School of Pharmacy, Mashhad University of Medical Sciences, Iran, * Presenting Author
leilaa.arabi@gmail.com, Arabil@mums.ac.ir

INTRODUCTION

Melanoma as one of the most immunogenic cancers, is considered as a good candidate to develop the immunotherapy treatment (1). In several studies, it has been shown that liposomal peptide-based vaccines can defeat cancer cells proliferation. To enhance the effectiveness of vaccination against cancer, we considered additional strategies. In this study, we evaluated the effect of combination of liposomal celecoxib with dendritic cells matured by melanoma antigen, gp-100 peptide for melanoma treatment. The therapeutic efficacy of this combination was evaluated in B16F10 bearing C57BL/6 mice. In this study, celecoxib as a cyclooxygenase-2 inhibitor would help to eliminate inhibitory mechanisms of tumor microenvironment and gp-100 peptide would enhance MHC I class presentation and cytotoxic T cell activation. Generally, we pursue three goals in this study: Determine the role of liposomal formulation as delivery system for drugs with low water solubility, understand the role of Dendritic cells in tumor growth, and evaluate the anti-tumor effects of cyclooxygenase-2 inhibitors

STUDY DESIGN AND METHODOLOGY

liposomal vaccine formulations used for immunization of C57BL/6 mice to induce CTL response against gp-100 peptide and treatment of B16F10 tumor mice.

Liposomal formulations containing gp-100 peptide and celecoxib were prepared and characterized (2). Linking of peptide to maleimide-PEG2000-DSPE through covalent binding between the thiol group of C terminal cysteine residue of peptide and maleimide (3).

C57BL/6 mice bearing B16F10 melanoma tumors were vaccinated with different formulations of gp-100 peptide in combination with intravenous administration of liposomal celecoxib.

Immunological tests such as ELISpot assay, flow cytometry and cytotoxicity assay were performed on splenocyte suspensions (3), and the remaining mice were evaluated for tumor growth and survival analysis.
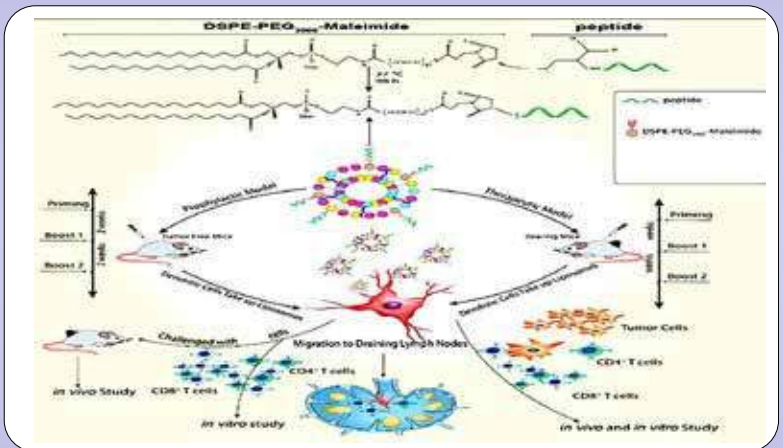

RESULTS

Therapeutic combination of liposomal celecoxib and gp-100 demonstrated an effective immune response and tumor regression in C57BL/6 mice bearing B16F10 melanoma.

The combinational therapy of dendritic cells + liposomal gp-100peptide + liposomal celecoxib leads to a significant amount of IFN-γ secretion and increased number tumor infiltrated lymphocytes (TILs) and cytotoxic activity

In this study, therapeutic combination of liposomal celecoxib and gp-100 demonstrated an effective immune response and tumor regression in C57BL/6 mice bearing B16F10 melanoma (figure). The significant tumor growth inhibition by combination therapy (DC+peptide/Lip-peptide+Lip-COX) could be a result of increased IFN-Y secretion alongside the cytottoxic activity of T cells.

In vivo therapeutic efficacy of different liposomal formulations and tumor volume (mm3) of each mouse in each treatment group were evaluated and compared with Buffer groups. The values are means of tumor size ± SEM. Survival analysis of therapeutic groups were monitored by the multiple comparison log-rank (Mantel–Cox) test. Effects of treatments on survival time were monitored for a period of 30 days among B16F10 tumor model of C57BL/6 mice (n=6).
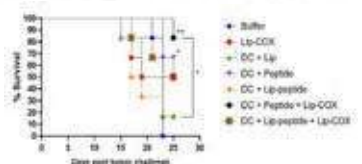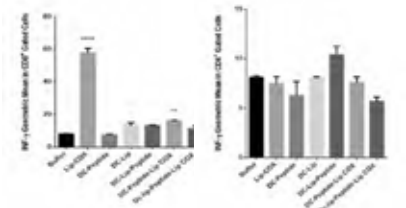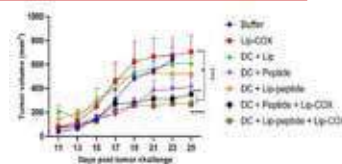
CONCLUSION

Taken together, our data supports the rational development of combination of liposomal gp-100 matured dendritic cells and liposomal celecoxib to overcome the immunosuppressive tumor microenvironment, improve immunologic response and enhanced therapeutic outcomes in melanoma model. All in all, this combination could be employed as a promising vaccine to generate potent CTL anti-tumor immune responses that could be beneficial to treatment of melanoma.
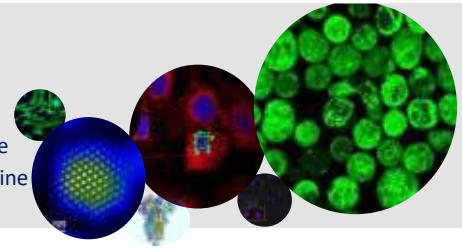
REFERENCES

1- Passarelli, A., et al. Oncotarget, 2017. 8(62): p. 106132-106142.
2- Matbou Riahi, M., et al. Int J Pharm, 2018. 540(1-2): p. 89-97.
3- Zamani, P et al., Journal of Controlled Release 303 (2019) 223–236

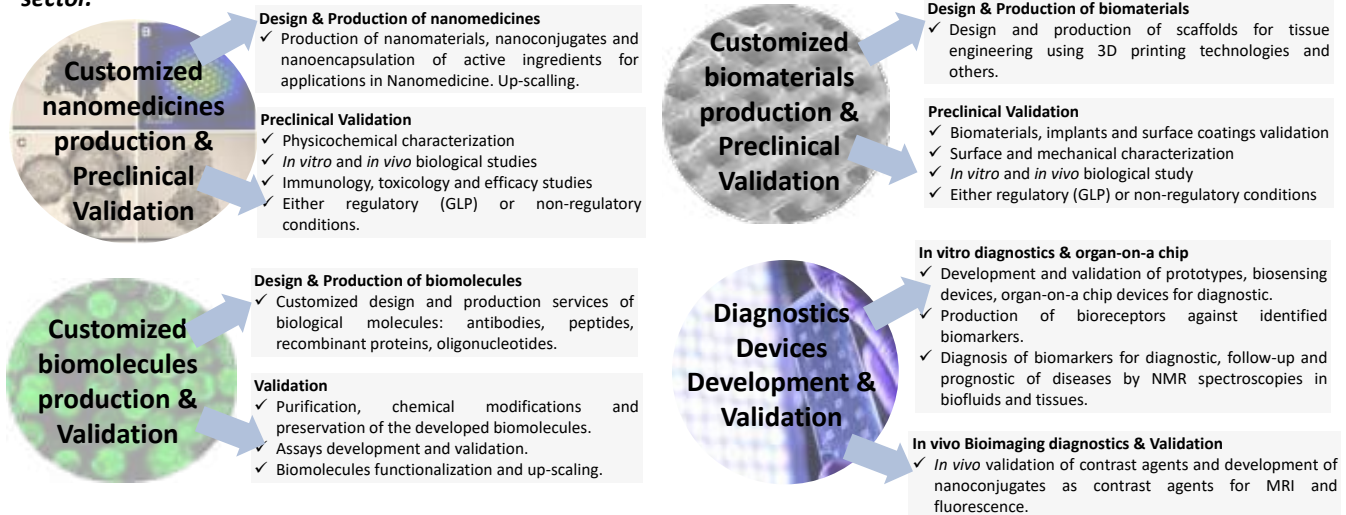# CUTTING-EDGE BIOMEDICAL SOLUTIONS in HEALTH

for Translation into CLINICs

Argarate Nerea, Bernardos Andrea, Casado Marga, Martínez-Máñez Ramón, Veciana Jaume
Biomedical Research Networking Center (CIBER), Bioengineering, Biomaterials & Nanomedicine Research Area (CIBER-BBN). Nanbiosis Spanish Research Infrastructure

Cutting-edge biomedical solutions

A new line of action has been launched named **Cutting-Edge biomedical solutions,** *where* **integrated solutions are offered to advance challenges in nanomedicine, tissue engineering and regenerative medicine, diagnostic and medical devices sector.**

Customized nanomedicines production & Preclinical Validation

Design & Production of nanomedicines
✓ Production of nanomaterials, nanoconjugates and nanoencapsulation of active ingredients for applications in Nanomedicine. Up-scalling.

Preclinical Validation
✓ Physicochemical characterization
✓ *In vitro* and *in vivo* biological studies
✓ Immunology, toxicology and efficacy studies
✓ Either regulatory (GLP) or non-regulatory conditions.

Customized biomaterials production & Preclinical Validation

Design & Production of biomaterials
✓ Design and production of scaffolds for tissue engineering using 3D printing technologies and others.

Preclinical Validation
✓ Biomaterials, implants and surface coatings validation
✓ Surface and mechanical characterization
✓ *In vitro* and *in vivo* biological study
✓ Either regulatory (GLP) or non-regulatory conditions

Customized biomolecules production & Validation

Design & Production of biomolecules
✓ Customized design and production services of biological molecules: antibodies, peptides, recombinant proteins, oligonucleotides.

Validation
✓ Purification, chemical modifications and preservation of the developed biomolecules.
✓ Assays development and validation.
✓ Biomolecules functionalization and up-scaling.

Diagnostics Devices Development & Validation

In vitro diagnostics & organ-on-a chip
✓ Development and validation of prototypes, biosensing devices, organ-on-a chip devices for diagnostic.
✓ Production of bioreceptors against identified biomarkers.
✓ Diagnosis of biomarkers for diagnostic, follow-up and prognostic of diseases by NMR spectroscopies in biofluids and tissues.

In vivo Bioimaging diagnostics & Validation
✓ *In vivo* validation of contrast agents and development of nanoconjugates as contrast agents for MRI and fluorescence.

NANBIOSIS ICTS - Unique Value proposition

➢ *Research Infrastructure* with an *academic spirit of scientific excellence.*
➢ **TOP-LEVEL technological resources** to the scientific community in the public and private sector.
➢ **Innovation process** to develop new nanomedicine products/applications/tools.
➢ Collaboration with experts on **Nanosafety**, **regulatory** issues, **investors** and **consultancy**.
➢ Preparation of **business plans**, creation of **new spin-offs** and **start-up** companies.

NANBIOSIS ICTS– Your research Infrastructure of Scientific Expertise

NANBIOSIS is a **Research Infrastructure** (RI) specialised in the design and production of **nanomaterials**, **biomaterials** and **devices to the preclinical validation**

NANBIOSIS is a distributed **ICTS** (Singular scientific and technical infrastructures) accredited by the Spanish Government

NANBIOSIS is composed by:

Standard of Quality
NANBIOSIS is capable of offering their services with laboratories accredited with **ISO 9001:2015 and GLP** required in the pharmaceutical, biotech and medtech sector.
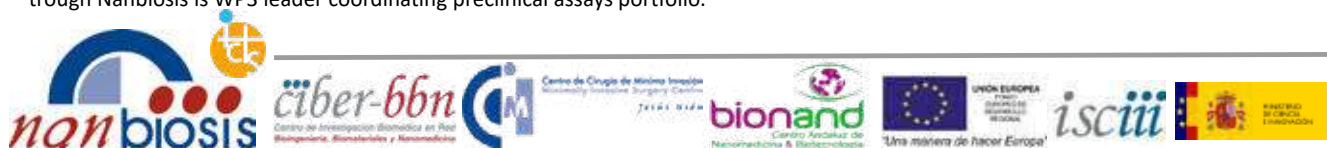
Being an ICTS
Access to public funds for the continuous improvement and updating of infrastructures. By contracting a service, our clients can benefit of this excellence

>**115** Scientists linked to ICTS

>**6000** Services since 2008

>**1600** Projects since 2008

>**4000** Publications since 2008

Participation in the SAFE-N-MEDTECH OITB

SAFE-N-MEDTECH H2020 project aims to develop an **innovative open access platform** that will offer to companies and reference laboratories the capabilities, knowhow, networks and services required for the development, testing, assessment, up scaling and market exploitation of **nanotechnology-based Medical and Diagnosis devices**. This OITB will have a deep understanding and knowledge of the **material-nanoproperties**, their advance use and applications in Medical Technologies and other aspects involved in MT safety. CIBER-BBN trough Nanbiosis is WP3 leader coordinating preclinical assays portfolio.

BIOMIMETIC MICROCAPILLARY-ON-A-CHIP TO MODULATE ENDOTHELIAL PERMEABILITY AGAINST NANODELIVERY SYSTEMS

Maria Grazia Barbato[1,2], Miguel Ferreira[1], Paolo Decuzzi[1]

[1]Laboratory of Nanotechnology for Precision Medicine, Italian Institute of Technology, Genoa, Italy.

[2]University of Genoa, Genoa, Italy

INTRODUCTION

By combining 3D cell cultures with flow systems that mimic the physiologically relevant conditions and functions of organs and tissues, microfluidic models have gained attention during last decade. So far, blood vessel-on-a-chip have been applied to study NPs margination, effect of vessel geometry, shear stress, vessel permeability and NPs translocation across the endothelium . Here, a double-channel microfluidic system was developed in order to mimic the vascular compartment in the upper channel, while the lower channel serves as the extravascular compartment, represented by a complex extracellular matrix (ECM). Endothelial permeability was modulated in order to enhance the accumulation of small tracers and nanoparticles.

RESULTS AND DISCUSSION
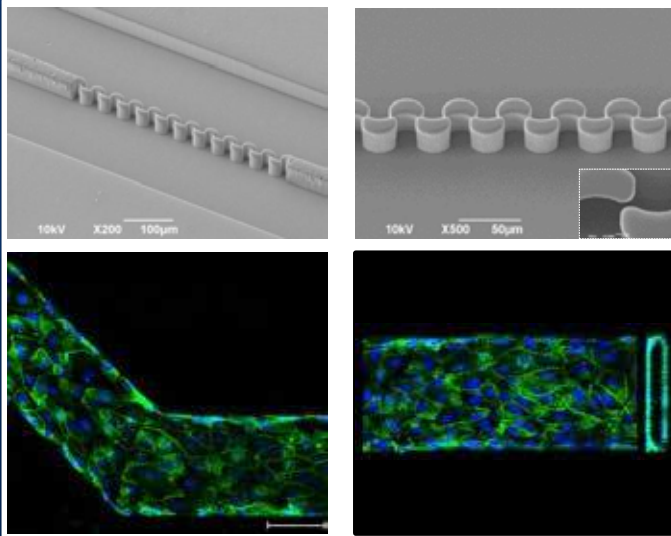
To explore and asses the functionality of human vasculature, a soft-lithography approach was employed to create a double-channel microfluidic device. The microfluidic system is composed of two parallel channels interconnected in the central section *via* an array of permeable micropillars. In particular, the permeable membrane has a characteristic length of 500 μm and a gap size between pillars of 3 μm. HUVEC, cultured in the vascular channel, formed a continuous endothelial barrier. Along cell-cell borders, endothelial cells displayed junctional integrity by expressing the VE-Cadherin junctional protein.

The extravascular space of the microfluidic device was filled with different extracellular matrix compositions and the influence of Matrigel on the crosslinking of the collagen fibrils was characterized. **Figure** shows four SEM images corresponding to four selected matrices (100% Collagen, 80% Collagen-20% Matrigel, 50% Collagen-50% Matrigel and 100% Matrigel). The increasing in Matrigel content resulted in porosity reduction and limited diffusion of Dextran 250kDa and Microspheres 0.2μm.
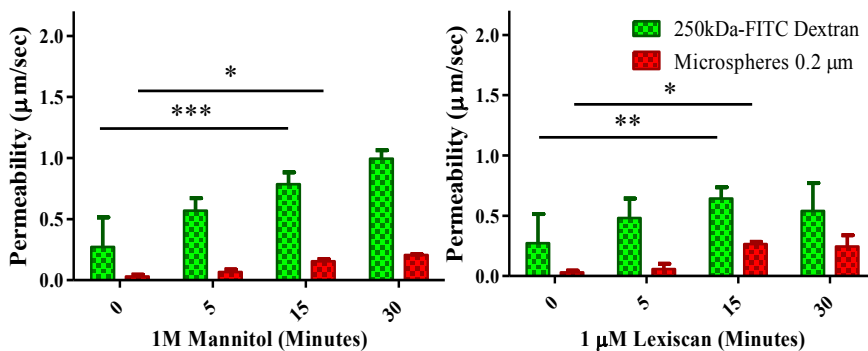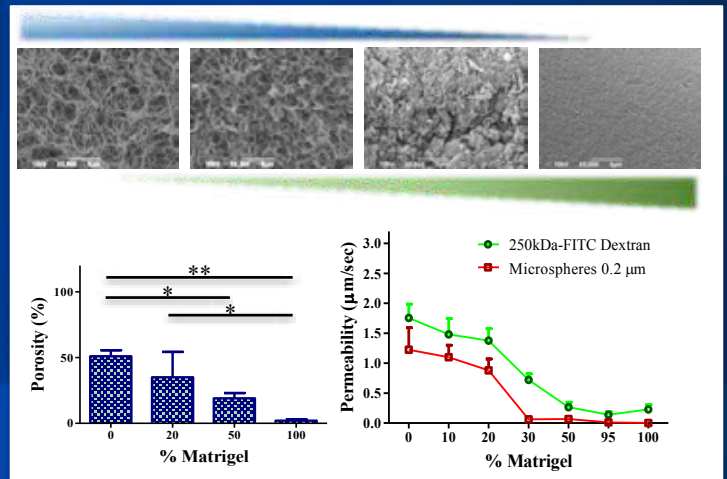
Endothelial permeability values reported in this work (from 0.27 to 0.02 μm/sec for Dextran 250 kDa and 0.2 μm microspheres, respectively) explored the size-selectivity characteristic of *in vivo* vasculature. Opening of the vascular barrier was achieved with two clinically relevant modulators, mannitol and Lexiscan®. Both modulators enhanced the accumulation of small molecules (~30 %) and NPs (~10%), suggesting the formation of small leaks into vascular barrier..

CONCLUSIONS

An *in vitro* vascular-tissue interfaced microfluidic chip was described in this study as a way to quantitatively measure the permeability coefficient of small tracers and NPs, facilitating modulation of vascular permeability and understanding the accumulation of nanomedicine into different extravascular compartments.

Size rather than targeting ligand and the inflammatory mediator used, dominate nanoparticle translocation and binding across the dysfunctional endothelium

Salime Bazban-Shotorbani [a,b], **Martin Dufva** [b], **Nazila Kamaly** [a,b*]

[a] Department of Chemistry, Molecular Sciences Research Hub, Imperial College London, London, W12 0BZ, UK

[b] Department of Health Technology, DTU Health Tech, Technical University of Denmark, 2800, Kgs. Lyngby, Denmark

Introduction

- The major cause of Cardiovascular disease (CVD) is atherosclerosis, which is an inflammation-driven disease of the arteries.
- Atherosclerosis is characterized by dysfunctional endothelium (Dys-EC).
- Enhanced permeability of Dys-EC is a promising strategy for non-specific targeting of nanoparticles to atherosclerotic lesions. Furthermore, overexpression of VCAM-1 on Dys-EC can be used as a site-specific targeting approach **(Figure 1)**.
- It was the goal of this study to assess the most optimal nanoparticle properties for binding and permeability across Dys-EC to target atherosclerotic lesions.
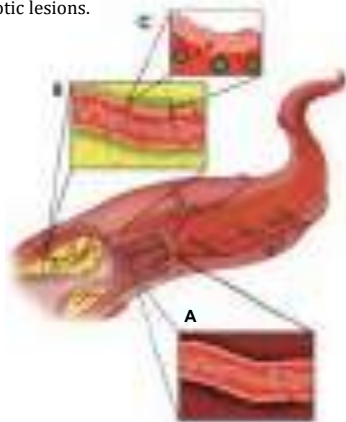

Figure 1. (A) Structure of a vasa vasorum on a healthy vessel wall.
(B) Structure of a leaky vessel sprout into the plaque.
(C) Overexpression of VCAM-1 receptors on endothelial cells

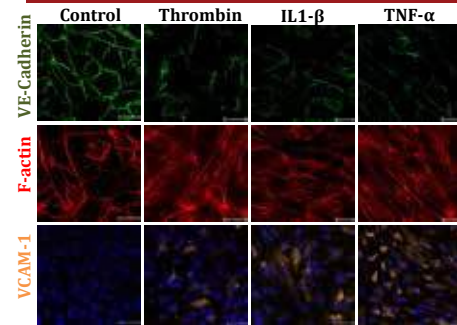## Development of *in vitro* models of endothelial dysfunction

Figure 2. Confocal microscopy of **(A)** VE-Cadherin to study the disruption of tight-junctions, **(B)** F-actin to study the formation of stress fibers, and **(C)** VCAM-1 to study the VCAM-1 overexpression.

Development of the NP library

Size: 30,60,120,250 nm
Peptides:
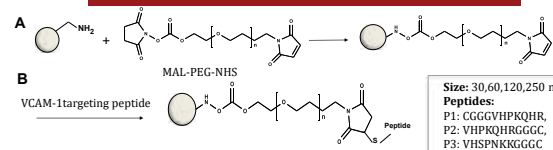P1: CGGGVHPKQHR,
P2: VHPKQHRGGGC,
P3: VHSPNKKGGGC

Figure 3. (A) PEGylation of the NPs using amide bond coupling between NHS ester on the PEG polymer and the amino functionality on the surface of the NPs.
(B) Conjugation of the peptides to the surface of the NPs via MAL-thiol reaction between MAL groups of the PEG polymer and cysteine of the peptide.

Nanoparticle translocation and binding across the healthy and dysfunctional endothelium

Figure 4. (A) Permeability of the NPs across the healthy and dysfunctional endothelium. **(B)** Binding of the NPs to the healthy and dysfunctional endothelium

Based on the permeability results:
- The permeability of NPs across Dys-EC was higher than healthy EC.
- For all nanoparticle groups, the permeability across the TNF-α model was the highest, followed by the IL1-β model, and then thrombin model.
- For all inflammatory models, the nanoparticle permeability was in the following order: NP30 > NP60 > NP120 > NP250.

Based on the binding results:
- For all nanoparticle groups, the binding of peptide-conjugated NPs to TNF-α induced EC was the highest, followed by IL1-β, and then thrombin-induced EC.
- For all models, the nanoparticle binding was in the following order: NP30 and NP60 > NP250 > NP120.
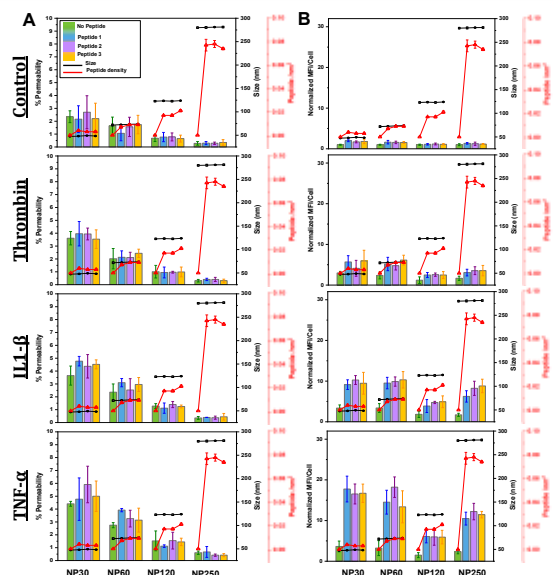
Conclusion

- NP size governs the NP permeability.
- The smaller the NPs are, the higher their permeability is.
- The binding of the NPs is firstly governed by size, then peptide density.
- Design of NPs with proper size (*i.e.,* in the range of 30-60 nm) can highly increase the permeability and binding of NPs across dysfunctional endothelium, therefore can improve the efficiency of the nanoparticles for treatment of inflammatory disease including atherosclerosis.

Contact Info.

sbaz@dtu.dk
s.bazban-shotorbani19@imperial.ac.uk

Cyclosporin A loaded lipid nanoparticles for the intravenous treatment of retinopathy of prematurity

Marilena Bohley, Achim Goepferich

Department of Pharmaceutical Technology, University of Regensburg, Universitaetstrasse 31, 93053 Regensburg, Germany

✉ Marilena.Bohley@ur.de

Introduction

Retinopathy of Prematurity (ROP), a neovascular ocular disease affecting premature infants, is still a leading cause of irreversible childhood blindness [1]. Currently, the most promising therapeutic approach is the inhibition of retinal neovascularization by neutralizing the vascular endothelial growth factor (VEGF) [2]. However, intravitreal anti-VEGF injections that counteract neovascularization are associated with severe side effects including infections, bleedings, retinal detachment, and cell death of retinal pigment epithelial (RPE) cells and photoreceptors due to their invasive administration and their unspecific and rigorous suppression of VEGF in the whole retina [3]. Therefore, to overcome the limitations and disadvantages an intravenous, cell specific anti-VEGF therapy would be a major accomplishment not only for the treatment of ROP but for all neovascular ocular diseases. To achieve this goal, nanoparticles that accumulate efficiently in retinal endothelial and RPE cells were used for targeted drug delivery. For anti-VEGF therapy, the nanoparticles were loaded with Cyclosporin A (CsA) that has been shown to interact with VEGF signaling pathway in both, endothelial cells and RPE cells [4]. Here, we investigate if CsA loaded nanoparticles can efficiently inhibit neovascularization *in vivo* using the mouse model of ROP.
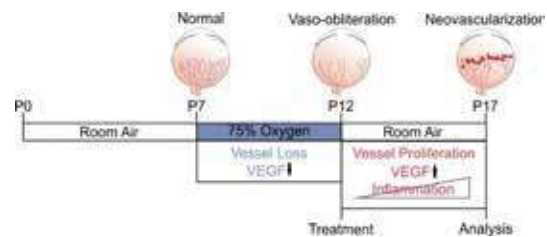

Results

Nanoparticle Composition
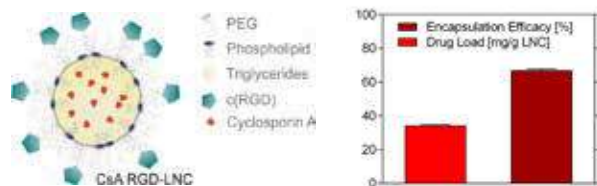
Lipid nanocapsules (LNC) were used a nanoparticulate drug delivery system. Due to their lipid character, they could be easily loaded with high amounts of the lipophilic CsA. For targeting endothelial and RPE cells, LNC were further grafted with the highly potent and αvβ3 integrin-specific ligand cyclo(-Arg-Gly-Asp-D-Phe-Cys) (RGD) [5].

### CsA loaded Nanoparticles successfully inhibit Neovascularization
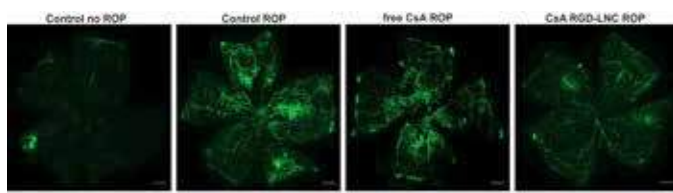
For the investigation of the effectiveness of the CsA loaded nanoparticles compared to the free CsA on the ROP, mice with oxygen induced retinopathy were treated at postnatal (P) day 12 and the effects were analyzed at day P17 and always compared to healthy control mice at P17.

Since the inhibition of retinal neovascularization is the clinically most relevant readout, first, retina whole mounts were prepared, and the retinal vasculature was examined. The microscopic analysis revealed that the magnitude of neovascular and leaky areas was efficiently diminished by the treatment with CsA loaded nanoparticles, whereas the treatment with free CsA caused no apparent changes. In order to validate this observation, the relative area of neovascularization and its quantitative change due to the treatment was determined. The analysis impressively demonstrated the efficacy of CsA loaded nanoparticles by reducing the extent of neovascularization down to levels comparable to the healthy control.

The results, therefore, indicate that already one single injection of CsA loaded nanoparticles can be sufficient to completely inhibit the pathological neovascularization of ROP.
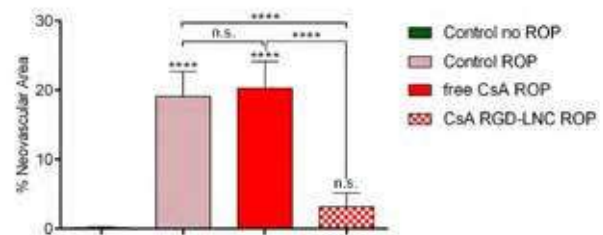
Since, in contrast to the drug loaded nanoparticles, free CsA of the same concentration, had no effect on neovascularization, we assumed that the nanoparticles dramatically enhance availability of CsA in the eye.

CsA Effectiveness entirely depends on Nanoparticles
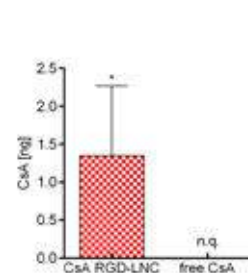
In order to verify this hypothesis, the CsA content in the eye after the intravenous application of either free CsA or CsA loaded nanoparticles was investigated using UHPLC-MS, revealing that detectable amounts of drug are only present in the case of the treatment with drug loaded nanoparticles. Thus, demonstrating that the specific nanoparticulate delivery system is essential to achieve sufficient amounts of CsA in the eye and therefore effectiveness against ROP.

Conclusion

Taken together, the results demonstrate the potential of CsA loaded nanoparticles as a novel therapeutic option for the systemic, single-dose therapy of infants with ROP. Furthermore, the therapeutic concept of cell-specific nanoparticles combined with a highly potent anti-angiogenic drug could also be a resounding treatment option for other neovascular diseases like proliferative diabetic retinopathy and wet age-related macular degeneration.

References

[1] Hellstrom, A. et al.: The Lancet. 2013, 382: 1445-1457
[2] Jain Fouzdar, S. et al.: Clin. Opthalmol. 2018, 12: 1003-1009
[3] Falavarhani Ghasemi, K. et al.: Eye. 2003, 27: 787-794
[4] Rafiee, P. et al.: Cell Commun. Signal. 2004, 2 :1-22
[5] Bohley, M. et al.: Eur. J. Pharm. Biopharm. 2019, 139: 23-32

Acknowledgements

Deutsche Forschungsgemeinschaft

DFG

Direct assessment of nanoparticle hydrophobicity

Loïc Burr[1], David Schmid[1], Stefano Cattaneo[1], Silvia Generelli[1]

[1]CSEM SA, Landquart, Switzerland

With the objective of improving efficacy, physicochemical properties and pharmacokinetic profiles of pharmaceutical substances, nanodrugs are being extensively investigated. Therapeutic compound uptake, biodistribution, and assimilation have always been major challenges for pharmaceutical companies. For nanodrugs, these parameters are strongly impacted by the surface properties of the nanoparticles such as the surface charge and hydrophobicity. In the frame of the European ACEnano project, CSEM is developing innovative characterization techniques to evaluate the hydrophobicity of nanoparticles. Three different approaches for hydrophobicity assessment of NMs are presented and evaluated with polystyrene (PS) latex nanoparticles with various functionalization:

00876: 100 nm – bare PS   **08691**: 50 nm – bare PS   **16586**: 100 nm – PS + amine surface groups   **16586**: 100 nm – PS + carboxylate surface groups

Surface Adsorption Assay with Field Flow Fractionation

Principle

Evaluate the adsorption of hydrophobic/hydrophilic dyes on nanomaterials by assessing the quantity of adsorbed dye and the particle size modification

Method

1. Dye adsorption on NM

2. Fractionation by size using FFF
   • Separate the unbound dye from the particles (alternative to ultracentrifugation) to quantify the dye-NM binding
   • Optimally fractionate the particle by amount of bound dye

Results

Porphin-based hydrophobic dye (non water-soluble) staining in methanol

• Modifying the particle size (swelling induced by methanol?)
• Lowering the retention time

BUT

Nile Blue hydrophilic dye/Rose Bengal hydrophobic dye staining in water/PBS
• Non permanent dye-membrane interaction

Membrane after elution of Nile Blue stained latex particles

Nile blue saturated membrane after elution of Nile Blue stained latex particles

Conclusion

Dye-membrane interaction hindering consistent assessment of NM hydrophobicity by surface affinity with field flow fractionation technique

Hydrophobic Interaction Chromatography

Principle

Separate NMs based on their reversible adsorption, according to their hydrophobicity

Method

1. Promote the hydrophobic binding of the nanomaterials to HIC column with hydrophobic stationary phase using high salt concentration as eluent
2. Elute the particles by increasing hydrophobic affinity to the column by decreasing the salt concentration

Hydrophobic NMs
Mid-hydrophobic NMs
Hydrophilic NMs

Retention number and Retention time by the column reflect NMs affinity to the stationary phase

Results

Retention on the phenyl functionalized column correlating with particle hydrophobicity

Reproducible and quantitative for latex particles

Binding Affinity - Waveguide Interrogated Optical System

Principle

Assess the adsorption of NM on surfaces with defined hydrophobicities by measuring the change of refractive index on the surface with a waveguide interrogated optical system (WIOS).

Method

1. Calibrate the system with reference solution
2. Flow the particles above the functionalized waveguide and measure the change of surface refractive index induced by NMs adsorption by monitoring the in-coupling wavelength enabling resonance

In-coupling wavelength proportional to the quantity of immobilized NMs on each individual sensing pad

Results

Adsorption on Teflon functionalized waveguides correlating with particle hydrophobicity

Measured increase of refractive index and latex particle adsorption partly confirmed by scanning electron microscopy

Conclusions & Outlook

Hydrophobic → 00876 / 08691 Polystyrene → 16688 Carboxylate → 16586 Amine → Hydrophilic

Hydrophobic Interaction Chromatography and **waveguide interrogated optical system assessment of the binding affinity** enable the hydrophobicity assessment of Latex nanoparticles

The major **challenges** for the future industrial use of both techniques are the **regeneration** and **re-use** of the same chromatography column/waveguide sensor for several measurements without cross-contamination.

LungCheck: Point-of-care device for multiplexed detection of chronic obstructive pulmonary disease biomarkers in sputum
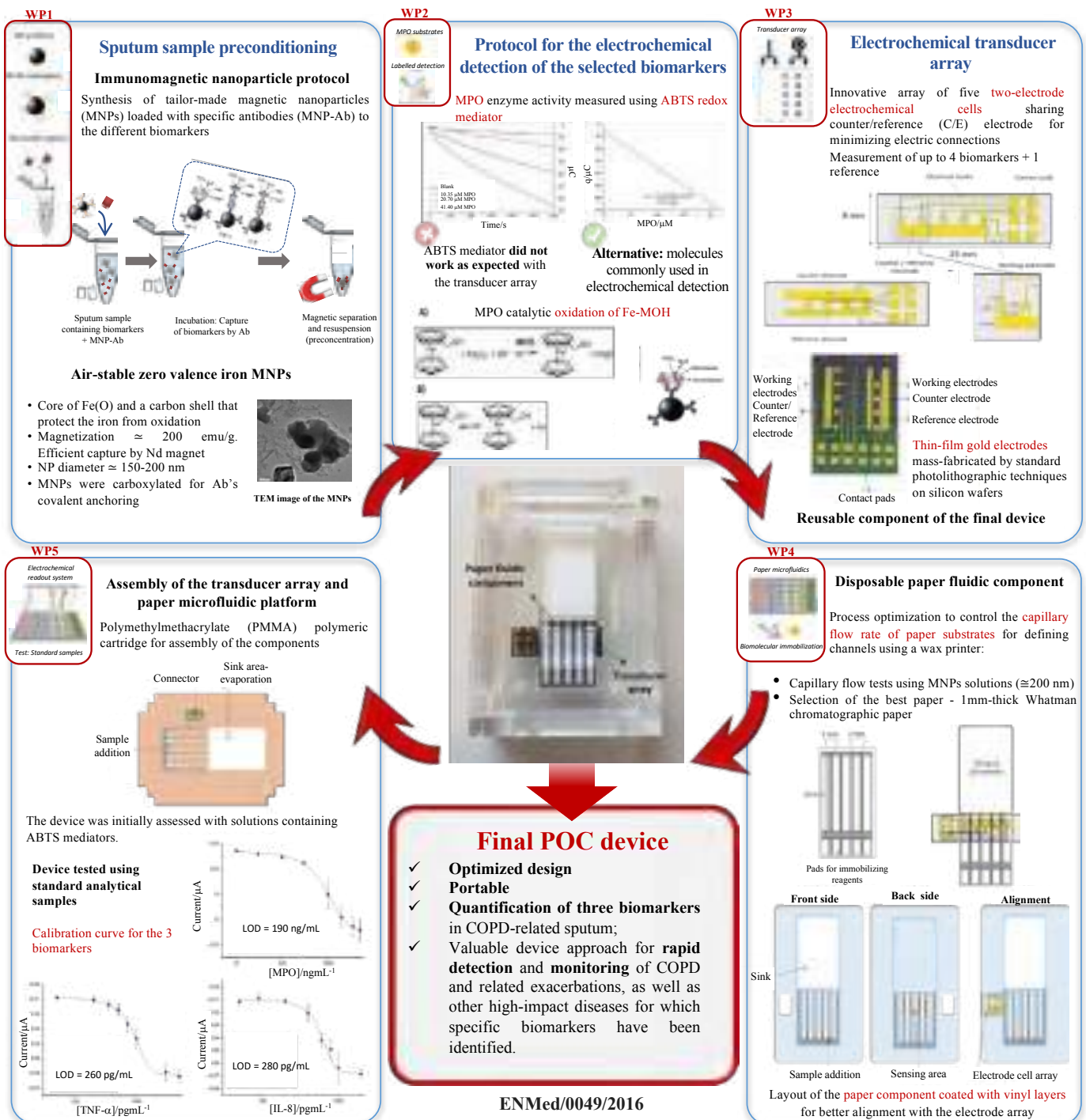
Estela O. Carvalho[1], Manuel Gutiérrez-Capitán[2], Antonio Baldi[2], Tzanko Tzanov[3], Javier Hoyo[3], Arnau Bassegoda[3], Aharon Gedanken[4], Ilana Perelshtein[4], Ming Wei[5], Vanessa F. Cardoso[1,6], Senentxu Lanceros-Méndez[1,7,8], César Fernández-Sánchez[2]*

[1]Centre of Physics, University of Minho and Porto, Braga, 4710-057 Portugal; [2]Instituto de Microelectrónica de Barcelona, IMB-CNM (CSIC), Campus UAB, 08193 Bellaterra, Spain; [3]Grup de Biotecnologia Molecular i Industrial, Department of Chemical Engineering, Universitat Politècnica de Catalunya, Rambla Sant Nebridi 22, Barcelona, 08222, Spain; [4]Bar-Ilan Institute for Nanotechnology and Advanced Materials, Department of Chemistry, Bar-Ilan University, Ramat-Gan, 52900, Israel; [5]Cellvax, Ecole Nationale Vétérinaire d'Alfort, 7 Avenue du Général de Gaulle, Maisons-Alfort Cedex, 94704, France; [6]CMEMS-UMinho, University of Minho, Guimarães, 4800-058, Portugal; [7]BCMaterials, Basque Center for Materials, Applications and Nanostructures, UPV/EHU Science Park, Leioa, 48940 Spain; [8]Ikerbasque, Basque Foundation for Science, Bilbao, 48013, Spain
*cesar.fernandez@csic.es

Respiratory system diseases are one of the main causes of death in EU-28. **LungCheck** project focuses on the **early diagnosis** of **chronic obstructive pulmonary disease (COPD)** in high-risk patients.

The **LungCheck** diagnostic approach is **point-of-care (POC) device,** integrating a **reusable array of electrochemical transducers** and a **disposable microfluidic paper component,** enabling the affordable, rapid and reliable detection of selected biomarkers. Quantitative detection of specific inflammatory biomarkers in **sputum**:
- **Myeloperoxidase (MPO):** Enzyme released by neutrophils upon activation of leukocytes – production of bactericidal hypochlorous acid (HOCL);
- **Interleukin-8 (IL-8):** Recruits and activates neutrophils - concentration related to exacerbation episodes;
- **Tumor necrosis factor-α (TNF-α):** Activates neutrophils and macrophages. Related to IL-8 as it induces expression of IL-8 during exacerbation episodes.

WP1 — Sputum sample preconditioning

Immunomagnetic nanoparticle protocol

Synthesis of tailor-made magnetic nanoparticles (MNPs) loaded with specific antibodies (MNP-Ab) to the different biomarkers

Sputum sample containing biomarkers + MNP-Ab → Incubation: Capture of biomarkers by Ab → Magnetic separation and resuspension (preconcentration)

Air-stable zero valence iron MNPs

- Core of Fe(O) and a carbon shell that protect the iron from oxidation
- Magnetization $\simeq$ 200 emu/g. Efficient capture by Nd magnet
- NP diameter $\simeq$ 150-200 nm
- MNPs were carboxylated for Ab's covalent anchoring

TEM image of the MNPs

WP2 — Protocol for the electrochemical detection of the selected biomarkers

MPO enzyme activity measured using ABTS redox mediator

Blank
10.35 µM MPO
20.70 µM MPO
41.40 µM MPO

Time/s

MPO/µM

ABTS mediator did not work as expected with the transducer array

Alternative: molecules commonly used in electrochemical detection

MPO catalytic oxidation of Fe-MOH

WP3 — Electrochemical transducer array

Innovative array of five two-electrode electrochemical cells sharing counter/reference (C/E) electrode for minimizing electric connections
Measurement of up to 4 biomarkers + 1 reference

Working electrodes
Counter/Reference electrode

Working electrodes
Counter electrode
Reference electrode

Thin-film gold electrodes mass-fabricated by standard photolithographic techniques on silicon wafers

Contact pads

Reusable component of the final device

WP5 — Assembly of the transducer array and paper microfluidic platform

Polymethylmethacrylate (PMMA) polymeric cartridge for assembly of the components

Connector
Sink area-evaporation
Sample addition

The device was initially assessed with solutions containing ABTS mediators.

Device tested using standard analytical samples

Calibration curve for the 3 biomarkers

LOD = 190 ng/mL
[MPO]/ngmL⁻¹

LOD = 260 pg/mL
[TNF-α]/pgmL⁻¹

LOD = 280 pg/mL
[IL-8]/pgmL⁻¹

Final POC device

- ✓ **Optimized design**
- ✓ **Portable**
- ✓ **Quantification of three biomarkers** in COPD-related sputum;
- ✓ Valuable device approach for **rapid detection** and **monitoring** of COPD and related exacerbations, as well as other high-impact diseases for which specific biomarkers have been identified.

ENMed/0049/2016

WP4 — Disposable paper fluidic component

Process optimization to control the **capillary flow rate of paper substrates** for defining channels using a wax printer:

- Capillary flow tests using MNPs solutions ($\cong$200 nm)
- Selection of the best paper - 1mm-thick Whatman chromatographic paper

Pads for immobilizing reagents

Front side
Back side
Alignment

Sink

Sample addition
Sensing area
Electrode cell array

Layout of the **paper component coated with vinyl layers** for better alignment with the electrode array

Personalized Nanomedicine Delivery: the Impact of Heparin on the Cellular Uptake

Carole Champanhac[1], Adelina Haller[2], Johanna Simon[1,2], Katharina Landfester[1], and Volker Mailänder[1,2]

1 - Max-Planck-Institute for Polymer Research, Ackermannweg 10, 55122 Mainz, Germany
2 - Department of Dermatology, University Medical Center of the Johannes Gutenberg-University Mainz, Langenbeckstrasse 1, 55131 Mainz, Germany

MAX-PLANCK-INSTITUT FÜR POLYMERFORSCHUNG

DFG Deutsche Forschungsgemeinschaft

BIONTECH

Nanomedicines are regularly used to improve the cellular uptake of conventional drugs and to limit the side effects arising from untargeted treatment. Nanocarriers (NCs) are susceptible to the environment and a change in the blood composition can lead to unexpected cellular uptake behavior. Here, we highlight how a common anticoagulant (heparin) can change the internalization rate of a NC. We used several heparin concentrations, centered around the clinically relevant value of 1.0IU/mL, to investigate the change in cellular uptake depending on the surface charge of the NCs, the composition of the NC, and the timing of the addition of heparin to the system. We observed that heparin interferes with the uptake of positively charged NCs independently of their composition. Primary phagocytes internalize to a higher extent positively charged liposomes in the presence of heparin, which could lead to an unexpected decrease in therapeutic efficiency for an heparinized patient.

Timing the addition of heparin

Aim: Determine the impact on the cellular uptake of the presence of heparin during the biomolecular corona (BMC) formation versus the addition of heparin after the BMC formed using a positively charged NC.

Pre-coating strategy:

Incubation for 2h at 37°C with cells.
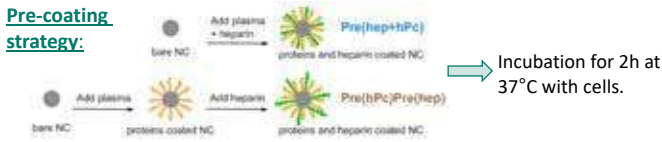
Cellular response:

Effect's overview:

In **primary phagocytes**, same effect for both addition times.
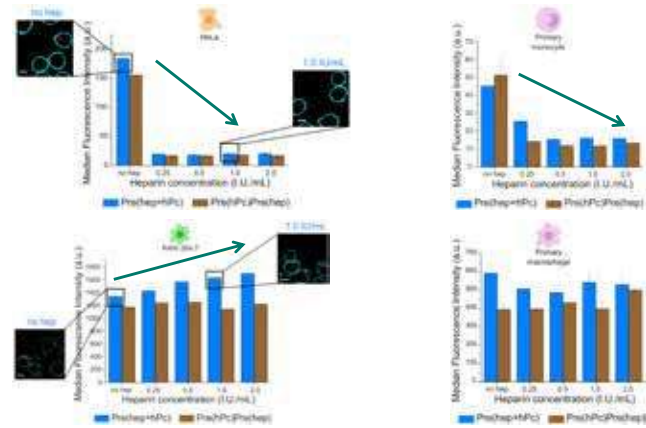
Clinical relevance: liposomal formulation

Aim: Determine the interference to expect depending on the nanomedicine used (two types of liposomes are tested) in a system containing heparin.

Cellular response:
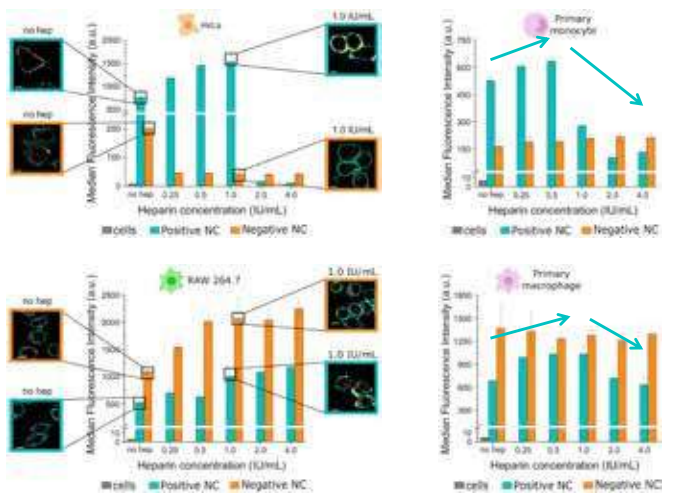
Incubation 3h at 37°C in media with 10% human serum and heparin.

Effect's overview:

In primary phagocytes, effect only for positively charged liposomes.
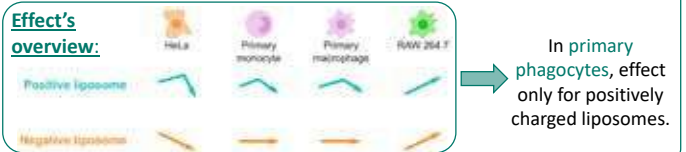
The nanocarrier surface charge matters

Aim: Determine the importance of the surface charge of a nanocarrier to the cellular response in the presence of heparin in the environment.

Experimental setup:

10% human serum + heparin + nanocarriers incubation with cells 3h at 37°C

Cellular response:

Only **positively charged nanocarriers** induce a cellular response to the presence of heparin in the media.
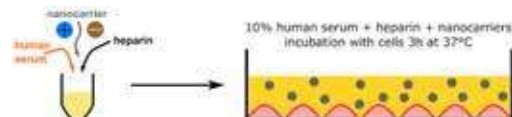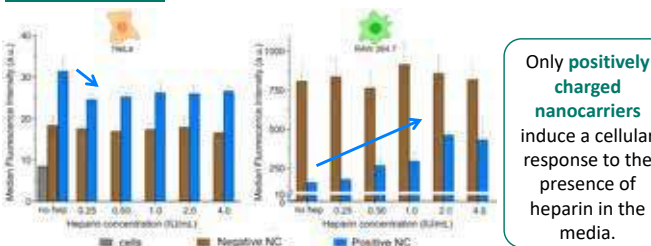
Overview – Take home message

- **No interference** observed *in vitro* with negatively charged liposomes (used for drug delivery).

- **Strong interference** observed *in vitro* with positively charged liposomes (used for gene therapy).

- Even if heparin is added after the nanomedicine, there is **still a risk** of interference.
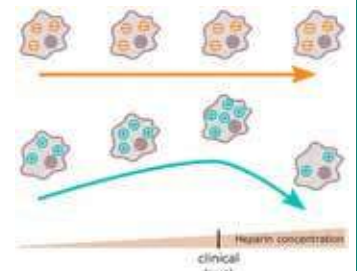
References:
1. C. Champanhac et al., *Biomacromolecules*, 2019, **20**, 3724-3732.
2. S. Schöttler et al., *Nanoscale*, 2016, **8**, 5526-5536.
3. G. Caracciolo, *Nanomedicine: NBM*, 2015, **11**, 543-557.

Modified Gold nanoparticles as gene editing adjuvants in cancer cells

Marco Cordani, Eduardo Garcia-Garrido, Begoña Sot*, Álvaro Somoza*
IMDEA Nanociencia, C/ Faraday 9, Ciudad Universitaria de Cantoblanco, 28049 Madrid, Spain.
marco.cordani@imdea.org

CLINAM
European foundation for Clinical Nanomedicine

SUMMARY

Although CRISPR/Cas-based strategies have great therapeutic potential, the safe and efficient delivery of the molecules involved in this edition remains a major challenge. In this regard, gold nanoparticles (AuNPs) have been exploited in biomedicine as drug delivery systems, because of their low toxicity, biocompatibility, and stability. This was due because the surface of AuNPs can be modified with a variety of bioactive molecules, such as chemotherapy drugs, nucleic acids, and proteins.

In our study, we developed a therapeutic system based on the CRISPR-Cas9, which can reduce the level of oncogenic mutant p53 proteins (mp53) and generate unspecific insertions and deletions (indels) in the TP53 gene, leading to a decrease in cell viability in cancer cells. To further increase the efficacy of the system, we improved the overall editing process by inhibiting critical genes involved in DNA repair (e.g., Kun70, Kun80) using therapeutic nucleic acids as antisense or gapmers.

Concomitantly, we prepared AuNPs with Turkevich's method and modified them with tailored PEI-based molecules developed in our group. Such structures containing stimulus-sensitive linkers can interact with negatively charged nucleic acids, ease their translocation into the cells, promote the endosomal escape and carry the nucleic acids in the cytoplasm.

We observed that these nanostructures could deliver nucleic acids targeting mp53 in cancer cells, which were able to reduce the chemoresistance to Gemcitabine (GEM). Thus, these nanostructures will serve as a multifunctional platform to deliver therapeutic nucleic acids in cancer cells to improve gene editing of key oncogenes involved in cancers (e.g., TP53), providing more effective and selective therapies against mp53-associated cancers.

BACKGROUND

Gain-of-function mutant p53 sustains oncogenic phenotype

CRISPR/Cas9: a versatile tool for genome editing

- Endonuclease Cas9 recognizes PAM motif
- Cas9 generates DSBs leading activation of DNA repair
- NHEJ is error-prone DNA repair pathway that leads indels
- HR occurs if a donor template is present and lead gene correction

CRISPR-Cas9 therapeutic system

CRISPR-Cas9 plasmids for gene editing of mutant p53

Cas9 plasmids
NT   p53.1   p53.2

T7 assay
p53
INDELS
FANC1 cells

p53
GAPDH

Cell viability
NT p53.1 p53.2

Nucleic acids for modulation CRISPR/Cas9 gene editing

p53
GAPDH

Therapeutic mixtures

DNA repair pathway

Gene editing modulation

Preparation and evaluation of AuNPs

Synthesis of AuNPs with Turkevich's method

Cell Internalization

Overcoming chemoresistance

Cell viability

p53   phospho-p70S6K   p70S6K   Bcl-2

CONCLUSIONS

This work focuses on the design of the CRISPR-Cas9 technique against mutant p53 associated cancer and its subsequent modulation through the use of nucleic acids as additives. We also functionalized and evaluated AuNPs for further application as a delivery system.

The analysis of the results obtained allowed us to conclude that:
- CRISPR-Cas9 plasmids knockdown mutated TP53 gene, induce indels generations, and decrease the viability of pancreatic cancer cells.
- Nucleic acids against DNA repair genes, as additivities, modulate mutant p53 expression, suggesting that blocking DNA repair pathway after double-strand breaks may be an efficient therapeutic strategy to counteract the oncogenic mutant p53 proteins.
- AuNPs functionalized with chemical groups deliver functional nucleic acids (e.g., 6-FAM, gapmers) in cell lines and revert chemoresistance to Gemcitabine.

FUTURE RUTES: We are generating a highly specific genome editing system, delivered by AuNPs, that recognizes the mutated TP53 gene in cancer cells. In this way, we could provide a capable tool that exerts good selectivity in future in vivo applications with little damaging side effects.

Antibody conjugation strategies towards an aimed cargo delivery and improvement of nanovaccines

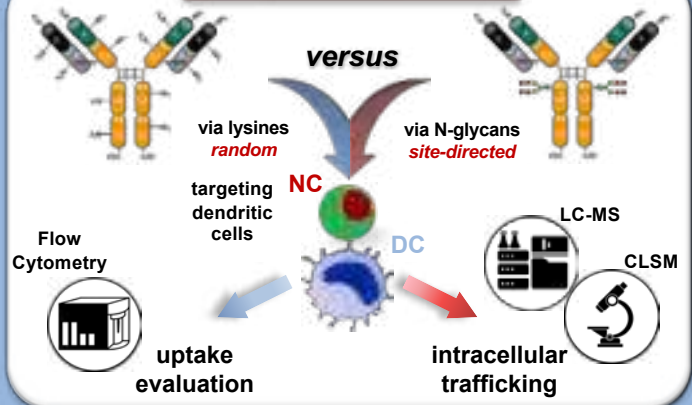**Maximilian Brückner[a,b], Richard da Costa Marques[a,b], Katharina Landfester[a], Volker Mailänder[a,b]**

[a]Max Planck Institute for Polymer Research, Ackermannweg 10, 55128 Mainz
[b]Dermatology Clinic, University Medical Center of the Johannes Gutenberg University Mainz, Langenbeckstr. 1, 55131 Mainz
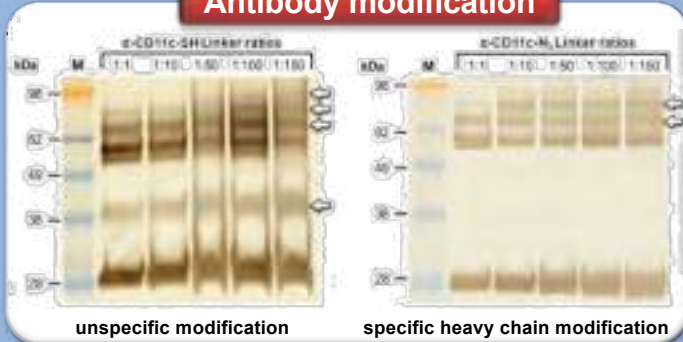
Basic concept

- Antibody-based nanocarrier targeting of dendritic cells
- **Two strategies:**

  modifying **lysine residues** (*thiol-maleimide*)

  vs. **glycosilation site** (*copper-free click chemistry*)
- Validation of antibody modification by SDS-PAGE
- **Flow cytometric** analysis of antibody-nanocarrier conjugates
- **Intracellular trafficking** analysis for unconjugated nanocarriers by LC-MS proteomics and CLSM

Graphical abstract

Antibody modification

unspecific modification   **specific heavy chain modification**

Blocking the targeting site

FcR-mediated uptake   **CD11c-mediated uptake**

The amount of antibodies

increase of unspecificity   **low unspecificity**

Intracellular trafficking

Uptake Scheme

CLSM: Endo-lysosomal stain

endo-lysosomal colocalization   **endo-lysosomal trafficking**   **time-dependent protein corona**

LC-MS: Endo-lysosomal proteins

LC-MS: TOP18 proteins
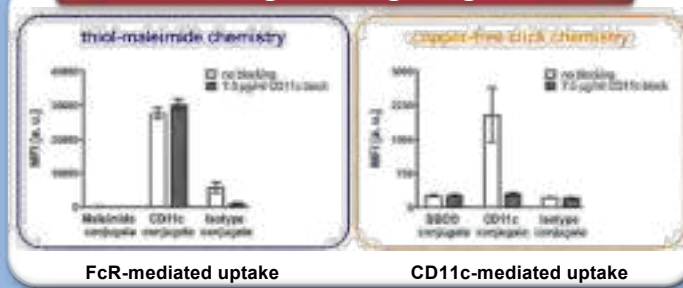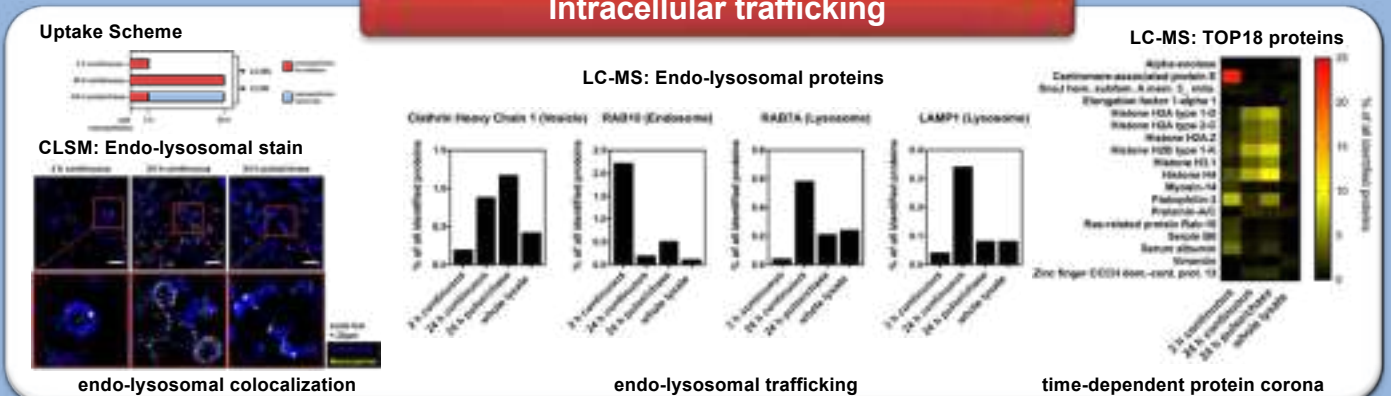
Conclusion

- Enzymatic antibody modification outperforms lysine modification due to a higher site-selectivity
- Site-specificity leads to a controlled orientational antibody attachment
- Targeting due to Fab-specificity and not due to FcR-mediated uptake
- LC-MS proteomics and CLSM indicate a clathrin-mediated uptake and endo-lysosomal trafficking

References

- Tonigold et al., Nat Nanotechnol. 2018 13(9): 862-869
- Paßlick et al., J Control Release 2018, 289, 23-34
- Schoettler et al, Nature Nanotechnology 2016, 11: 372-377
- Hofmann et al, ACS Nano 2014, 8, 10, 10077–10088

SPHERICAL NANOPARTICLES FOR THE DELIVERY OF METHOTREXATE TO ATHEROSCLEROTIC PLAQUES

Valentina Di Francesco[1,2], Danila Gurgone[3,4], Roberto Palomba[1], Miguel Ferreira[1], Pasquale Maffia[3,4,5], Paolo Decuzzi[1]

[1]Laboratory of Nanotechnology for Precision Medicine, Fondazione Istituto Italiano di Tecnologia
[2]Department of Informatics, Bioengineering, Robotics and System Engineering, University of Genoa, Via Opera Pia, 13 Genoa 16145,
[3] Centre for Immunobiology, Institute of Infection, Immunity and Inflammation, College of Medical, Veterinary and Life Sciences, University of Glasgow, Glasgow, United Kingdom
[4] Department of Pharmacy, University of Naples Federico II, Naples, Italy
[5] Institute of Cardiovascular and Medical Sciences, College of Medical, Veterinary and Life Sciences, University of Glasgow, Glasgow, United Kingdom

INTRODUCTION

Atherosclerosis is a chronic inflammatory disease affecting the blood vessel walls. Its pathogenesis is based on the transformation of macrophages into foam cells, following the uptake of oxidized low density lipoproteins (oxLDL). Recent discoveries found that methotrexate (MTX) can modulate cholesterol transport in macrophages. However, MTX is characterized by low water solubility and poor bioavailability. In this work, new MTX nanocarriers are presented to improve MTX based therapies by ameliorating its bioavailability and reducing its toxicity.

RESULTS AND DISCUSSION

A lipid-based prodrug was realized by conjugating MTX to 1,2-distearoyl-sn-glycero-3-phosphoethanolamine. The resulting lipid-MTX was then used as a constituent of spherical nanoparticles: liposomes (MTX-LIP) and spherical polymeric nanoparticles (MTX-SPN). (Stigliano, Ramirez et al. 2017). LIP were prepared by thin layer evaporation (TLE) while SPNs were synthetized using a sonication-emulsion technique. Both nanoparticle formulations presented similar features. For the lipidic nanoparticles, the size is 174±2 nm (PdI: 0.15 ± 0.0007), and Zeta Pot -48 ± 0.02 mV; for the polymeric nanocarriers, the size is 208±2 nm (PdI: 0.15 ± 0.02), and Zeta Pot 45.8 ± 0.02 mV. MTX encapsulation efficiency (EE%) 70±5% for MTX-LIP and 1.5±0.2% for MTX-SPN.
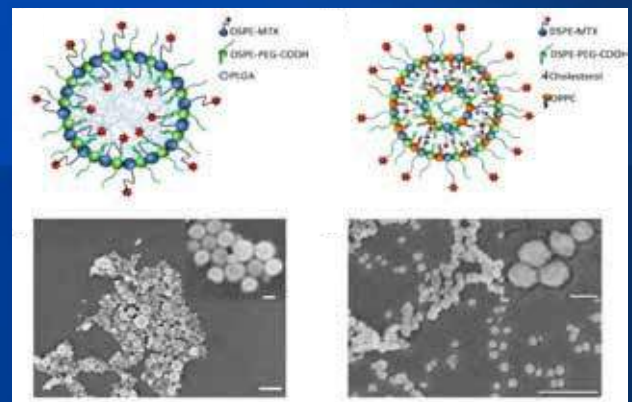
Foam cells were obtained by treating rat bone marrow derived monocytes (BMDM) with oxLDL. The treatment with the two nanoformulations was able to reverse foam cells maturation into macrophages. Both MTX-LIP and MTX-SPN decreased cholesterol amounts after 24 hours in BMDM. The efficacy of the treatment was also proved by gene expression analysis. RT-PCR showed the down-regulation of CD36 and SRA-1 genes (foam cell markers) and up-regulation of the reverse cholesterol transporter (ABCA1) in foam cells treated with the nanoformulations. MTX-LIP and MTX-SPNs reduced also inflammatory gene expression (IL-6, IL-1β and TNFα). Cytotoxicity tests of MTX-LIP and MTX-SPN were performed on BMDM, cells showed a good tolerance to the treatment at the used doses.
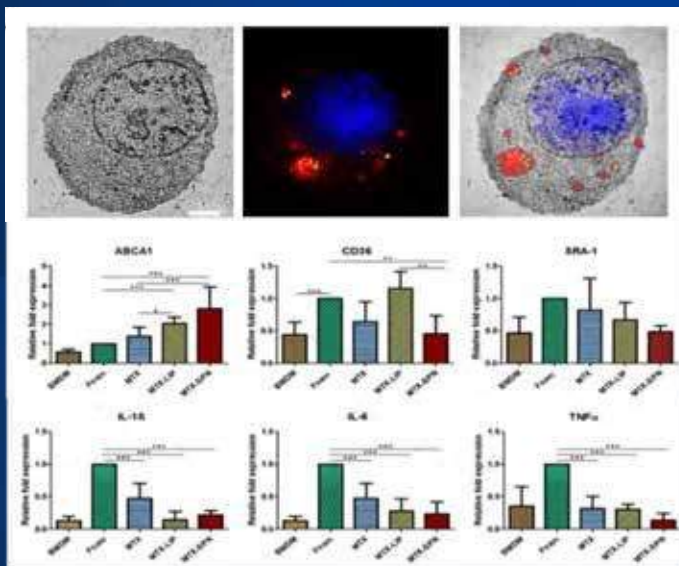
MTX-LIP were used in vivo in murine experimental atherosclerosis. ApoE^{-/-} mice, fed with high-fat diet for 28 days were treated for 4 weeks (once every three days) and plaque burden was measured. Results show that this treatment reduces the plaque area supporting the concept that a systemic delivery of MTX particles may constitute an effective strategy to inhibit early atherogenesis

CONCLUSION

Data revealed that both formulations are able to reverse macrophage inflammation and maturation into foam cell phenotype. MTX-LIP effectively reduced plaque area in ApoE^{-/-} supporting the concept that a systemic delivery of MTX loaded particles may constitute an effective strategy to inhibit early atherogenesis.
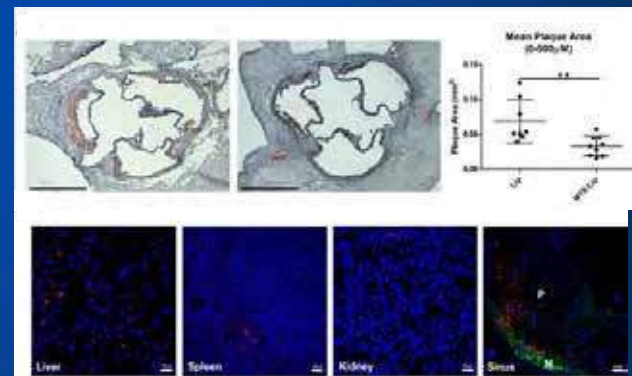
Programmed self-assembly of peptide based inhibitor toward hypoxic cancer therapy

Zeinab Farhadi Sabet†‡, Jiayang Li†, Kejian shi, Chunying Chen†‡

†CAS Key Laboratory for Biomedical Effects of Nanomaterials and Nanosafety, CAS Center of Excellence in Nanoscience, National Center for Nanoscience and Technology, Beijing 100190, P. R. China,
‡University of Chinese Academy of Sciences, Beijing 100049, P. R. China

Abstract

CAIX as a marker of hypoxia, has over expression on membrane of cancer cell and control the acidity of tumor microenvironment provide resistance and aggressive cells. Here by delivering a small molecule of CAIX inhibitor with short peptide motif which has self assembly to form nanofibers in low pH of cancer cell, overcome to this abnormality. Meanwhile the CAIX related endocytosis enhance the uptake of nanofibers inside of the cell and in lower pH of acidic vesicle, the diameter of the nanofibers increases by sticking to each other and finally causes the vesicle damage the blocking autophagy. Moreover in vivo study show the antitumor efficacy, antimetastatic and antiangiogenesis effects in breast tumor of mouse model. As a biocompatible compound, which has been effective in targeting hypoxic cell, this system can be used as a new route for hypoxia targeting .

Materials

1- Synthesis of self-assemble motif ⟩⟩⟩ N-pep

2- Synthesis of isothiocyanate-benzensulfonamide (CAIX inhibitor) ⟩⟩⟩ ABS

3- Conjugation of peptide motif to CA inhibitor ⟩⟩⟩ N-pepABS

4- Synthesis peptide without self-assembly ability + CA Inhibitor ⟩⟩⟩ pep-ABS

Results and Discussion
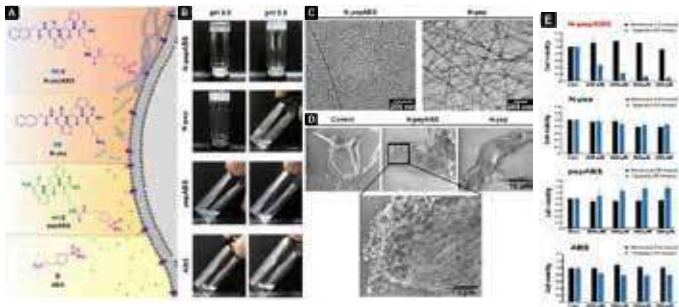
Molecular design of self-assembled CA IX inhibitors and hypoxic cancer cell–targetting.
(A) chemical structure of N-pepABS and different control group. (B) In vitro gelation performance of N-pepABS, N-pep, pepABS, and ABS at pH 6.5 and 5.5. (C) Transmission electron microscope (TEM) images of 0.75 wt % of N-pepABS and N-pep hydrogel formed at pH 6.5. (D) Environment scanning electron microscope images of MDA-MB-231 cells treated with 500 M medium control, N-pepABS, or N-pep under hypoxia condition after 24-hour. (E) Cell viability of of MDA-MB-231 with treatment of N-pepABS, N-pep, pepABS, and ABS, for 72 hours under both hypoxia (sky blue) and normoxia (black).
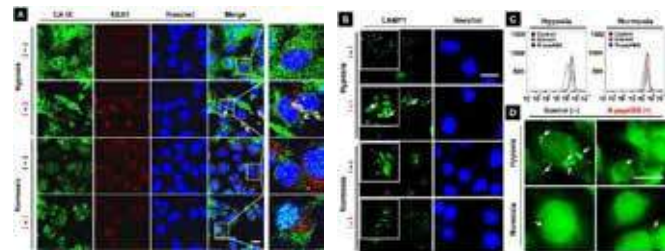

CA IX–regulated endocytosis. (A) Endocytosis regulation by CA IX of N-pepABS nanofibers under hypoxia after 24-hour treatment of 500 µM N-pepABS (+) or medium control (−). Scale bar, 20 µm. (B) endolysosomal swelling and (C and D) and damaging intracellular acid vesicles after 48-hour treatment of 500 µM N-pepABS under hypoxia. Scale bars, 20 µm.
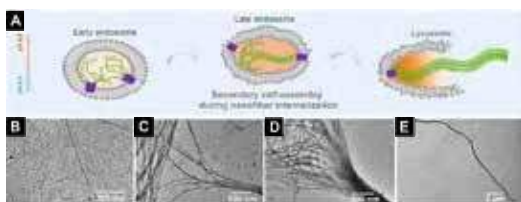
CA IX–induced nanofiber internalizations in hypoxic cancer cells. (A) scheme of endocytosed nanofibers and vesicle damage. TEM images of nanofibers formed by 0.75 wt % of N-pepABS at (A) pH 6.5 or (B to D) pH 5.5. TEM images of nanofibers
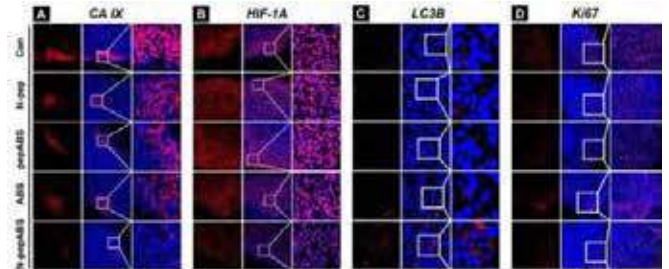
Antihypoxia performance of N-pepABS in MDA-MB-231 tumor model. Immunofluorescence images of expression alterations on (A) CA IX, (B) HIF-1A, (C) LC3B, and (D) Ki67 after treatments of phosphate-buffered saline (PBS) control, N-pep, pepABS, ABS, and N-pepABS. Inhibition of tumor growth and metastasis in 4T1 tumor model.
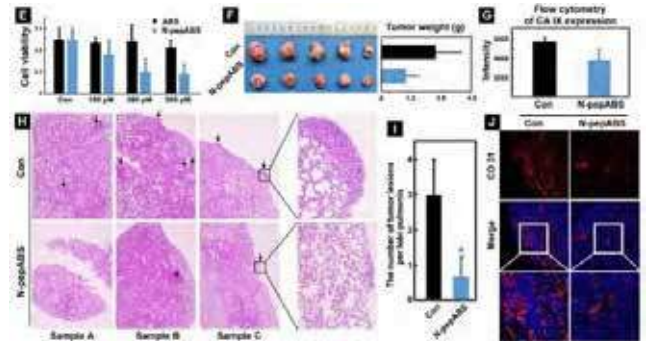
Antimetastasis effect of N-pepABS in 4T1 breast tumor model. Inhibitory effects of N-pepABS on (E) hypoxic 4T1 cell growth; (F) tumor growth and decreases tumor weight of 4T1 cancer. (G) CA IX expression in tumor tissues after N-pepABS treatment. (H) Hematoxylin and eosin staining images of lung tissues with metastasis of 4T1 tumor cells from six different samples and (I) its statistical analysis of the number of tumor lesions per lobi pulmonis. (J) Immunofluorescence images of endothelial marker CD31, indicating blood vessel variation after N-pepABS treatment.

Conclusion

Hypoxia not only prevents the drug spreading to the target tissue, but also causes tumor resistance to radio/chemo therapy. Here we modify the CA inhibitor with self-assemble peptide which can successfully target the CA IX on cell membrane and with the favorable effect of nanofibers cased increasing the inhibitor circulation retention time, endocytosis regulation of nanofibers and damage intracellular vesicle can obviously inhibit hypoxic condition and tumor growth.

Future Direction

In addition to the rapid growth and proliferation of tumor, hypoxic regions have a profound effect on cancer progression and metastasis. Here we introduce a biocompatible system which effetely could target hypoxia. Codelivery of anticancer drug with this system can have an increasing effect on inhibition of cancer cells.

Acknowledgment

Synthesis and reproducibility of functionalized hydroxylethyl starch (HES) and protein nanocapsules by inverse miniemulsion and their biological properties
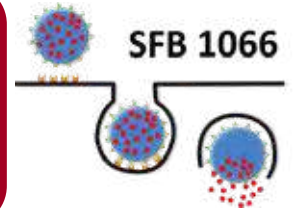
TP B6

SFB 1066

Marie-Luise Frey[1], Matthias P. Domogalla[2], Johanna Simon[1,2], Volker Mailänder[2,1], Svenja Morsbach[1], Kerstin Steinbrink[2] and Katharina Landfester[1]
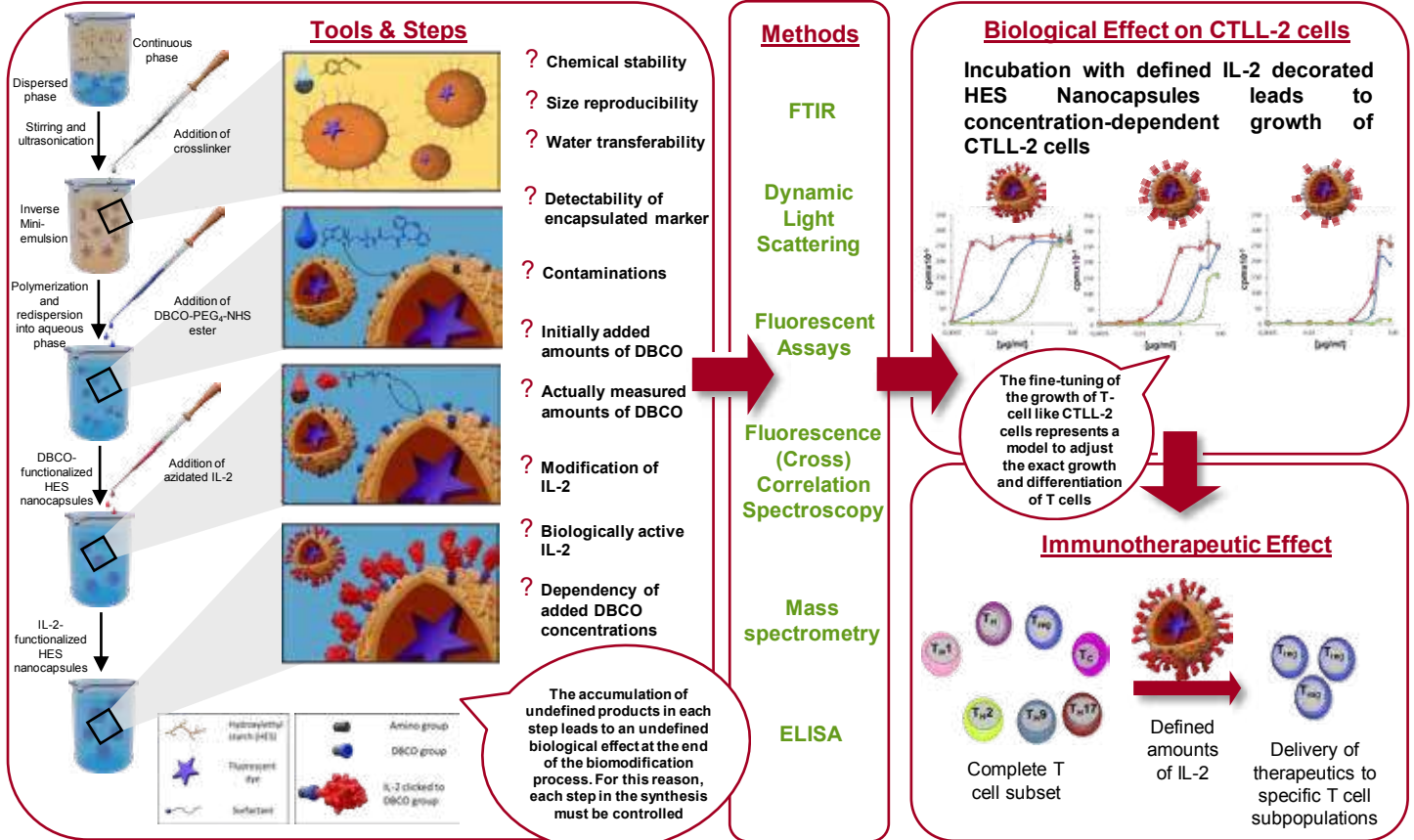
[1]Max-Planck-Institute for Polymer Research Mainz
[2]Department of Dermatology, University Medical Center of the Johannes Gutenberg-University Mainz

Concept

Process Control of the Nanocarrier Synthesis Leads to Reproducibility of the Biological Effect

Complex physicochemical properties and a **high process dependency** complicate the **synthesis of nanocarriers** in a reproducible manner. We demonstrate that **by splitting up the synthesis** into smaller steps and **controlling** them, reproducibility is achieved.

Tools & Steps

Continuous phase
Dispersed phase
Stirring and ultrasonication
Addition of crosslinker
Inverse Mini-emulsion
Polymerization and redispersion into aqueous phase
Addition of DBCO-PEG$_4$-NHS ester
DBCO-functionalized HES nanocapsules
Addition of azidated IL-2
IL-2-functionalized HES nanocapsules

? Chemical stability
? Size reproducibility
? Water transferability
? Detectability of encapsulated marker
? Contaminations
? Initially added amounts of DBCO
? Actually measured amounts of DBCO
? Modification of IL-2
? Biologically active IL-2
? Dependency of added DBCO concentrations

The accumulation of undefined products in each step leads to an undefined biological effect at the end of the biomodification process. For this reason, each step in the synthesis must be controlled

Methods

FTIR

Dynamic Light Scattering

Fluorescent Assays

Fluorescence (Cross) Correlation Spectroscopy

Mass spectrometry

ELISA

Biological Effect on CTLL-2 cells

Incubation with defined IL-2 decorated HES Nanocapsules leads to concentration-dependent growth of CTLL-2 cells

The fine-tuning of the growth of T-cell like CTLL-2 cells represents a model to adjust the exact growth and differentiation of T cells

Immunotherapeutic Effect

Complete T cell subset

Defined amounts of IL-2

Delivery of therapeutics to specific T cell subpopulations

Concept

Bioorthogonal Triazolinedione (TAD) Crosslinking of Protein Nanocapsules leads to a Change in Protein Adsorption in Comparison To Conventional Unspecific Toluene Diisocyanate (TDI) Crosslinking

Different **crosslinking** of protein nanocapsules **changes the capsule surface** and therefore also the **protein adsorption and uptake into cells.**

Tools

Conventional TDI mainly crosslinkes lysines. TAD crosslinkes tyrosines and tryptophans in the interior of a protein.

Physicochemical Properties of the Nanocapsules

Sample	Average Diameter in toluene*/ nm	Average Diameter in water*/ nm	Zeta Potential/ mV
BSA-TAD	115 ± 55	193 ± 150	-34 ± 5
OVA-TAD	189 ± 82	214 ± 135	-38 ± 5
HSA-TAD	145 ± 69	192 ± 91	-25 ± 5
BSA-TDI	122 ± 53	199 ± 75	-27 ± 5
OVA-TDI	108 ± 45	200 ± 54	-30 ± 5
HSA-TDI	152 ± 51	178 ± 46	-16 ± 5

*determined by DLS at 90°

TEM micrograph of BSA-TAD nanocapsules

The protein corona composition reveals slight differences in the adsorbed amounts of immunoglobulins and coagulation cascade proteins of the differently crosslinked protein nanocapsules

Biological Effect on HeLa cells

HeLa

Human serum incubation prior to HeLa cell incubation changes the uptake behaviour of TAD crosslinked nanocapsules in comparison to TDI crosslinked ones

References

[1] S. Frick, M. P. Domogalla, G. Baier, F. R. Wurm, V. Mailänder, K. Landfester, K. Steinbrink, *ACS Nano*, **2016**, *10*, 9216-9226.
[2] M. P. Domogalla, P. V. Rostan, V. K. Raker, K. Steinbrink, *Front Immunol*, **2017**, *8*, 1764.
[3] G. Baier, J. M. Siebert, K. Landfester, A. Musyanovych, *Macromolecules*, **2012**, *45*, 3419-3427.

[4] K. Landfester, A. Musyanovych, V. Mailänder, *J. Polym. Sci. Part A: Polym. Chem.*, **2010**, *48*, 493-515.
[5] M-L. Frey, J. Simon, M. Brückner, V. Mailänder, S. Morsbach, K. Landfester, *Polym. Chem.*, **2020**, *11*, 3821-3830.

JGU Johannes GUTENBERG UNIVERSITÄT MAINZ

Max-Planck-Institut für Polymerforschung
Max Planck Institute for Polymer Research

UNIVERSITÄTSmedizin.
MAINZ

A Bio-orthogonal Functionalization Strategy for Site-specific Coupling of Antibodies on Vesicle Surfaces after Self-assembly

Meiyu Gai [a,l], Johanna Simon [a,b,l], Ingo Lieberwirth [a], Volker Mailänder [b,a], Svenja Morsbach [a,*] and Katharina Landfester [a]

a Max Planck Institute for Polymer Research, Ackermannweg 10, 55128 Mainz, Germany

b Department of Dermatology, University Medical Center of the Johannes Gutenberg-University Mainz, Langenbeckstrasse 1, 55131 Mainz, Germany

INTRODUCTION

Background: The modification of liposomal surfaces, especially coupling with targeting ligands, is interesting for a mass of applications and a variety of chemistries (e.g. maleimide–thiol coupling) bring this into reality. In the conventional approaches, the surface functionalization mostly takes place before the amphiphilic molecules (block-copolymers, lipid etc.) complete the self-assembly, by introducing specific functional groups directly into the amphiphilic molecules.

Current problems: 1) the introduced functional groups may react with loaded cargo; 2) natural carriers like extracellular vesicles should be functionalized making chemical pre-assembly modification impossible; 3) the attached targeting antibodies are not specifically conjugation-site controlled, which will dramatically decrease the antibody targeting efficiency.

Our solutions: Here, we would like to present the site-specific coupling of antibodies to the surface of amino group-terminated liposomes via bio-orthogonal copper-free click chemistry after liposome self-assembly.

MATERIAL & METHODS

Schematic step-by-step illustration of liposome synthesis, surface functionalization and site-selective antibody attachment.
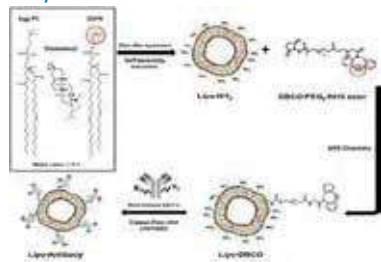
Liposomes production strategy and characterizations.
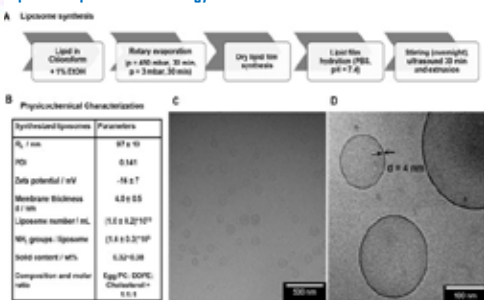
Figure 1. A) Schematic overview of liposome preparation. **B)** Physicochemical characterization of synthesized liposomes. **C, D)** Cryo-TEM images of liposomes. From images with high magnification **(D)** the membrane thickness of the liposomes d was determined.

Quantification of DBCO groups on the liposomes' surface.
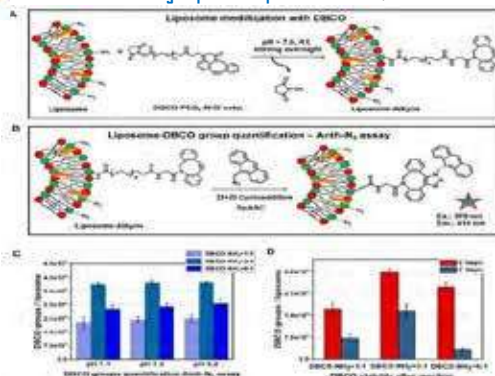
Figure 2. Schematic illustration of **A)** the functionalization procedure with a DBCO-PEG$_4$-NHS ester. **B)** The anthracene-azide assay: the coupling of anthracene provides fluorescence emission proportional to the number of DBCO groups. **C)** Anthracene-Azide assay quantification results for different reaction conditions (varied DBCO/NH$_2$ group ratio and different reaction pH). **D)** DBCO group quantification after different storage times.

RESULTS

Antibody functionalization and attachment to surface-modified liposomes.
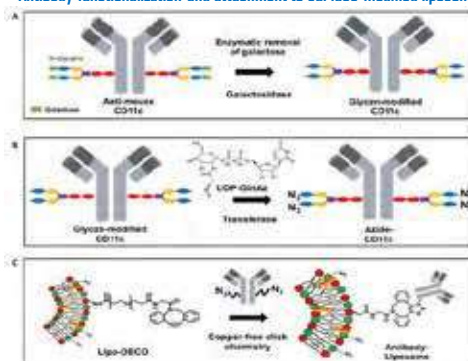
Figure 3. A) Enzymatic removal of galactose from the Fc-part of the CD11c-antibody with galactosidase. **B)** Site-specific, enzymatic attachment of an azide functionality using UDP-N-azidoacetylgalactosamine (UDP-GalNAz) to the sugar residues on the Fc-part of the CD11c-antibody **C)** Bio-orthogonal copper-free click reaction to attach the azide-modified antibody on the DBCO-modified liposome surface.

Characterization of the azide-modified antibody.
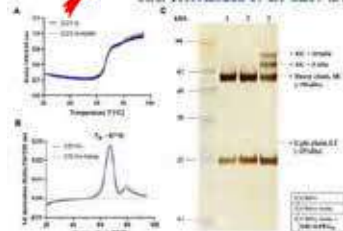
Figure 4. A) and B) nanoDSF measurements of the unmodified and azide-modified anti-mouse CD11c antibody (10 µL, ~0.5 mg/mL). The ratio of the fluorescence intensity (350/330 nm, A) and the first derivation (B) is plotted. The melting temperature T_M is determined from the maximum of the 1st derivation of the ratio. **C)** SDS-PAGE of unmodified (1), azide modified CD11c (2) and PEGylated CD11c antibody.

Verification of antibody presence on the liposomes' surface.
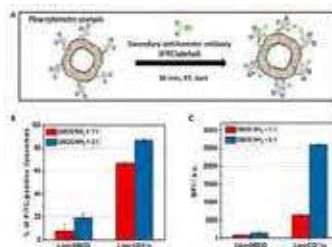
Figure 5. A) Schematic illustration of the flow cytometry measurements for the antibody quantification on the liposome surface. **B) and C)** Flow cytometry measurements for liposomes functionalized with anti-mouse-CD11c antibodies. A secondary labeled FITC-anti-hamster antibody was used to detect the antibodies on the liposome surface.

Physicochemical characterization of liposomes before and after functionalization with DBCO/antibodies.
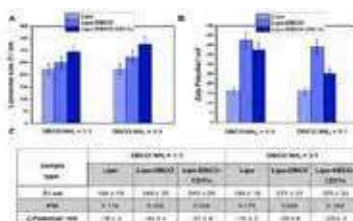

Figure 6. A) Size of liposomes before/after DBCO and antibody attachment using 1:1 and 3:1 DBCO/NH$_2$ ratios. **B)** Surface charge before and after liposome functionalization. **C)** Overview of the physicochemical properties of the liposomes for the different reaction conditions.

CONCLUSIONS

1 ➢ The amine group-terminated liposomes via lipid dry film rehydration followed by extrusion can be successfully produced and can be further conjugated with functional groups and performed antibody coupling (Fc fragment) via bio-orthogonal copper-free click chemistry after liposome self-assembly in physiological conditions.

2 ➢ This surface functionalization procedure offers the advantage to be transferred to all self-assembled systems bearing primary surface amino groups without damaging the assembled structure, which applicable for a wide range of drug delivery systems as well as straightforward and robust in terms of handling.

Raman Spectroscopy, a sensitive method for bone quality evaluation. Iternative to histology.

E. Gatin[1, 2], P. Nagy[3], O. Dubok[4], C. Luculescu [5], C. Berlic [1], C. Cosconel [2]

1 University of Bucharest, Faculty of Physics, Magurele – Bucharest, Romania; **2** University of Medicine "Carol Davila", Blv. Eroii Sanitari 8, Sector 5, Bucharest, Romania; **3** Semmelweiss University, Faculty of Dentistry, Periodontology Department, Budapest, Hungary; **4** Frantsevich Institute for Problems of Materials Science, Kyiv, Ukraine; **5** INFLPR – CETAL, Magurele – Bucharest, Romania.

INTRODUCTION

The majority of studies evaluating the effects of different surgical procedures aimed at defect fill with bone grafts and only employed clinical outcome measures, such as probing pocket depth, probing attachment level, radiological analysis and direct visualization, following surgical re-entry procedures. Such approaches did not facilitate the determination of true bone regeneration, an outcome that requires histologic investigation.

OBJECTIVE

A non-invasive and quick method for evaluation of chemical compounds from bone tissues is requested. We suggest a new method, based on the Raman spectroscopy. This non-destructive optical method is able to characterize and differentiate initial normal cortical bone, initial augmentation material and final regenerated bone.

Materials and Methods

Regarding our study, for harvested bone samples were selected 2 patients, before and after maxillary - sinus lift augmentation procedure (Cerabone material from **Botiss GmbH** as bone substitute it was used)[2]. The healing period was approximatively 8 months for both patients. Bioethitical approval was obtained. Raman Spectroscopy was performed respecting same geometrical conditions for data recording. Corresponding spectra were acquired before and after surgical augmentation

Results

Differences in peaks intensity on raw spectra reflect the differences in the quantities of the chemical components (related to specimens concentration) for investigated specimens. Sensitive information obtained from the Raman spectra (shape related to fluorescence) using raw data, were compared with the histological results (collagen matrix / quantity / bone substitute integration).

For both patients' bone samples, higher PPi peak intensities were obtained before treatment (73.04 % - patient #1 and 81.22 % - patient #2; highest value recorded for patient #2 with previous periodontal problems) and lower values after treatment (48.76% - patient #1 and 38.39% – patient #2). PPi is known acting as a potent inhibitor of HAP crystals precipitation (biological mineralization), aspect that might causes periodontal disease. From histology investigation, morphometric results for ratio areas (bone tissue / implant material) are: 1.6067 - patient #1 and 0.6970 – patient #2. Histological results confirm Raman evaluation of bone samples.
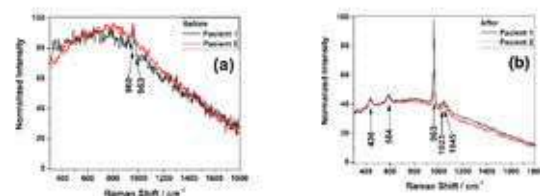
Fig. 1 Raman spectra for bone samples. Details:
before treatment (a) and after healng (b).

Fig.2 Histological results (after healing) versus SEM results for patient #1.

TABLE 1. Targeted Raman shift for bone specimens, **"list of four"**.

Raman shift	Characteristics	Assignment	References
430 - 450 cm^{-1}	very strong	$v_2 PO_4^{3-}$	
955 - 960 cm^{-1} 955 cm^{-1} 957 cm^{-1}	very strong	**Extensive mineral immature bone;** $v_1 PO_4^{3-}$, P – O phase; $v_1 PO_4^{3-}$, extensive HPO_4^{2-}	[3]
960 – 965 cm^{-1}	very strong	**Mineral mature bone;** $v_1 PO_4^{3-}$ tetrahedral internal mode.	[3]
1,023 cm^{-1}	strong	**PP_i ($P_2 O_7^{4-}$), inorganic pyrophosphate**; symmetric P••O stretch modes of PO_3^{2-} moieties; $v_S PO_3$ and of P–O– P bridging.	[4, 5, 6]

Conclusions

Raman technique is capable to offer a complete bone evaluation (qualitative / quantitative), in the meantime being an independent method.

References:

1) Sfeatcu R, Luculescu C, Ciobanu L, Balan A, Gatin E, Patrascu I. Dental Enamel Quality and Black Tooth Stain: A New Approach and Explanation by using Raman and AFM Techniques. Particulate Science and Technology 2015: 33(4): 429-435

2) Trajkovski B, Jaunich M, Müller WD, Beuer F, Zafiropoulos GG, Houshmand A. Hydrophilicity, Viscoelastic, and Physicochemical Properties Variations in Dental Bone Grafting Substitutes. Materials. Bone Substitute Materials 2018, 11(2);

3) Nathanael AJ, Sun Ig Hong, Mangalaraj D, Pao Chi Chen. Large scale synthesis of hydroxyapatite nanospheres by high gravity method. Chemical Engineering Journal 2011: 173: 846 – 854;

4) Daizy P, Bini LG, Aruldhas G. IR and Polarized Raman Spectra of - Na4P2O7. 10H20. Journal of Raman spectroscopy 1990: 21: 523-524;

5) Bouchaib M, Brahim El Bali, Surendra KS, Revansidha PG. High-pressure studies of SrNi3 (P2O7)2 pyrophosphate by Raman spectroscopy and X-ray diffraction. J Mol Struct 2006: 794:334–340;

6) Hua D, Callender R, Schramm VL, Grubmeyer C. Pyrophosphate activation in Hypoxanthine-Guanine phosphoribosyltransferase with transition state analogue. Biochemistry 2010: 30; 49(12): 2705–2714.

ETH zürich

Empa
Materials Science and Technology

Design and Development of Inorganic Nano-particles for Radio-enhancement Therapy

Lukas RH Gerken[1,2], Anna Lena Neuer[1,2], Inge K Herrmann[1,2]

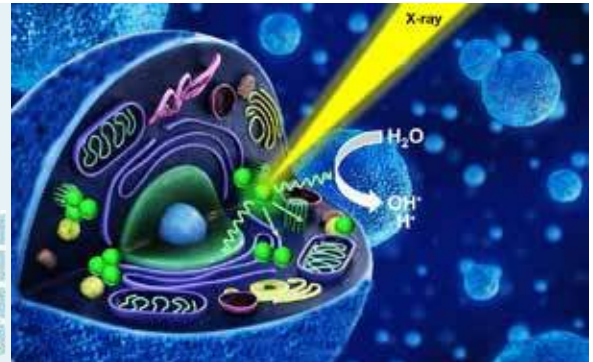[1] Nanoparticle Systems Engineering Lab, Department of Mechanical and Process Engineering, ETH Zürich, Sonneggstrasse 3, CH-8093 Zürich, Switzerland

[2] Particles 4D, Laboratory for Particles Biology Interactions, Swiss Federal Laboratories for Materials Science and Technology (Empa), Lerchenfeldstrasse 5, CH-9014, St. Gallen, Switzerland

Email: lukas.gerken@empa.ch

1 Introduction

- Radiotherapy is an important part of cancer therapy but bears risks, including the development of radio-resistance, damage to healthy tissue and occurrence of secondary cancers.[1]

- Nanoparticle-based radio-enhancement may selectively amplify the damage caused by (X-ray) irradiation through ejection of secondary particles in proximity of the nanoparticles.

- While promising results have been reported for Au and HfO_2, treatment plans are empirically designed and show highly variable efficiency ranging from significant radio-enhancement to radio-protection for the same nanoparticle system.[2]

- Clinical translation is hampered by the challenge of scalable manufacturing of high quality nanoparticles (pilot-plant scale: kg/day) and the lack of experimental standardization and mechanistic insights.[3]

- Here, we systematically investigate the radio-enhancement properties of metal oxide nanoparticles with different atomic number (TiO_2, ZrO_2, HfO_2) in relatively radio-sensitive (HeLa) and radio-resistant (HT1080) cancer cells as well as healthy fibroblasts (NHDF).

2 Results & Discussion

Figure 1: Wet-chemical (WetChem) synthesis methods allow the production of high-quality, crystalline 5 nm TiO_2, ZrO_2 and HfO_2 nanoparticles at production rates of grams/day (A, C-E, I). Flame-spray pyrolysis (FSP) can yield industrial scale production rates (kg/day) with comparable physico-chemical nanoparticle characteristics (B, F-H, J).
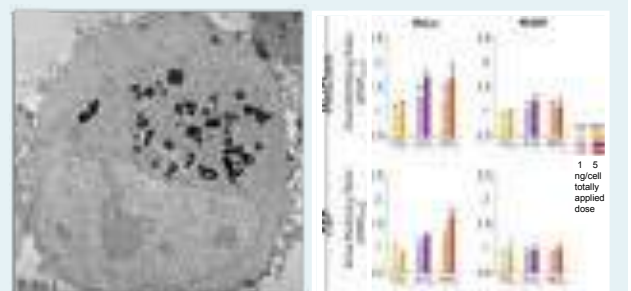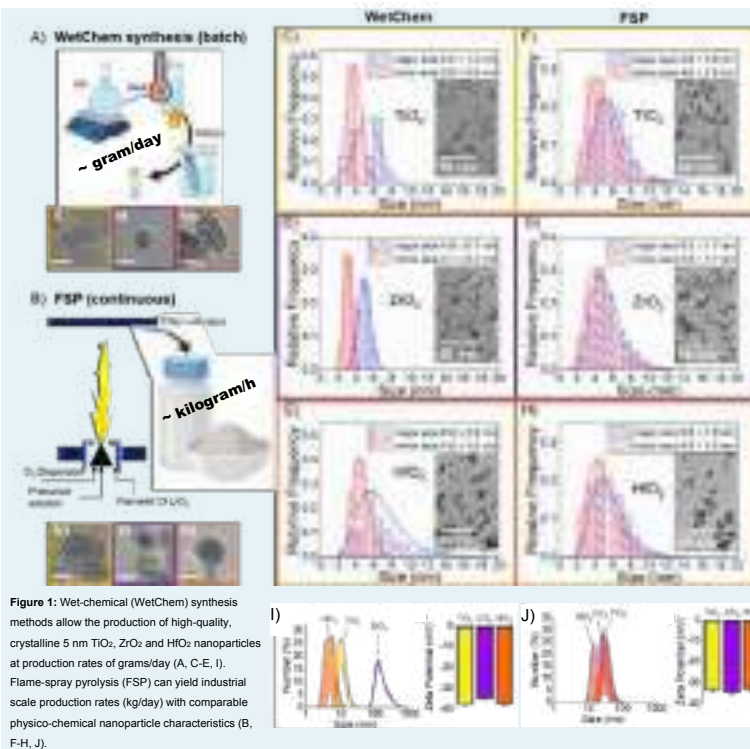
Figure 2: STEM image of a HT1080 cancer cell with taken up WetChem HfO_2 nanoparticles.

Figure 3: Radio-enhancement effect from oxide nanoparticles observed in cancerous HeLa cells (TiO_2 < ZrO_2 < HfO_2), but not in normal fibroblasts (NHDF).
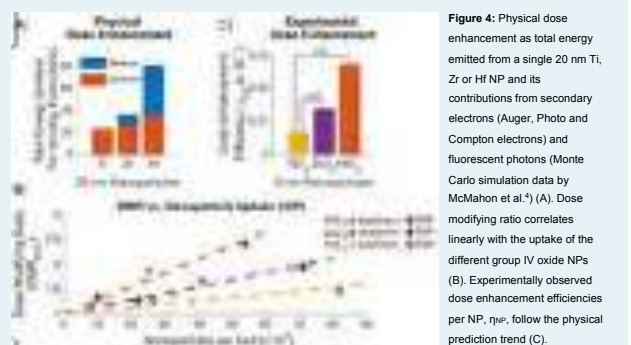
Figure 4: Physical dose enhancement as total energy emitted from a single 20 nm Ti, Zr or Hf NP and its contributions from secondary electrons (Auger, Photo and Compton electrons) and fluorescent photons (Monte Carlo simulation data by McMahon et al.[4]) (A). Dose modifying ratio correlates linearly with the uptake of the different group IV oxide NPs (B). Experimentally observed dose enhancement efficiencies per NP, η_{NP}, follow the physical prediction trend (C).

3 Materials & Methods

- Synthesis of metal oxide nanoparticles via benzyl alcohol route and Flame Spray Pyrolysis.
- Size and morphology analyzed using TEM (200 keV), XRD and DLS.
- Sub-lethal concentrations were determined by Lactate dehydrogenase (LDH) and ATP release (CellTiter Glo) assays.
- Uptake/Nanoparticle-Cell association was measured using ICP-MS.
- Irradiation of cancerous (HeLa, HT108) and normal (NHDF) cell lines within a 8 cm thick phantom were performed using 150 kVp x-rays.
- Surviving cell fractions were analyzed using ATP release assay (CellTiter-Glo).

4 Conclusion

- Nanoparticles with comparable size and morphology but different atomic number allow systematic radio-enhancement study.
- First-in field comparative study shows pronounced radio-enhancement effects for HfO_2 and ZrO_2 in HeLa cells as well as in the more radio-resistant HT1080 cells.
- Little to no dose-enhancement in healthy fibroblast cells (NHDF).
- Dose modifying ratios follow a physical enhancement rationale

Radio-enhancement effect (@150kVp): HfO_2 > ZrO_2 > TiO_2

D MAVT
Nanoparticle Systems Engineering Laboratory

1. Kim, B. M., Hong, Y., Lee, S., Liu, P., Lim, J. H., Lee, Y. H., … Hong, Y. (2015). Therapeutic Implications for Overcoming Radiation Resistance in Cancer Therapy. International Journal of Molecular Sciences, 16(11), 26880–26913.
2. Ricketts, K., Ahmad, R., Beaton, L., Cousins, B., Critchley, K., Davies, M., Evans, S., Fenuyi, I., Gavriilidis, A., Harmer, Q. J., Jayne, D., Jefford, M., Loizidou, M., Macrobert, A., Moorcroft, S., Naasani, I., Ong, Z. Y., Prise, K. M., Rannard, S., … Royle, G. (2018). Recommendations for clinical translation of nanoparticle-enhanced radiotherapy. The British Journal of Radiology, 91(1092), 20180325.
3. Retif, P., Pinel, S., Toussaint, M., Frochot, C., Chouikrat, R., Bastogne, T., & Barberi-Heyob, M. (2015). Nanoparticles for Radiation Therapy Enhancement: the Key Parameters. Theranostics, 5(9), 1030–1044.
4. McMahon, S. J., Paganetti, H., & Prise, K. M. (2015). Optimising element choice for nanoparticle radiosensitisers. Nanoscale, 8(1), 581–589.
5. Gerken, L.H.R, Neuer, A.N., Gschwend P., Keevend, K. Aengenheister, L., Anthis. A.H.C, Pratsinis, S.E., Plasswilm, L., Herrmann, I.K., in revision, 2020.

Email: lukas.gerken@empa.ch

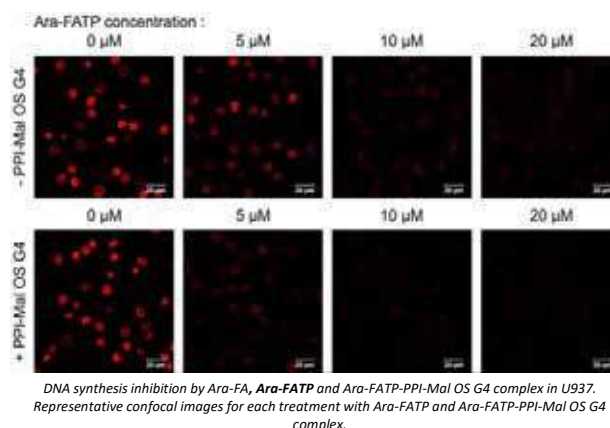# Poly(propyleneimine) dendrimers as carriers of anticancer adenosine nucleotides
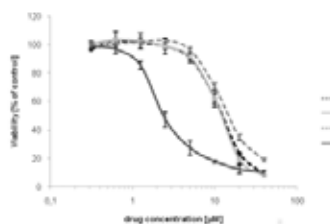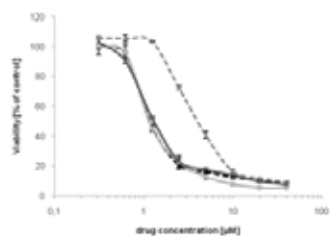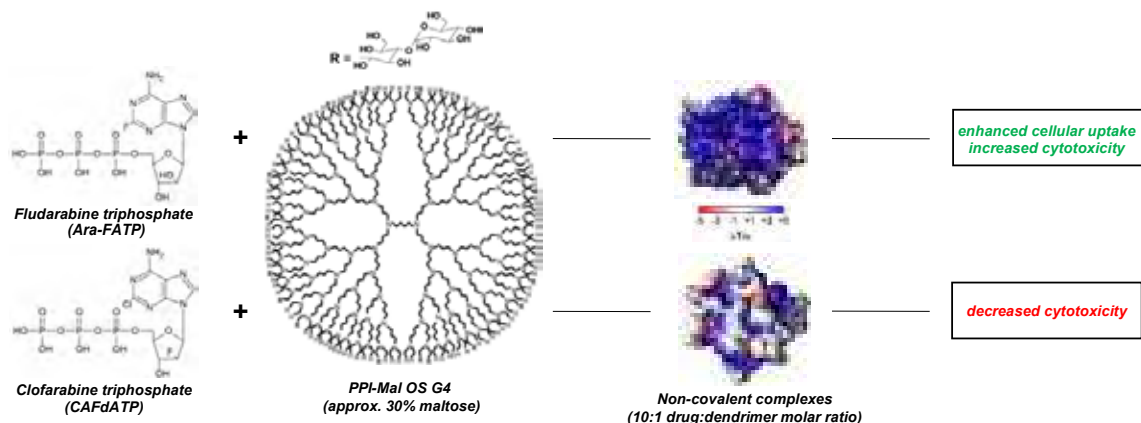
Michał Gorzkiewicz[1], Barbara Klajnert-Maculewicz[1,2]

[1] Department of General Biophysics, Faculty of Biology and Environmental Protection, University of Lodz, 141/143 Pomorska St., 90-236 Lodz, Poland
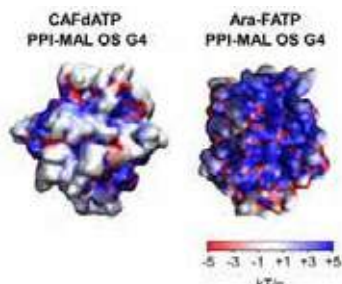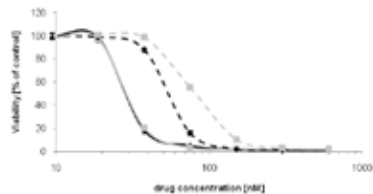[2] Leibniz Institute of Polymer Research Dresden, Hohe Str. 6, 01069 Dresden, Germany

Introduction

Anticancer nucleoside analogues have complicated pharmacokinetics requiring facilitated transmembrane transport and intracellular conversion to triphosphate nucleotide forms, causing their susceptibility to emergence of drug resistance. We evaluated a promising strategy to improve their clinical efficacy by direct delivery of triphosphates utilizing a biocompatible glycodendrimer nanocarrier system. Here, we present results of a proof-of-concept experiments using non-covalent complexes of **maltose-modified poly(propyleneimine) dendrimer of the 4th generation (PPI-Mal OS G4)** with fludarabine (Ara-FATP) and clofarabine (CAFdATP) triphosphates. We showed that Ara-FATP has limited cytotoxic activity towards leukaemic cells relative to free nucleoside, but complexation with glycodendrimer (which does not otherwise influence cellular metabolism) drastically increases its toxicity. Moreover, we demonstrated that transport via hENT1 is a limiting step in fludarabine toxicity, while complexation with dendrimer allows Ara-FATP to enter and kill cells even in the presence of hENT1 inhibitor. Thus, the use of glycodendrimers for drug delivery would allow to circumvent naturally occurring drug resistance due to decreased transporter activity. Finally, we proved that complex formation does not change intracellular pharmacodynamics of Ara-FATP, preserving its capability to inhibit DNA and RNA synthesis and induce apoptosis via intrinsic pathway. By contrast, we showed that clofarabine, a more toxic nucleoside analogue drug, is characterized by significantly different molecular interactions with poly(propyleneimine) dendrimers than fludarabine, leading to different cellular outcomes (decreased rather than increased treatment efficiency). The most probable mechanistic explanation for uniquely dendrimer-enhanced fludarabine toxicity points to a crucial role of alternative cellular uptake pathway, avoidance of intracellular phosphorylation of nucleoside drug form, and stability of complexes.

Fludarabine triphosphate (Ara-FATP)

Clofarabine triphosphate (CAFdATP)

PPI-Mal OS G4 (approx. 30% maltose)

Non-covalent complexes (10:1 drug:dendrimer molar ratio)

enhanced cellular uptake increased cytotoxicity

decreased cytotoxicity

*Cytotoxic effect of Ara-FA, **Ara-FATP** and their complexes with PPI-Mal OS G4 dendrimer on U937 cells. Data presented as percentage of viability of control (untreated) cells, average ± S.E.M., n = 8.*

*Cytotoxic effect of Ara-FA, **Ara-FATP** and their complexes with PPI-Mal OS G4 dendrimer on U937 cells in the presence of hENT1 inhibitor NBMPR. Data presented as percentage of viability of control (untreated) cells, average ± S.E.M., n = 6.*

*DNA synthesis inhibition by Ara-FA, **Ara-FATP** and Ara-FATP-PPI-Mal OS G4 complex in U937. Representative confocal images for each treatment with Ara-FATP and Ara-FATP-PPI-Mal OS G4 complex.*

Gorzkiewicz M. et al. (2018), Biomacromolecules, 19(2):531-543

Representative snapshots of nucleotide-dendrimer (1:1 ratio) configurations.

The electrostatic map presented for nucleotide-dendrimer complexes (10:1 ratio).
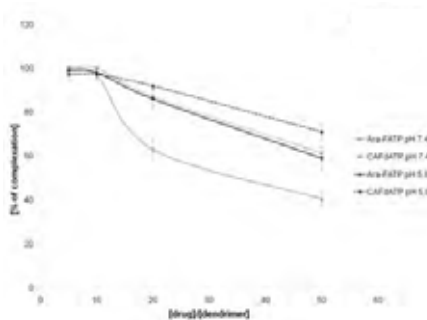
Stability of nucleotide-dendrimer complexes. Results of AF4 experiments, presented as percentage of drug complexation, average ± SD, n = 8.

Gorzkiewicz M. et al. (2019), Biomacromolecules, 20(3):1429-1442
Gorzkiewicz M. et al. (2019), Macromol. Rapid. Commun., 40(15):1900181

FACULTY OF BIOLOGY AND ENVIRONMENTAL PROTECTION
University of Lodz

Amsterdam UMC
University Medical Centers

Specific silencing of microglial gene expression in rat brain by siRNA-delivering lipid and polymer hybridized nanoparticles

Shanshan Guo[1,2#], Fernando Cázarez-Márquez[1,2#], Nikita L. Korpel[1,2], Andries Kalsbeek[1,2], Guangjun Nie[3], Chun-Xia Yi[1,2*]

1 Department of Endocrinology and Metabolism, Laboratory of Endocrinology, Amsterdam Gastroenterology and Metabolism, Amsterdam University Medical Centers (UMC), location AMC, Amsterdam, the Netherlands.
2 Netherlands Institute for Neuroscience, an Institute of the Royal Netherlands Academy of Arts and Sciences, Amsterdam, the Netherlands.
3 CAS Key Laboratory for Biomedical Effects of Nanomaterials and Nanosafety, National Center for Nanoscience and Technology, Beijing, China.

*Corresponding author: c.yi@amsterdamumc.nl

Background

Microglia are the brain innate immune cells and are essential for maintaining homeostatis in the microenvironment. Currently, a genetic tool for modifying microglial gene expression in specific brain regions is lacking. Here we introduce a novel method that uses a lipid and polymer hybridized nano-carrier (LNP) for the local delivery of siRNAs, allowing the local silencing of microglia genes in the mediobasal hypothalamus.

We firstly tested the gene silencing efficiency of the LNP-siRNA *in vitro* and *in vivo*. In the cultured BV2 microglial cells, both LNP-CD11b siRNA and LNP-TLR4 siRNA were able to efficiently silence cluster of differentiation molecule 11b (CD11b) or Toll-like receptor 4 (TLR4) protein expression. The silencing efficiency of LNP-CD11b siRNA was also demonstrated after infusion into the hypothalamus. Finally, we tested the effectiveness of LNP-TLR4 siRNA by infusing it into the MBH and challenging the animal with a lipopolysacharide (LPS) immune stimulation. Microglia in the LNP-TLR4 siRNA treated animals showed less reactivity upon LPS stimulation.

Schematic diagram
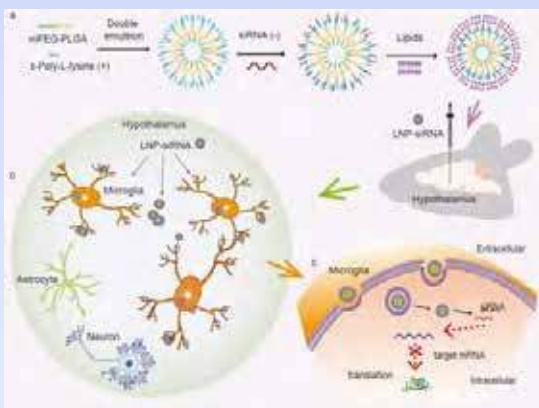
(a) LNP-siRNA preparation; (b) The LNPs are taken up by the microglia surrounding the stereotactic injection spot; (c) The processing of LNP-siRNA in the microglia and its inhibition of translation of the targeted genes in the microglia.

Specific accumulation of LNP-RhoB in microglia
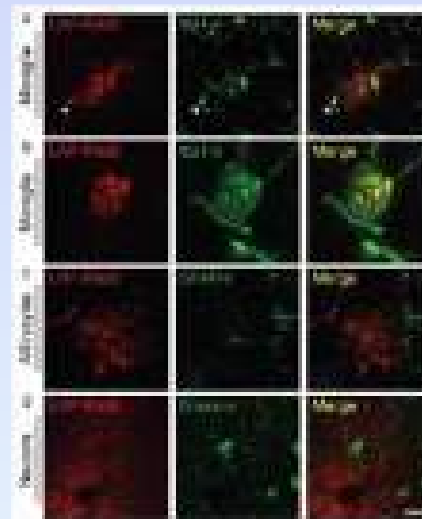
(a) LNP-RhoB (red) accumulation in iba1-ir microglial cells (green);
(b) the higher magnification of the microglial cell pointed by the arrowhead in (a);
(c) LNP-RhoB (red) was not observed in GFAP-ir astrocytes (green),
(d) LNP-RhoB (red) was not observed in orexin-ir neurons (green) in the rat hypothalamus 24 h after injection.

Silence of microglia gene by LNP-siRNA
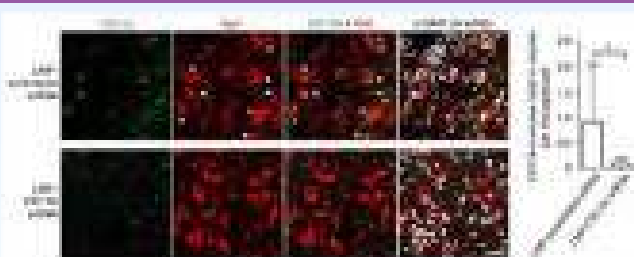
Evaluation of gene silencing efficiency of LNP-CD11b siRNA at protein expression level in the rat hypothalamus.

LNP-TLR4 siRNA reduces microglial responses to LPS
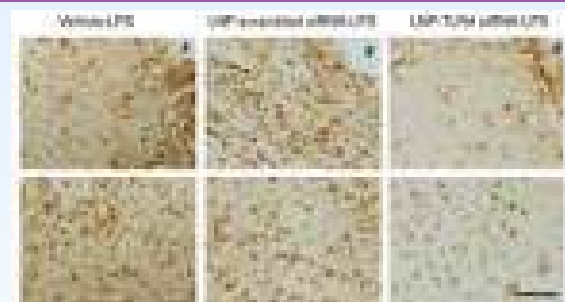
Less activated microglia (iba1-ir) in the LNP-TLR4 siRNA group in response to LPS comparing to the LNP-scrambled siRNA control group.

Conclusion

Our results suggest that LNP-siRNA is a promising tool for the spatial and temporal manipulation of microglia activity in the brain, and thereby investigate the involvement of microglia in different pathological conditions.

European Commission

Automatic tools for systematic review of the scientific literature on nanomedicines

Blanka Halamoda-Kenzaoui, Etienne Rolland, Jacopo Piovesan, Antonio Puertas Gallardo, Susanne Bremer-Hoffmann

Joint Research Centre, Directorate F - Health, Consumers and Reference Materials, Ispra (VA), Italy

Introduction

Limited regulatory experience with innovative health products and existing knowledge gaps leave open questions on what are the crucial physical, chemical and biological properties of nanomedicines needed for regulatory decision making. This uncertainty for product developer prevents the generation of high quality datasets on quality and safety of nanotechnology-based products, which would support a better definition of regulatory requirements. Scientific literature could be an additional source of information on the innovative health products such as nanomedicines. Thousands of scientific publications related to physicochemical characteristics and biological effects of nanotechnological applications are released every year. However, screening of huge amount of publications to extract necessary data is laborious and time consuming. In this study we investigated whether automatic tools are available to perform all necessary steps of a systematic review of the scientific literature.
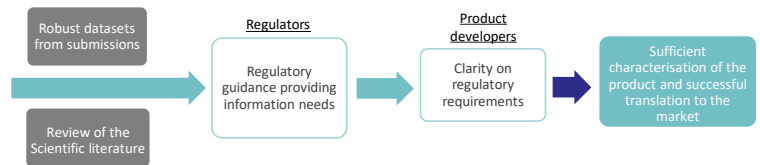
Strategy of the Scientific Literature Review on Toxicity Effects of Nanomedicines by using Automatic Tools

Identification

Targeted searches in several sources
- PubMed MeSH[1]
- Snowball approach (additional citations from reviews)[2]

1143 records

Curation

Removal of duplicates
Screening of abstracts
- Mendeley[3]
- Swift Review[4]

821 publications

Segmentation

Extraction of specific article section
- Development of a new tool[5] for article segmentation

801 full texts

Evaluation of quality

Scoring of articles based on nanomaterial characterisation
- Analysis of Materials & Methods sections

664 articles

Synthesis

Extraction of the toxicity effects
- Analysis of the Result sections based on developed ontology

494 articles

Results

QUALITY EVALUATION of scientific articles

Removed from further analysis | Selected for further analysis

36 | 130 | 222 | 182 | 77 | 18
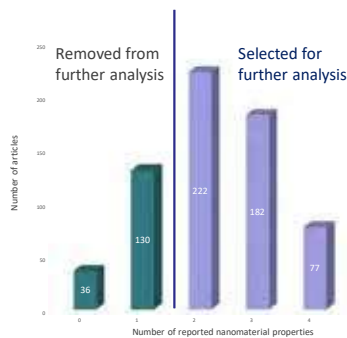
Figure 1: Evaluation of the quality of articles dependent on the reported physico-chemical characterisation of nanomaterial[6]

TOXICITY EFFECTS
Automatically extracted from result sections
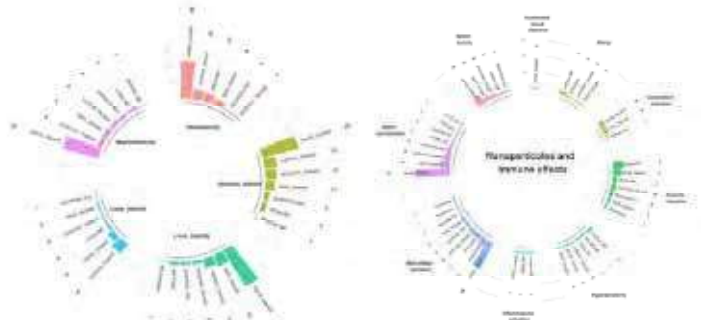
Figure 2: Main patterns of toxicity effects correlated with types of nanomaterials

Figure 3: Most reported immune reactions induced by different types of nanomaterials

References

[1] NCBI PubMed MeSH (Medical Subject Headings):
https://www.ncbi.nlm.nih.gov/mesh/
[2] EFSA (2018). Machine Learning Techniques for Literature and Systematic Reviews. Supporting publication 2018:EN-1427
[3] Mendeley Reference Manager:
https://www.mendeley.com/
[4] Sciome Workbench for Interactive computer-Facilitated Text-mining (Swift Review):
https://www.sciome.com/swift-review/
[5] Article segmentation tool (R package) in preparation
[6] Faria, M.et al (2018). Minimum information reporting in bio-nano experimental literature. *Nature Nanotechnology*, 13, 777–785

Conclusions

We **confirmed the feasibility** of performing a systematic review of the literature using automatic tools. For certain steps of the procedure, such as targeted searches, refining and deduplication, automatic tools are available. For the analysis of full texts regarding the quality evaluation and extraction of relevant information we applied **text parsing technique** based on the developed ontology. A **new tool for the article segmentation** was developed allowing an analysis of a s specific section of a document.
Further development of such tools is needed to improve their reliability and applicability and to allow the use of good quality published data for the regulatory decision-making, in particular in the area of innovative health products.

- Systematic analysis and use of published data to progress regulatory science
- Raise regulatory awareness on safety issues associated with innovative health products
- Reduce uncertainty for product developer through evidence-based guidance
- Reduce time for the translation of urgently needed innovative health products

Contact:
Blanka Halamoda-Kenzaoui
blanka.halamoda-kenzaoui@ec.europa.eu
European Commission, - Joint Research Centre
Directorate F - Consumer Products Safety Unit

The European Commission's science and knowledge service
Joint Research Centre

Joint Research Centre

Temozolomide Acid-Loaded Nanoparticles: A Protein-Based Platform for Glioma Therapy

Dina Helal[1,2], Nadia Rouatbi[1], Shunping Han[1], Mona M.A. Abdel-Mottaleb[2], Amany O. Kamel[2], Ahmed-Shawky Geneidy[2], Julie Wang[1], Gehanne A.S. Awad[2], Khuloud T. Al-Jamal[1]

[1] School of Cancer and Pharmaceutical Sciences, Faculty of Life Sciences & Medicine, King's College London, 150 Stamford Street, London SE1 9NH, United Kingdom.
[2] Department of Pharmaceutics and Industrial Pharmacy, Faculty of pharmacy, Ain Shams University, Monazzamet El Wehda El Afrikeya Street, Abbasseya, Cairo, Egypt .

Email: dina.helal@kcl.ac.uk

Introduction

• Brain cancer is one of the most leading causes of death worldwide. The brain–blood barrier (BBB) is the main challenge for chemotherapy[1]
• Temozolomide (TMZ) is the first line chemotherapy treatment for glioma. Temozolomide acid (TMZA) is a metabolite of TMZ with demonstrable anticancer activity *in vitro* and preferential aqueous solubility[2].
• Albumin NP is a versatile drug delivery system that is biocompatible, non-immunogenic & non-toxic. It can be internalized into cells through SPARC receptors, which are overexpressed in glioma[1].
• The **aim** of this study is to optimize TMZA loading in HSA NPs, study their cellular uptake, *in vitro* cytotoxicity and *in vivo* uptake into glioma-bearing mice.

Hypothesis
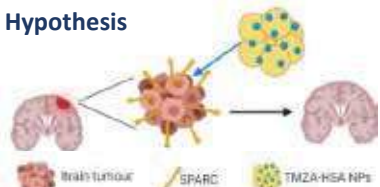
Scheme1: The loading of TMZA into HSA NPs (TMZA-HSA NPs) is hypothesized to improve the physical/biological stability of TMZA, improve its accumulation into glioma and intracellular uptake of the NP through SPARC receptors. Overall, this will result in better efficacy of glioma therapy.

Methodology

Scheme2: Fabrication of TMZA-HSA-NPs by the de-solvation method.

Results

I- Formulation optimization

TMZA was successfully loaded in HSA-NPs.
• Increasing TMZA amount significantly increased Percentage Drug Loading (DL%) and reduced Particle Size (PS).
• Increasing Na cholate concentration led to increase in PS with no significant effect on DL% **(Fig. 1A & B)**.
• The highest DL% achieved was ≈5% with particle size ≈112nm, confirmed by TEM **(Fig. 1C)**.
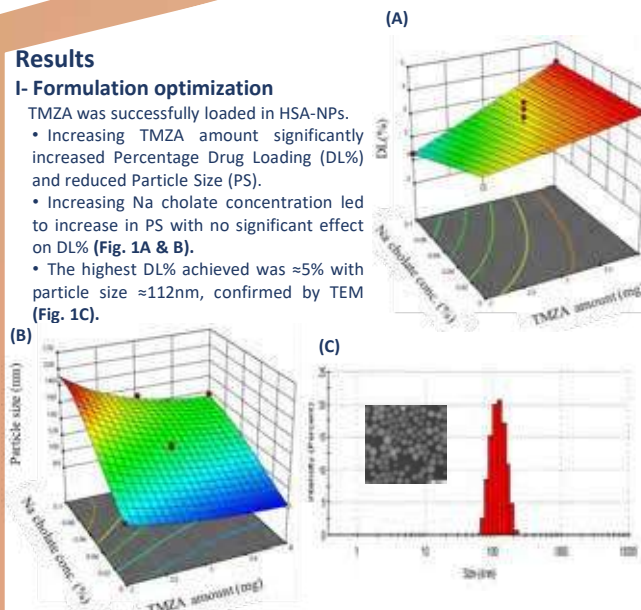
Figure 1: Design of Experiment (DoE) of TMZA-HSA-NPs formulation showing the effect of TMZA amount and Na cholate concentration on (A) DL% and (B) particle size. (C) A representative TEM image (inset) and size histogram.

II- *In vitro* studies

• Fluorescently-labelled NPs showed preferentially high internalization by BL6 (brain cancer stem cells) compared to GL261 (glioblastoma) cells **(Fig.2 A & B)**.
• The prepared NPs showed high cytotoxicity on both cell lines at 1mM drug concentration **(Fig.2 C & D)**, suggesting that the formulation process did not compromise the drug chemical stability.
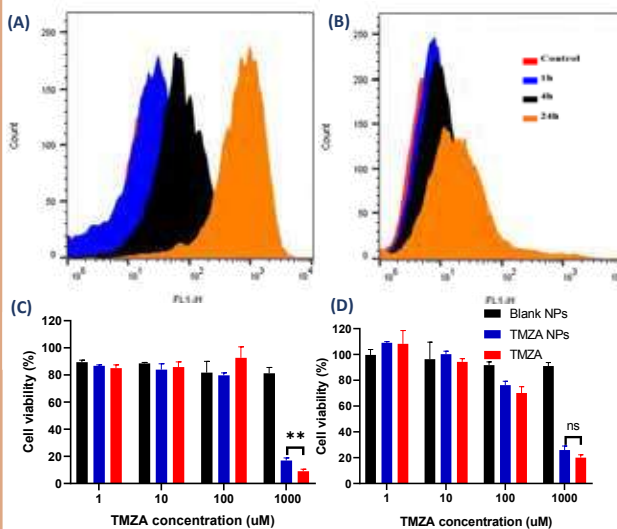
Figure 2: Cellular uptake study of HSA-NPs by BL6 (A) andGL261 cells (B). Cytotoxicity of Blank NPS, TMZA-NPs and free TMZA on BL6 (C) and GL261 cells (D) by MTT assay.

III *Ex vivo* imaging studies

Sulfo cy7.5-Labelled HSA NPs showed preferential uptake by BL6 and GL261 tumours after intravenous administration to glioma-bearing mice (Fig. 3).
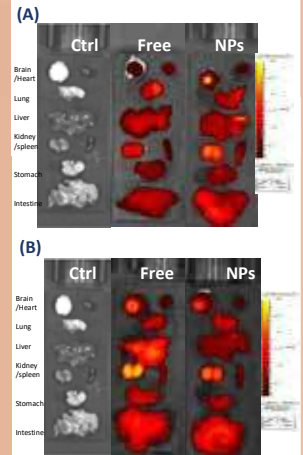
Figure 3: *Ex vivo organ* biodistribution of Cy7.5 labelled HSA NPs and the free dye control in the intra-cranially implanted (A) BL6 tumour model and (B) GL261 in mouse model.

Conclusion

• TMZA loaded HSA NPs with suitable DL% and PS were fabricated.
• The NPs could internalize in glioblastoma and brain cancer stem cell lines *in vitro*. The drug cytotoxicity was maintained upon encapsulation.
• The NPs could reach both types of tumour models after intravenous injection.
• TMZA-HSA-NPs is a promising nano-carrier platform warranting additional testing for anticancer activity *in vivo*.

References

(1) Lin, Tingting et al (2016).Blood–Brain-Barrier-Penetrating Albumin Nanoparticles for Biomimetic Drug Delivery via Albumin-Binding Protein Pathways for Antiglioma Therapy. ACS Nano 2016,10, 9999-10012

(2) Zhang, Yunhui, et al201.4 Simultaneous determination of temozolomide acid and its hexyl ester in plasma by LC-MS/MS: application to the first pharmacokinetic study of temozolomide hexyl ester in rats. Analytical Methods 6(22):8973-8978

Acknowledgment

Multicomponent Encapsulation of Adjuvants into Protein Nanocapsules by Azide-Alkyne Click Chemistry

Natkritta Hüppe[a], Jenny Schunke[b], David Paßlick[b], Keti Piradashvili[a], Frederik Wurm[a], Volker Mailänder[b], Katharina Landfester[a]

[a]Max-Planck Insitute for Polymer Research, Ackermannweg 10 55128 Mainz
[b]University Medical Center Johannes Gutenberg University Mainz, Langenbeckstraße 1, 55131

SFB 1066
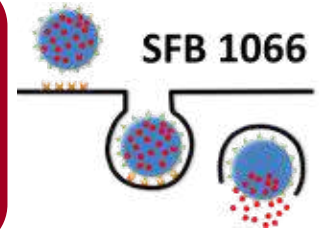
Concept

GOAL: Superadditive Stimulation of dendritic cells and enhanced T cell proliferation by **simultaneous delivery** of adjuvants through encapsulation into nanocapsules as **nanovaccines**

- **Multicomponent Encapsulation** of Adjuvants with defined concentration in inverse Miniemulsion
- Biocompatible and **Degradable Nanocapsules** from Biopolymers (Carbohydrates, Proteins)
- **Bioorthogonal Encapsulation** of therapeutic cargoes through Azid-Alkyne Click reaction

REQUIREMENTS
1) Defined concentration of Adjuvants
2) Dense Nanocarrier
3) Degradable Nanocarrier
4) Bioorthogonal Reaction
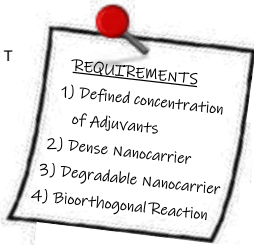
Next steps

- All-in-one nanocapsule as nanovaccine → **OVA as antigen** AND shell material
- **In vivo** studies
- **Quantification** of adjuvants encapsulated into nanocapsules
- Variation **density and degradablity** of NCs by crosslinker amount

Stimulation

- Upregulation of CD80 and CD86 by adjuvant-loaded nanocapsules
- Higher Stimulation of DCs by nanocapsules loaded with three adjuvants compared to one adjuvant
- Higher Stimulation of DCs by triple combination compared to mixture of single-loaded NC

→ **All-in-one delivery creates superadditive stimulation**

Therapeutic Cargo
Protein-repelling Coating
Targeting with Antibody
Protein-based Nanocapsules

Encapsulation

Adjuvants: Difference in chemical characteristics hamper simultaneous and efficient encapsulation
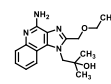
Resiquimod (R848):
- TLR 7 / TLR 8
- M = 314.38 g/mol
- DMSO as solvent
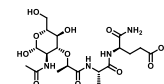
Muramyldipeptide (MDP):
- NOD 2
- M = 492.48 g/mol
- High water-solubility
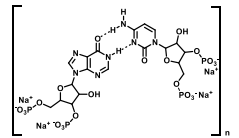
Polyinosynic:polycytidylic acid
- TLR 3
- M = 100-500 kDa
- Low water-solubility

Requirement 1: Defined Concentration of Adjuvants

Inverse water-in-oil Miniemulsion:
- Broad range of crosslinking reactions
- Multicomponent encapsulation
- Defined concentration of cargo
- High encapsulation efficiency
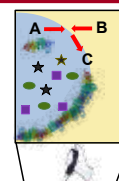
Requirement 2: Dense Carrier

Interfacial Crosslinking:
- Shell formation
- Amount of crosslinker influences density & degradability of shell

Protein Nanocapsules

Requirement 3: Degradable Carrier

Proteins as Shell Material:
- Biocompatible → Human Serum Albumin
- Biodegradable by proteases (Trypsin, Proteinase K)
- Biofunctional → Ovalbumin as model antigen or enzymes (Horse Radish Peroxidase, Glucoseoxidase, Lipases)
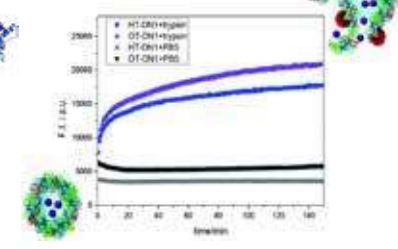
Requirement 4: Bioorthogonal Reaction
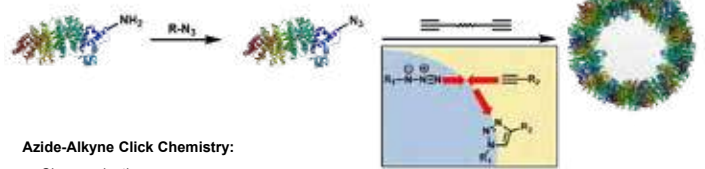
Azide-Alkyne Click Chemistry:
- Chemoselective
- No side products
- Mild reaction conditions

→ no integration of cargo in shell
→ Preserves bioactivity of cargo
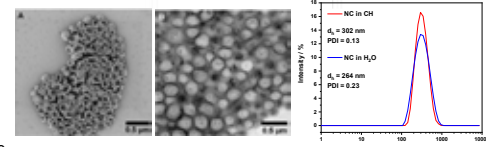
Publications
1. Paßlick, D., Piradashvili, K., Bamberger, D., Li, M., Jiang, S., Strand, D., ... & Mailänder, V. (2018). *Journal of Controlled Release*, 289, 23-34.
2. Landfester, K.; Weiss, C. K., *Modern Techniques for Nano- and Microreactors/-reactions*, 2010; pp 1-49.
3. Piradashvili, K.; Fichter, M.; Mohr, K.; Gehring, S.; Wurm, F. R.; Landfester, K., *Biomacromolecules* 2015, 16 (3), 815-821.
4. Siebert, J. M.; Baier, G.; Musyanovych, A.; Landfester, K., *Chem Commun (Camb)* 2012, 48 (44), 5470-2.

Max-Planck-Institut für Polymerforschung
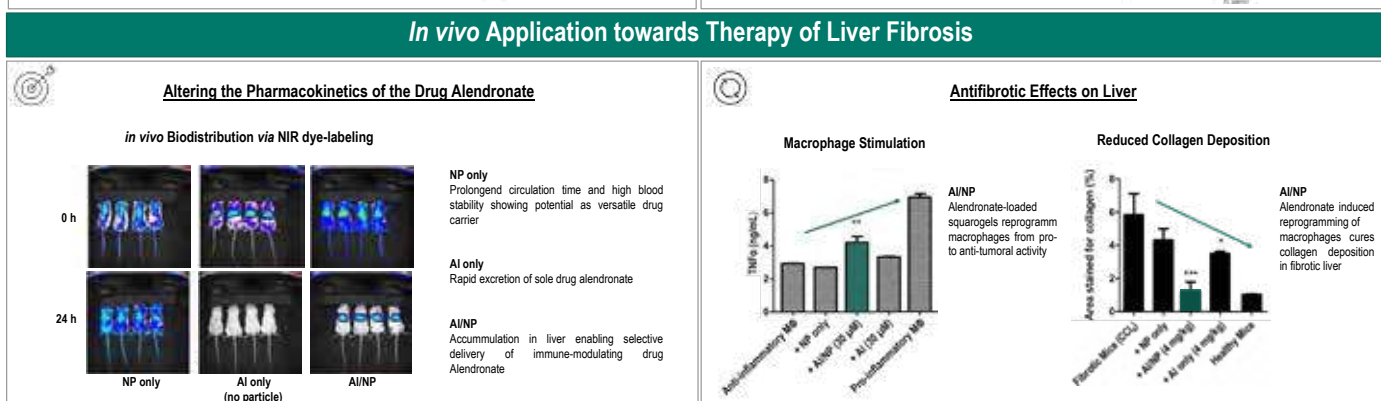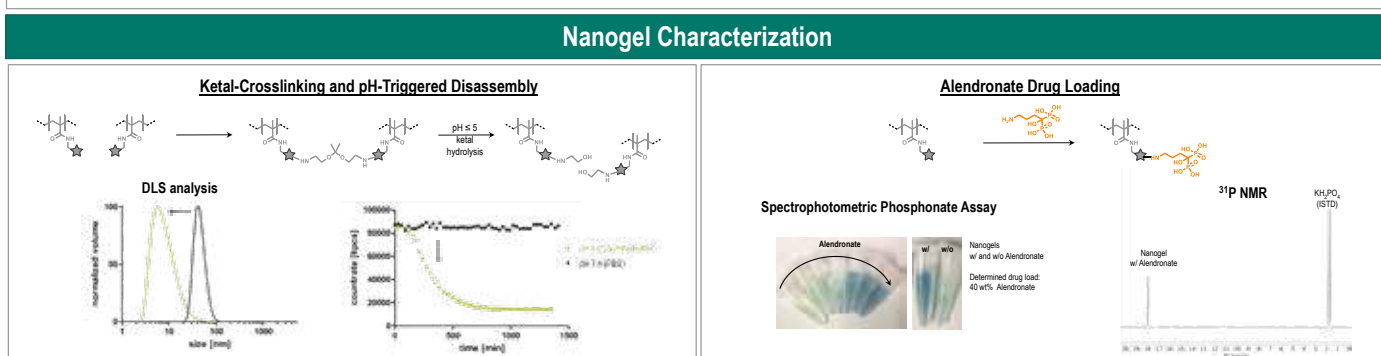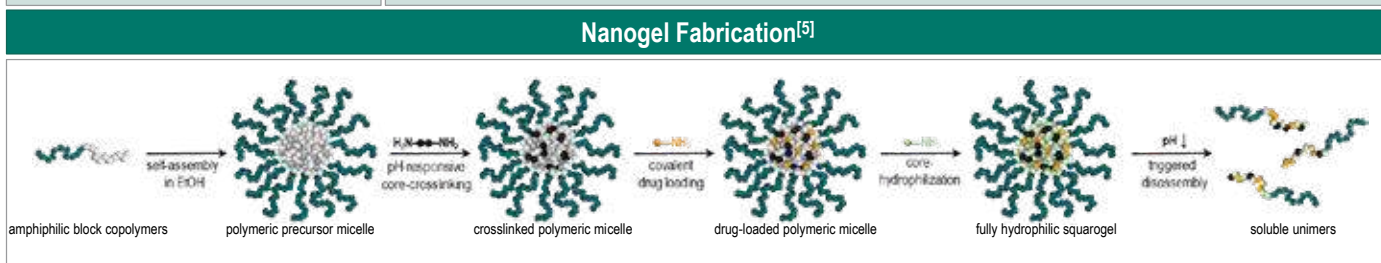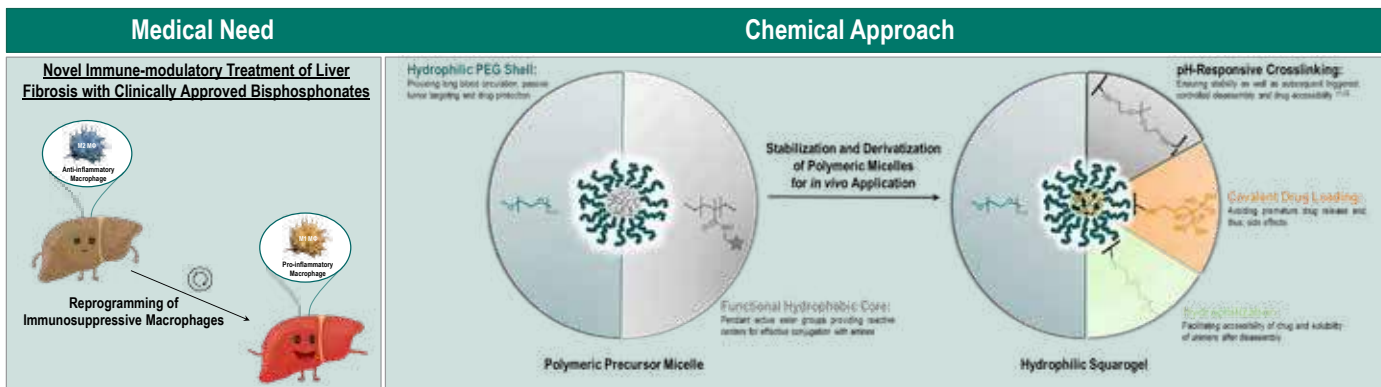Max Planck Institute for Polymer Research

UNIVERSITÄTSmedizin.

Selective Targeting and Reprogramming of Liver Macrophages by Nanoparticular Bisphosphonate

Anne Huppertsberg,[1] Alina Heck,[1] Patric Komforth,[1] Leonard Kaps,[2] Detlef Schuppan,[2] Hansjörg Schild,[2] Lutz Nuhn[1*]

1. Max Planck Institute for Polymer Research (MPIP), Ackermannweg 13, 55128 Mainz, Germany
 * lutz.nuhn@mpip-mainz.mpg.de
2. Institute for Translational Immunology, JGU University Medical Center, Langenbeckstraße 1, 55131 Mainz, Germany

Medical Need

Novel Immune-modulatory Treatment of Liver Fibrosis with Clinically Approved Bisphosphonates

Reprogramming of Immunosuppressive Macrophages

Chemical Approach

Polymeric Precursor Micelle → Stabilization and Derivatization of Polymeric Micelles for in vivo Application → Hydrophilic Squarogel

Nanogel Fabrication[5]

amphiphilic block copolymers → self-assembly in EtOH → polymeric precursor micelle → pH-responsive core-crosslinking → crosslinked polymeric micelle → covalent drug loading → drug-loaded polymeric micelle → core-hydrophilization → fully hydrophilic squarogel → pH↓ triggered disassembly → soluble unimers

Nanogel Characterization

Ketal-Crosslinking and pH-Triggered Disassembly

DLS analysis

Alendronate Drug Loading

Spectrophotometric Phosphonate Assay

^{31}P NMR

Nanogels w/ and w/o Alendronate
Determined drug load: 40 wt% Alendronate

In vivo Application towards Therapy of Liver Fibrosis

Altering the Pharmacokinetics of the Drug Alendronate

in vivo Biodistribution via NIR dye-labeling

0 h / 24 h — NP only / Al only (no particle) / Al/NP

NP only
Prolonged circulation time and high blood stability showing potential as versatile drug carrier

Al only
Rapid excretion of sole drug alendronate

Al/NP
Accumulation in liver enabling selective delivery of immune-modulating drug Alendronate

Antifibrotic Effects on Liver

Macrophage Stimulation

Al/NP
Alendronate-loaded squarogels reprogram macrophages from pro- to anti-tumoral activity

Reduced Collagen Deposition

Al/NP
Alendronate induced reprogramming of macrophages cures collagen deposition in fibrotic liver

References

[1] M. Talelli, M. Barz, C.J.F. Rijcken, F. Kiessling, W.E. Hennink, T. Lammers, *Nano Today* **2015**, 10, 93-117.
[2] L. Nuhn, S. Van Herck, A. Best, K. Deswarte, M. Kokkinopoulou, I. Lieberwirth, K. Koynov, B.N. Lambrecht, B.G. De Geest, *Angew. Chem. Int. Ed.* **2018**, 57, 10760-10764.
[3] Z. Zhang, N. Vanparijs, S. Vandewalle, F.E. Du Prez, L. Nuhn, B.G. De Geest, *Polym. Chem.* **2016**, 7, 7242-7248.
[4] H.A. Klok, F. R. Wurm, *Chem. Soc. Rev.* **2013**, 42, 8220-8236.
[5] J. Stickdorn, L. Nuhn, Eur. Polym. J. **2020**, *124*, 109481.

Development of nanoparticle-based mRNA carrier systems for transient immunomodulation of immune cells

Isabell Sofia Keil[1], Meike Schinnerer[2], Philipp Heller[2], Heinrich Haas[2], Sebastian Kreiter[1,2], Mustafa Diken[1,2], Ugur Sahin[2]

[1]TRON–Translational Oncology at the University Medical Center of the Johannes Gutenberg University Mainz, Mainz, Germany; [2]Biopharmaceutical New Technologies (BioNTech) SE, Mainz, Germany

Background & Objectives

Nanoparticle (NP) - based carrier systems are a potentially tool for non-viral gene transfer. More specifically, the targeted delivery of mRNA as a therapeutic in cancer immunotherapy is of interest, as it allows the transient expression of factors for modulation of immune cells.

The identification of NP-based mRNA carriers for targeted delivery into leukocyte subpopulations, such as **monocytes, T-, B- and NK cells** in the **human** or **murine** system is the aim of this study.
- **Evaluation of** NP-based mRNA **carriers** based on polyplexes (**PLXs**) and lipid nanoparticles (**LNPs**)
- **Identification of** antibodies and derivates as potent **ligands** for NP functionalization via electrostatic interactions or copper-free click reactions
- **Characterization of** physico-chemical compositions and functional properties of **NPs**
- **Investigation of** targeted and unspecific **transfection efficiency** of reporter protein (Thy1.1), **dose-dependency** and **viability** in human peripheral blood mononuclear cells (PBMCs), human whole blood and murine splenocytes

Targeted transfection of T cells by anti-CD3e f(ab)'2-coated nanoparticles

Human PBMCs
Human whole blood
Murine
splenocytes
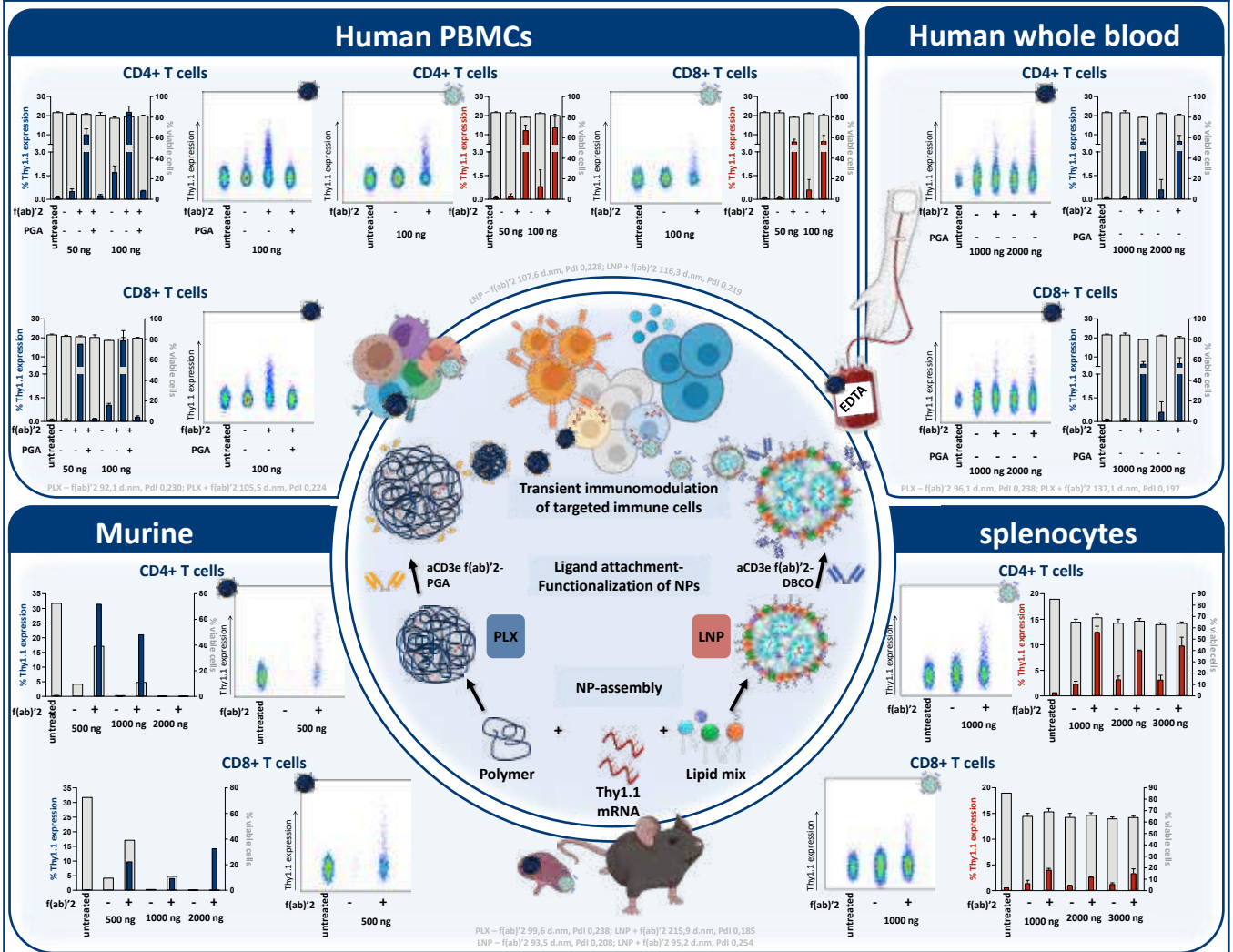
Current Results

- Transfection assays in human PBMCs, in human EDTA-coated whole blood and in murine splenocytes were successfully established
- Targeted transfection was achieved in human und murine T cells by anti-human and anti-mouse CD3e f(ab)'2-coated PLXs and LNPs
- Transfection efficiency was mRNA-dose-dependent without loss of viability
- Off-target transfection mainly in human monocytes and slightly in B cells (data not shown)

Perspectives

- As we already identified potent ligands for human and murine targets, selection of lead candidate for *in vivo* studies will be the next step
- Our currently used ligands are composed of f(ab)'2 fragments to avoid unspecific binding caused by the Fc part. Unfortunately, the main attachment strategy we are following leads to an uncontrolled orientation of f(ab)'2 to NP surface
- We therefore want to optimize the ligand-NP attachment to achieve a controlled orientation of our ligands. Hence we are focusing on a side-specific azido modification strategy[1] of whole IgG by avoiding unspecific binding due to modified Fc part and with no further need of f(ab)'2 generation [1] *Gai M. et al. (2020) Polym. Chem., 11, 527*
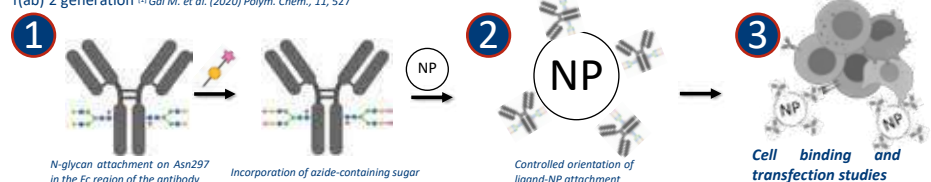
1 — N-glycan attachment on Asn297 in the Fc region of the antibody — Incorporation of azide-containing sugar

2 — Controlled orientation of ligand-NP attachment

3 — *Cell binding and transfection studies*

CLINAM
European Foundation for Clinical Nanomedicine

Automated nerve fibres identification and morphometry analysis with neural network based tool in MATLAB

Michał Kopka Medical Student [a] **Wiktor Paskal, MD, PhD** [a] **Adriana M. Paskal, MD** [a], **Piotr Pietruski, MD, PhD** [b], **Ryszard Kopka PhD** [c] **and Pawel K. Wlodarski, MD, PhD, DMD** [a]

[a] *Department of Methodology, Laboratory of Centre for Preclinical Research, Medical University of Warsaw, Warsaw, Poland*
[b] *Timeless Plastic Surgery Clinic, gen. Romana Abrahama 18/322, 03-982 Warsaw, Poland*
[c] *Department of Electrical Control and Computer Engineering Opole University of Technology, Opole, Poland*

Introduction

Preclinical research of neuroregeneration requires assessment of nerve fibers histology. The most reliable results contain histomorphometry parameters of axons and myelin sheaths. Manual methods are prone to human error and are time consuming. Computer-based techniques may improve the above and deliver the accuracy comparable with a experienced researcher. The study aimed to prepare a neural-network MATLAB script, with a novel approach to contrast-based method used for whole nerve section analysis.

Materials and methods

Semithin sections of a rat sciatic nerve stained with toluidine blue were a input data. They were scanned at 40x magnifications. Firstly, the analysis includes grey-scale conversion and contrast improving modifications e.g. CLAHE Unlike other described methods, which analyze objects after binarization, we worked with the grey-scale image. Objects found with regionprops function were then filtered. Our protocol offers manual verification and removal of false-positive objects. We also applied Neural Net Pattern Recognition from Matlab for filtering results.
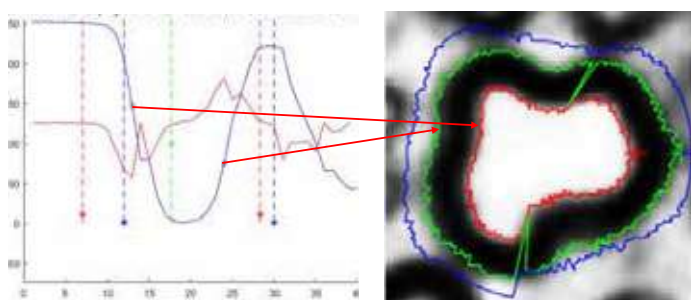
Fig. 1. Acquiring histogram from one particular line segment and setting boundaries.

Then, a rectangle enclosing each border of an object was defined. From the center to the edge of the acquired area line segment was lead and histogram on this length was set. The border of each axon was determined in the point of highest contrast between neighbour pixels. The borders of myelin sheaths were defined likewise. This operation was repeated 360 times, around the analyzed nerve cell (radial histogram scanning and thresholding). The method resembles manual analysis since local contrast is used to mark the axon. Finally, the main morphometric parameters may be determined (radius, G ration,, area etc.).

Results were compared with manual measurements of 28 random nerve images, estimated by 3 researchers in ImageJ. Comparison to manual data was shown as ratios: script: manual.

Results

After optimization of brightness and contrast parameters, axon area overlay at level 1,010 and 1,009 of the myelin sheaths was achieved. Paired T-test showed no significant differences between these two methods (p-value = 0,321).

Parameter	Manual	Script
Density	$0.0066/mm^2$	$0.0091/mm^2$
Mean axon area	$14,9\mu m^2$ SD = 15,123	$14,7\mu m^2$ SD=16,57
Mean myelin area	$42,84\mu m^2$ SD = 30,84	$42,46\mu m^2$ SD = 28,53

Tab.1 Comparision between methods.

Use of Neural Net enables to reach 93,6% of accuracy of axons recognition versus 3 researchers. A run time of the script is about 12 times shorter than the manual method.
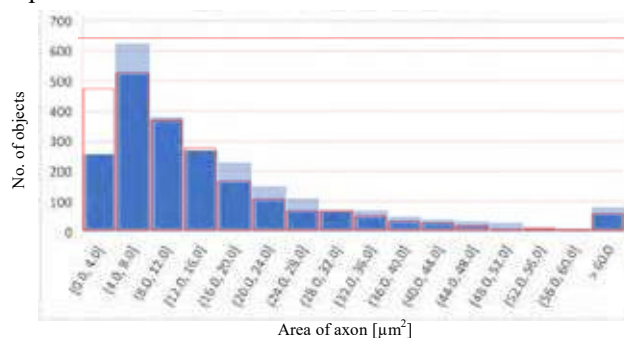
Fig. 2. Distributions of axons measurements - blue histogram—script measurements, red histogram—manual measurements.

Conclusions

The presented script performs an accurate analysis of nerve sections on a grey-scaled image. It overcomes bias of a binarization. The method decreases time of analysis and remains repeatable.

References

Moiseev, D., et al. (2018). "Morphometric analysis of peripheral myelinated nerve fibers through deep learning." J Peripher Nerv Syst. Isaacs, J., et al. (2014). "Modification of commercially available image analysis software for semi-automated qualitative analysis of axon regeneration and myelination in the rat sciatic nerve." J Neurosci Methods **233**: 45-49.
McCreedy, D. A., et al. (2016). "Semi-automated counting of axon regeneration in poly(lactide co-glycolide) spinal cord bridges." J Neurosci Methods **263**: 15-22

Corresponding author: Wiktor Paskal, E-mail: wiktor.paskal@gmail.com

DiaChemo – Development of a point-of-care device for the quantification of chemotherapeutics

C. Siebel[1], J. Boos[1], S. Krol[2] on behalf of the DiaChemo consortium

[1]Department of Paediatric Haematology and Oncology, University Children's Hospital of Muenster, Muenster, Germany
[2]Laboratory for Personalized Medicine, IRCCS Ospedale Specializzato in Gastroenterologia "Saverio de Bellis", Castellana Grotte, Italy

DiaChemo consortium: Silke Krol (coordinator) - Ospedale Specializzato in Gastroenterologia "Saverio de Bellis" (Italy), Oliver Panzer – European Research Services GmbH (Germany), René Heideman – LioniX International BV (Netherlands), Giuseppe Toffoli – National Cancer Institute Aviano (Italy), Joachim Boos – Westfälische Wilhems-Universität Münster (Germany), Francesco Stellacci – École polytechnique fédérale de Lausanne (Switzerland), Stefan Guldin – University College London (United Kingdom), Jürgen Städtler – Vermes Microdispensing GmbH (Germany)

Background

Therapeutic drug monitoring has been repeatedly proposed to individualize the administration of anticancer agents and improve cancer treatment. However, manifold challenges have to be overcome. One of these is the reliance on labour and cost intensive chromatographic techniques which require specialised laboratories and complex logistics. For some agents, such as doxorubicin, pre-analytical errors represent an additional difficulty. Pharmacokinetic analyses of anticancer agents will clearly benefit from improved analytical techniques that allow determination of drug concentrations within small sample volumes, without error-prone sample processing and within a short time frame.

Methods & Results

- selective binding of drugs by **functionalised gold nanoparticles**
- transfer of drug-bound nanoparticles into **liquid crystal phase**
- temperature-controlled **phase separation**
- **photometric** determination of drug concentration

  ➢ integration of the whole analytical process in a **microfluidic point-of-care** device

  Model substances: doxorubicin, irinotecan, methotrexate, paclitaxel

  ➢ Scalability to other drugs (platform technology)
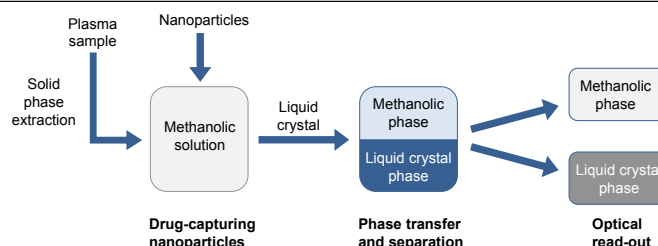
Figure 1: Basic concept of the DiaChemo microfluidic point-of-care device.

Functionalised gold nanoparticles

- Development of a modular synthetic approach and facile binding screening
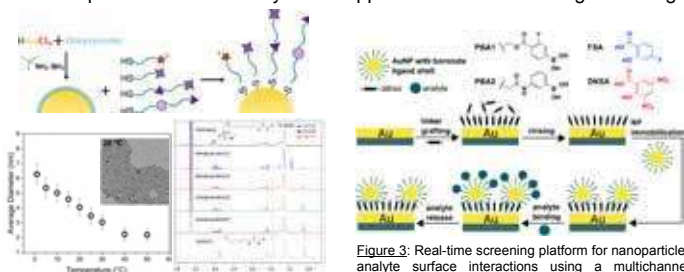
Figure 2: Two-step gold nanoparticle synthesis based on thiol-for-oleylamine ligand exchange for independent core size control and ligand shell variation.

Figure 3: Real-time screening platform for nanoparticle-analyte surface interactions using a multichannel quartz crystal microbalance with dissipation monitoring (QCM-D).

Langmuir 2018, 34, 23, 6820-6826
Nanoscale, 2019, 11, 11107-11113

Liquid crystal phase transfer and separation

Figure 5: Partitioning of model compounds. Percentage of Eosin Y (EO), Doxorubicin (DOX), Rhodamine 6G (RH), Crystal Violet (CV) and Sudan IV (SU) extracted into the 5CB and MeOH phases at $3.5°$ C, respectively.
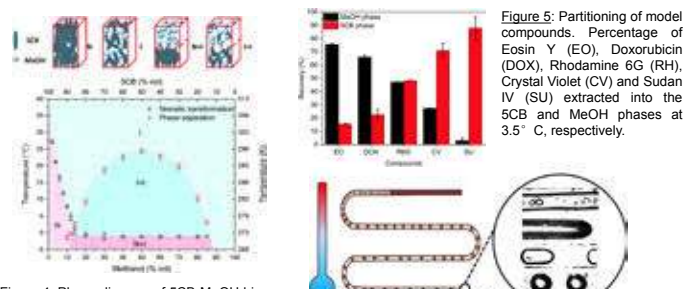
Figure 4: Phase diagram of 5CB-MeOH binary mixtures. The phase space is divided into four zones: isotropic (I), nematic (N), isotropic + isotropic (I + I) and nematic + isotropic (N + I).

Figure 6: Temperature-dependent mixing of 5CB and MeOH with fine-tuning of flow patterns.

Soft Matter, 2018, 14, 4615-4620
Mol. Syst. Des. Eng., 2020, 5, 358-365

Optofluidic detection platform

- measurement of wavelength specific absorption employing the evanescent field

- increased path length allow for higher sensitivity and lower detection limit

Figure 7: Design of the optofluidic sensor (D3). The path length within the fluidic channel can be varied by changing the number of waveguide loops.

Figure 8: Absorbance of red light ($\lambda = 638$ nm) by bromothymol blue solutions in water (20 mM NaOH) as a function of dye concentration at different path lengths.

Integration into automated microfluidic device

- fully automated analysis
- modular design
- operation via integrated touch display
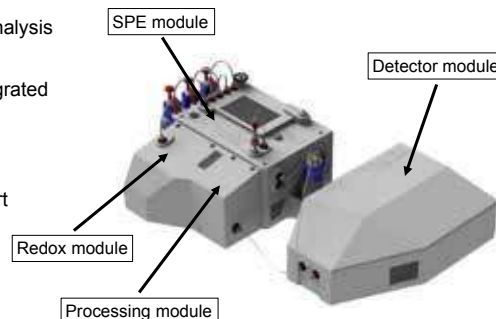- user-friendly GUI
- sample input via integrated luer port

SPE module
Detector module
Redox module
Processing module

Figure 9: Image of the device prototype.

Conclusions & Outlook

- ➢ the prototypic device will be cross-validated against established analytical methods using patient samples which reflect the spectrum of typical co-medications
- ➢ first usability tests within a clinical environment are envisaged
- ➢ availability of a robust, fast and reliable bedside analytical platform will facilitate pharmacokinetic analyses and might pave the way for future therapeutic drug monitoring approaches in oncology

Anti-tumor response and distribution of free and nanoformulated doxorubicin in four human cancer cell lines

Kullenberg, F[1]; Degerstedt, O[1]; Calitz, C[2]; Pavlovic, N[2]; Balgoma, D[3]; Gråsjö, J[1]; Sjögren E[1]; Hedeland, M[3]; Heindryckx, F[2]; Lennernäs, H[1]

(1) Department of Pharmacy, Uppsala University, Sweden (2) Department of Medical Cell Biology, Uppsala University, Sweden
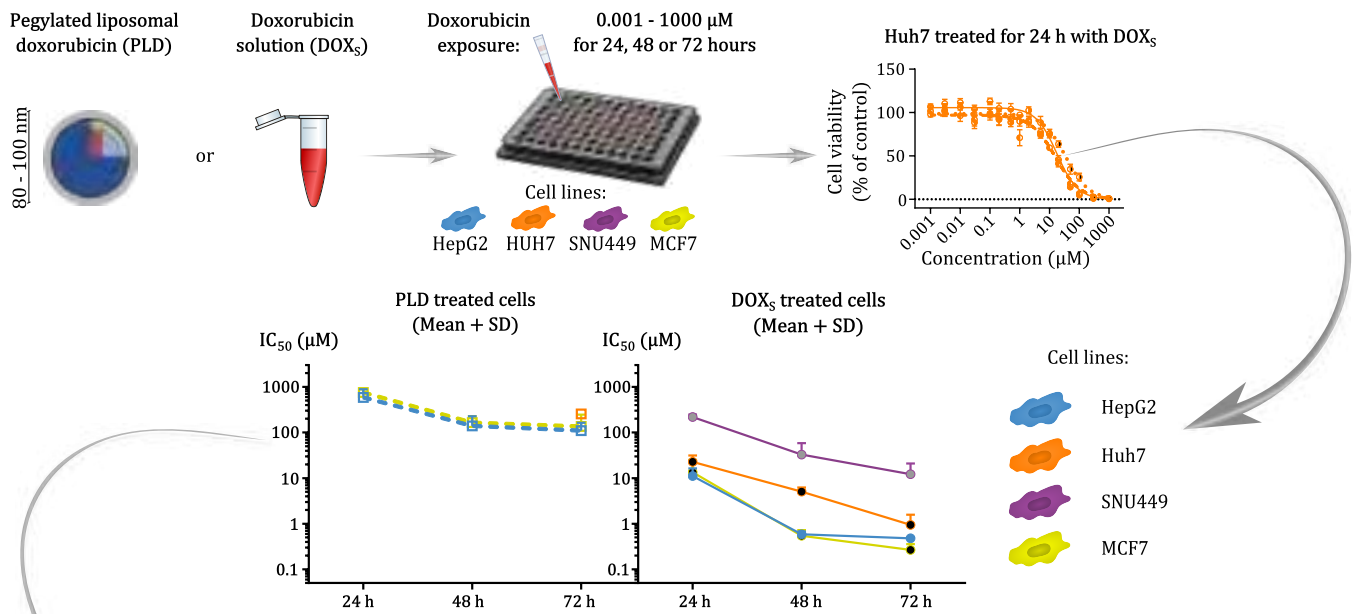(3) Department of Medicinal Chemistry, Uppsala University, Sweden

Introduction

Doxorubicin (DOX) is a well-established chemotherapeutic, but it suffers from many severe side effects. In an effort to reduce side effects and improve efficacy, the pegylated liposomal DOX (PLD) formulation Doxil (Caelyx in Europe) was developed and approved by the FDA in 1995, making it the first approved nanomedicine.[1]

A common way of testing chemotherapeutics *in vitro* is by use of cell lines.[1] To improve the understanding of cytotoxicity for PLD in this system, cell viability was compared between four different cancer cell lines after treatment with either PLD or a DOX solution (DOX$_S$) for up to three days. Three hepatocellular cancer cell lines were used: HepG2, Huh7, SNU449, as well as the breast cancer cell line MCF7. After treatment the inhibitory concentrations (IC$_{50}$), the concentration needed to kill half of the cells, at different exposure times was determined by using an AlamarBlue assay.

It is known that the mechanism of action of DOX occurs inside the cell, but as only parts of the dose given to the cells will enter it, the next question to answer was how much entered the cell and where the rest of the dose was distributed in the *in vitro* system. To find out, the cells were exposed to the concentration corresponding to their IC$_{50}$ values (up to 200 µM) for the different formulation and time points. The exposure media (EM) was then collected and the cells were washed twice with PBS (Wash). They were then trypsinized to detach them from the flasks, and this solution was centrifuged. The supernatant (SN) was collected and the pellet, after a lysis protocol, was collected and termed the intracellular (IC) portion.

These four portions were finally analyzed for both DOX and DOXol, the main metabolite of DOX, which is shown in the pie charts below as percentage of total given amount of DOX.

Methods and Results

Huh7 treated for 24 h with DOX$_S$

PLD treated cells (Mean + SD)

DOX$_S$ treated cells (Mean + SD)

Cell lines:
- HepG2
- Huh7
- SNU449
- MCF7

Cellular Distribution of DOX in Huh7

Abbreviations and collor coding:

EM DOX = Doxorubicin in Exposure Media
Wash DOX = Doxorubicin in PBS Wash
SN DOX = Doxorubicin in Supernatant
IC DOX = Doxorubicin Inside Cells
EM DOXol = Doxorubicin in Exposure Media
IC DOXol = Doxorubicinol Inside Cells
UL = Unspecified Loss of Doxorubicin
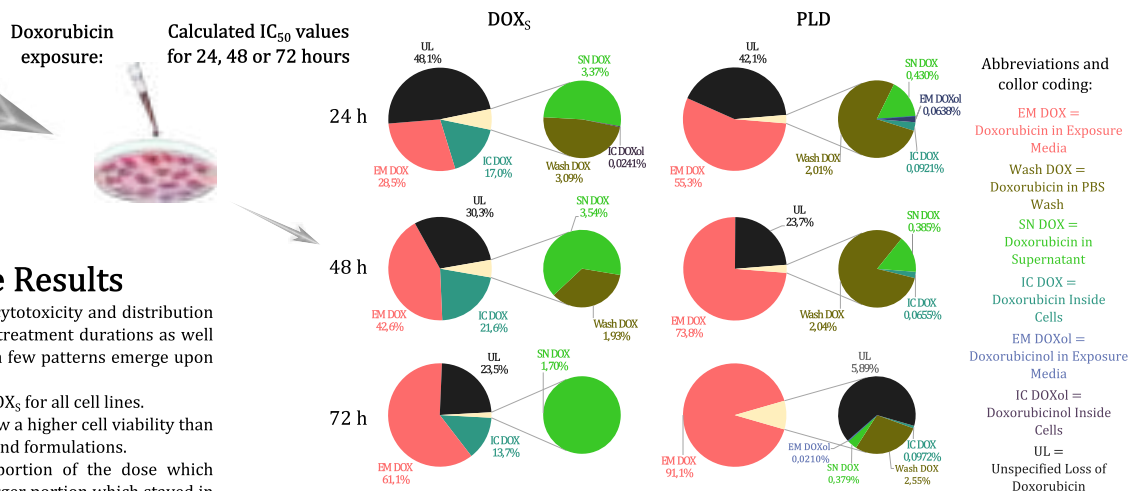
Highlights from the Results

There was a large variation in both cytotoxicity and distribution between the different formulations, treatment durations as well as the different cell lines. However, a few patterns emerge upon closer inspection:
- PLD is always less cytotoxic than DOX$_S$ for all cell lines.
- Huh7 and SNU449 consistently show a higher cell viability than HepG2 and MCF7 for all time points and formulations.
- DOX$_S$ consistently had a larger portion of the dose which entered the cells, while PLD had a larger portion which stayed in the EM for all cell lines and time points.
- For Huh7, 14-22 % of the added dose was detected inside the cell when exposed to DOX$_S$, while less than 0.1 % of the dose was detected inside when exposed to PLD.
- Contrary to what was assumed, the percentage of unspecified loss often decreased over exposure time, despite the lower dose given to the cells at longer exposure times.

Conclusions

There was a clear ranking of sensitivity to DOX between the cell lines, with SNU449 being the most resistant, followed by Huh7 and finally the two most sensitive cell lines, HepG2 and MCF7, which are also the most commonly used in the literature. This emphasizes the importance of selecting not only the most common cell lines when investigating tumor effects, as that may give skewed results. There were also interesting and unexpected effects seen in the cellular distribution, which will be further researched this autumn.

1: Kanwal, U., et. al. (2018). Advances in nano-delivery systems for doxorubicin: an updated insight. *Journal of drug targeting*

Questions or comments? Please contact me at *Fredrik.Kullenberg@farmaci.uu.se*

A novel bionanotechnology platform for the development of best-in-class enzyme therapeutics.

Emilie Laprévotte[1], Jasmina Djuric[1], Rita Correro[2], Yves Dudal[1], and Patrick Shahgaldian[3]

1. Perseo pharma AG, Muttenz, Switzerland;
2. INOFEA AG, Muttenz, Switzerland;
3. School of Life Science, University of Applied Sciences and Arts Northwestern Switzerland, Muttenz, Switzerland.

Introduction

Therapeutic enzymes are used in a wide variety of pathologies. However, existing therapeutic enzymes exhibit efficacy issues (lack of systemic stability, low residence time) and toxicity issues (up to 80% anti-drug reactions, immunogenicity). Perseo pharma has developed a proprietary **platform technology** called **enzzen®**[1,2] to shield any therapeutic enzyme of interest. The end-product is a nanomedicine designed to keep its integrity throughout its time in the body. Perseo Pharma initiated a non-clinical proof of concept with a first compound PER001 using the native form of an approved enzyme. Here, we report preclinical results for this nanomedicine and validate the enzzen® plateform for the further development of enzyme therapeutics.

enzzen® technology

Figure 1: PER001 manufacturing steps. The enzyme is immobilized on non-porous silica nanoparticles (1), then organosilanes building blocks are self-assembled at the surface of the enzyme (2) and a polycondensation reaction produces a soft layer of controlled thickness (3). Finally, a biocompatible coating is added on the nanomedicine (4).

Activity

High stabilization
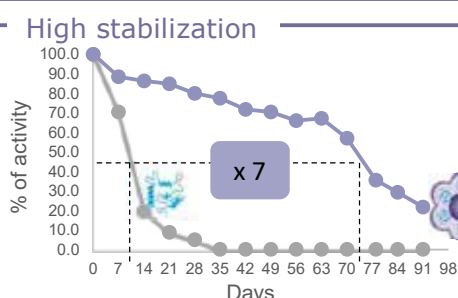
Figure 2: Sustained activity of PER001 compared to free enzyme. Enzymatic activity was measured on PER001 and compared to the equivalent amount of free enzyme over a period of 13 weeks. Data values are expressed as percentage of control at day 0.

Stable in blood
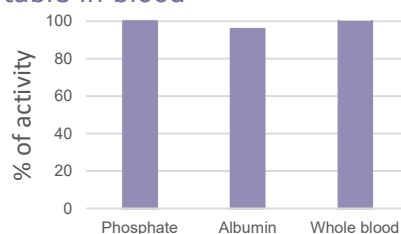
Figure 3: Sustained activity of PER001 in biological fluids. Enzymatic activity of PER001 in biological fluids was assessed and compared to its activity in phosphate buffer. Activity data values are expressed as percentage of control in phosphate buffer.

Protection

Absence of enzyme recognition
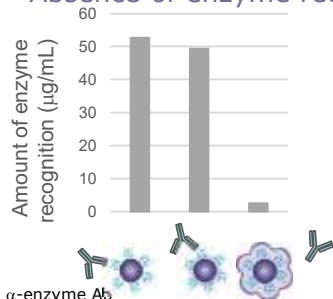
Figure 4: Lower Ab-enzyme binding on PER001. ELISA was assessed on nanomedicines at different stages of their development. ELISA data are expressed as enzyme concentration (μg/mL).

Resistance to proteolysis
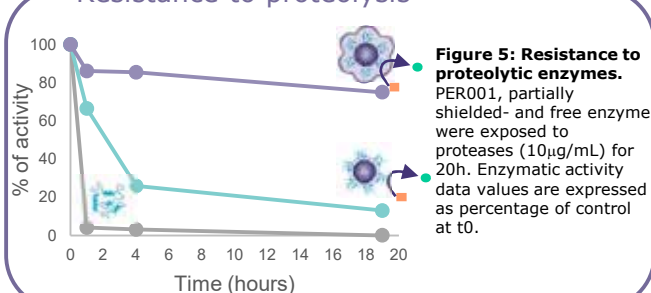
Figure 5: Resistance to proteolytic enzymes. PER001, partially shielded- and free enzyme were exposed to proteases (10μg/mL) for 20h. Enzymatic activity data values are expressed as percentage of control at t0.

Biocompatibility

No cytotoxicity
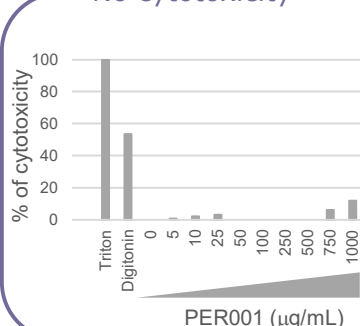
Figure 6: Cytotoxicity assessment of PER001 with LDH assay. HepG2 were exposed to increasing concentrations of enzyme-inactivated nanomedicine for 48h. Cell damages were assessed using the lactate deshydrogenase (LDH) assay. Cytotoxicity data values of PER001 are expressed as percentage of control cells treated with triton (1mg/mL).

No hemolysis
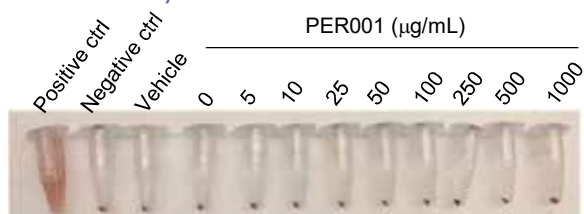
Figure 7: Hemolysis assessment of PER001. Whole blood was incubated with PER001 for 3h at 37°C, mixing the samples every 30min. Photograph shows samples after centrifugation at 800g for 15 min. Triton (10mg/mL) and PBS were used as positive and negative control, respectively.

Conclusion

Herein, we show that the enzzen® technology provides the enzyme with key features including a long-lasting stability of the biocatalytic activity, and a protection from antibody recognition as well as from external stresses. In addition, we report an unperturbed enzyme activity in biological fluids (plasma and whole blood). Moreover, the nanomedicine do not exert any toxicity, making them suitable candidates for various biological applications. Altogether, these results validate the enzzen® plateform for the further development of enzyme therapeutics by Perseo pharma.

1. Correro MR et al., Angew Chem Int Ed Engl, 2016
2. Patent WO2015/014888

European Commission

Assessing inter-individual activation of the complement system to increase the safety of liposomal formulations

Dorelia Lipsa[1], Cloé Desmet[1], Giacomo Della Camera[2], Sabrina Gioria[1], Ivana Bianchi[1], Dora Mehn[1], Otmar Geiss[1], Pascal Colpo[1], Susanne Bremer-Hoffmann[1]

[1] European Commission, Joint Research Centre (JRC), Directorate for Health, Consumers and Reference Materials, Ispra, Italy
[2] National Research Council (CNR), Institute of Biochemistry and Cell Biology (IBBC), Naples, Italy

Introduction

Policy needs

- Council of EU Health Ministers asked Commission to implement personalised medicine (Fig1) (2015: Council of EU Health Ministers)
- The implementation requires particular health products
- An adaptation of the current way of performing safety assessments might be necessary
- Human(ized) *in vitro* tests can help to identify individual risks of medicinal products (2017: EMA's Committee for Medicinal Products for Human)

Fig 1:The *right* patient with the *right drug* at the *right* dose at the *right* time."

Individual diversity of the human immune system: A challenge for nanomedicine development and regulation

Patients

Emerging health products support the implementation of personalised medicine

Drug delivery systems

Immune responses to foreign material

Biocompatibility of the foreign material

Biological drugs and smart (nano)materials are crucial for the implementation of personalised medicines but they often provoke immunological reactions which are difficult to predict in (pre)clinical studies due to

- Interspecies variations
- Inter-individual immunological responses depending on genetic factors, age, sex and environmental factors

Aim

The Complement system – A key component of the innate immune system
crucial for defense from infections and for clearance of 'non biocompatible materials'

- to investigate the **inter-individual variations of complement activation** using ex vivo test systems in contact with smart nanomaterials;
- to develop a prototype of a blood-on-a-chip that assess the immune responses using **high throughput and droplet like volume of whole blood**;
- to link immune responses with physicochemical characteristics of the smart nanomaterial.

Patient stratification

Blood sample
Liposome

Negative outcome:
Biocompatible liposomes

PIRAT blood-on-a-chip
Immunoreaction testing chamber

Positive outcome:
Immunoreaction present

New liposomal formulation needed

Methods

(1) Enzyme immunoassay (EIA) to quantify the complement fragments (e.g. iC3b, sC59b etc.)

01 Blood sampling · Donors grouped by sex and blood type
02 Phys-chem Char · LAL assay · DLS and AF4
03 Enzyme immunoassay · ELISA assay · Kinetic runs

(2) Blood-on-a-chip to assess immune reactions (e.g. L-SPR assay)

Results

Establishment of a relevant *in vitro* immunoassay for complement activation assessment

Crucial assay parameters were critically analysed:

A identification of the optimum ratio human serum and PBS;
B selection of positive controls and their concentration ranges
C assessment of the incubation times between human serum and positive controls
D evaluation and selection of the best negative controls

Systematic evaluation of the inter-individual variations of the complement system

female   male   pooled sera   female   male   pooled sera   female   male   pooled sera
Branched Polyethylenimine   Kolliphor-EL   Cobra Venom

Pooled serum (brown bar) will not correctly predict individual immune responses

Conclusions

- An *in vitro* assay based on pooled serum **will not predict correctly individual immune responses**
- **understanding the inter-variability of the immune reactions will reduce side-effects for patients** who are often in critical situations;
- **developing a predictive, quick and easy to use immunoassay** is relevant throughout the whole development pipeline of the nanoformulation.

Preclinical safety assessment
Providing information on complement activation as required for regulatory purposes

Clinical studies
Assessing individual immune responses before drug injection/application

PIRAT

Nanoformulation development
Evaluating biological effects of nanoformulations with various physicochemical properties

Post market surveillance
Assessing individual risk for personalized medicine by developing a blood-on-chip device

CONTACT:
P. Colpo
Directorate F – Health, Consumer and Reference Materials
Consumer Products Safety
Via E. Fermi, 2749. TP 125, I-21027 Ispra (VA), Italy
+39 0332 789979, Pascal.colpo@ec.europa.eu

IMPROVED INTESTINAL RESIDENCE TIME OF NANOSYSTEMS USING NOVEL CHITOSAN BIOSCAFFOLDS

A. Rosso[1], V. Andretto[1], Y. Chevalier[1], D. Kryza[1], J. Sidi-Boumedine[1], A.C. Montembault[2], L. David[2], S. Briançon[1] and G. Lollo[1]

1. CNRS, LAGEPP UMR5007, 43 bd du 11 Novembre 1918, F-69622; 2. Univ Lyon, CNRS, IMP UMR5223, 15 bd Latarjet, F-69100, UCBL1, Villeurbanne, France

Aim

The aim of this work has been to develop an innovative oral drug delivery platform based on nanocomposites. To reach this objective chitosan (CH) scaffolds loaded with nanoemulsions (NEs) have been designed to improve intestinal residence time of drugs following oral administration.

Methods

CH scaffolds loaded with NEs (CH-NE) were obtained using the freeze-casting technique [1-3] and a structural analysis using scanning electron microscopy (SEM) and optical images was performed.

To evaluate the intestinal residence time of these systems, fluorescent-labeled NEs and CH-NE were administered as physical mixture and as re-hydrated scaffold by oral gavage to healthy mice (n=15 for time point). *In vivo* fluorescence images of mice whole body were taken via a back-thinned CCD-cooled camera (ORCAIIBT-512G).
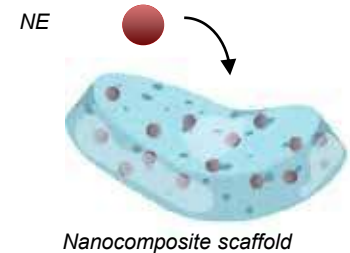
Fig. 1. Representation of CH-NEs scaffold

Results

CH scaffolds loaded with NEs (CH-NE) were successfully obtained (Figure 1 and 2-A) and using microscopy techniques (SEM and optical microscope) we were able to characterize the cell-walls structure of the system. *In vivo* fluorescence studies following oral administration demonstrated that NEs alone were rapidly cleared from the GI tract and following 6h, they were mainly located in the rectum. CH-NE physical mixture and re-hydrated scaffold were retained up to 4 h in cecum and colon and no fluorescent signal was detected in the rectum up to 6 h (Figure 2 B and C). No alteration of intestinal mucosa underlying toxicity was observed in all the cases.
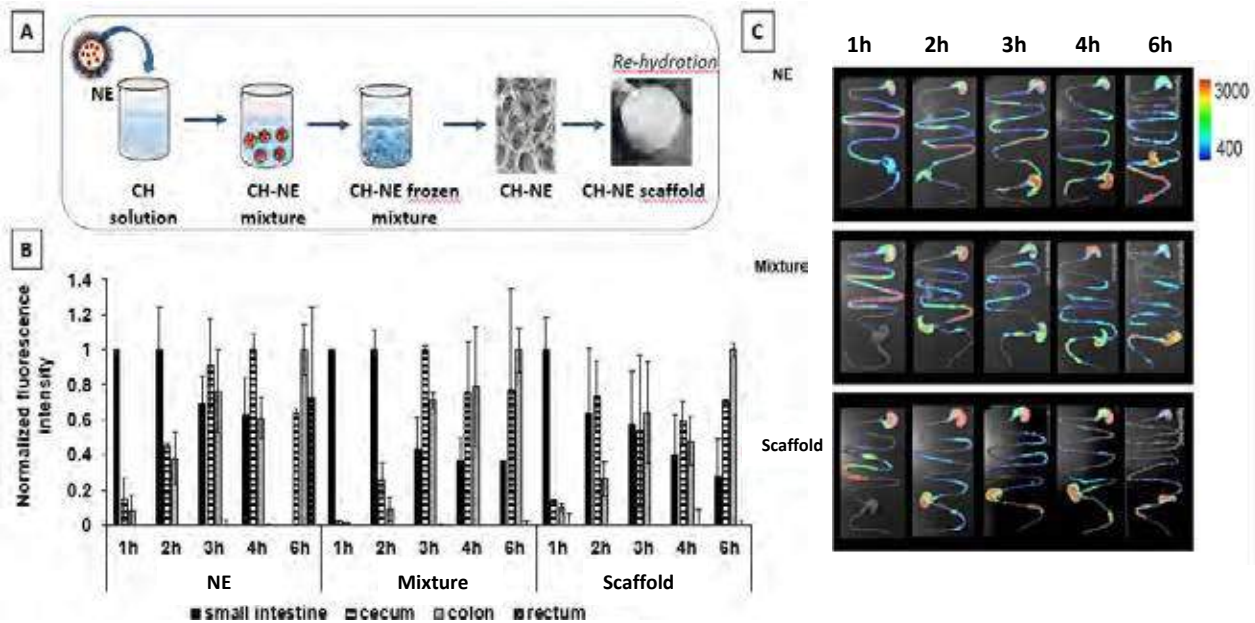
Fig. 2. A) preparation and SEM image of CH-NE scaffold B) contents of NE, NE-CH mixture, NE-CH scaffold in different parts of the intestinal tract following oral administration at time 1, 2, 3, 4 and 6 h C) ex vivo fluorescence images of intestines of mice sacrificed at 1, 2, 3, 4 and 6h after oral administration of NEs and CH-NEs mixture and scaffolds.

Conclusions

In vivo and *ex vivo* biodistribution studies showed that the nanocomposite increased the intestinal residence time of NEs. These results highlight the benefits offered by this novel platform as intestinal delivery system with a view to the local or systemic improvement in therapeutic efficacy.

References [1] A. Rosso et al., *Colloids Surfaces A Physicochem. Eng. Asp.* 2020, 593,124614; [2] T. De Witte et al., *J Biomed Mater Res.* 2020, 1–14; [3] M. Alfatama et al., *Mol. Pharm.* 2018, 15, 3369–3382.

Synthesis and characterization of citrate-stabilized gold-coated superparamagnetic iron oxide nanoparticles for biomedical applications

René Stein[1], Bernhard Friedrich[1], Marina Mühlberger[1], Nadine Cebulla[1], Eveline Schreiber[1], Rainer Tietze[1], Iwona Cicha[1], Juray Vrabel[4], Sami Haddadin[4], Christoph Alexiou[1], Silvio Dutz[2], Aldo R. Boccaccini[3], Harald Unterweger[1] and Stefan Lyer[1]

[1] Department of Otorhinolaryngology - Head and Neck Surgery, Section of Experimental Oncology and Nanomedicine (SEON), Else Kroener-Fresenius-Stiftung-Professorship, Universitätsklinikum Erlangen, Germany; [2] Institute of Biomedical Engineering and Informatics, Technische Universität Ilmenau, Ilmenau, Germany; [3] Institute of Biomaterials, University of Erlangen-Nuremberg, Erlangen, Germany; [4] Lehrstuhl für Robotik und Systemintelligenz, Munich School of Robotics and Machine Intelligence, Technische Universität München, Munich, Germany

The properties of superparamagnetic iron oxide nanoparticles (SPIONs) can be utilized for different biomedical applications. The superparamagnetic core offers opportunities as contrast agents in magnet resonance imaging (MRI), magnetic particle imaging (MPI) or ultrasound and magnetic targeting. The surface of SPIONs usually has to be surrounded by a coating to provide colloidal stability and biocompatibility in body fluids and tissue but can also be modified to bind drugs for the treatment of different diseases. The aim of the work presented here, was to add new properties to the core of SPIONs by developing bimetalic SPIONs with an iron core surrounded by a thin gold layer. This gold surface adds plasmon resonance as a property to the SPION-core, while it also serves as an anchor for covalent binding of coating molecules. In this poster we show the successful synthesis of Cit-Au-SPIONs, an initial magnetic and biocompatibility survey and a size tunability. We also show efficient binding of L-cysteine on the surface of those nanoparticles via covalent sulfide binding. Due to the bifunctional core, we believe that such particles in the future can be exploited by AI-approaches for a better medicine.

Methods

Starting from citrate-coated SPIONS, a reduction of chloroauric acid created Au-SPIONs, which again were coated with citrate to for colloidal stable Cit-Au-SPIONs. For investigating the influence on size and other properties, the synthesis parameters reaction time, temperature, citrate and gold concentration were varied. Iron and cold content was measured with atom emission spectroscopy (AES, Agilent Technologies), while ζ–potential and hydrodynamic diameter were acquired by a Zetasizer Nano (Malvern Instruments). Magnetic properties were measured using a vibrating sample magnetometer (Micromag 3900, Princeton Measurement) and magnetic susceptibility meter (MS2G, Bartington Instruments). Surface parameters were measured by fourier transform infrared spectroscopy (FTIR) (Alpha-P, Bruker) and UV-Vis spectrophotometer (Libra S22, Biochrom). Initial *in vitro* biocompatibility (apoptosis, necrosis) and cell uptake were measured with flow cytometry (Gallios, Beckmann Coulter).

Results

Basic differences between Cit-, Au-, and Cit-Au-SPIONS
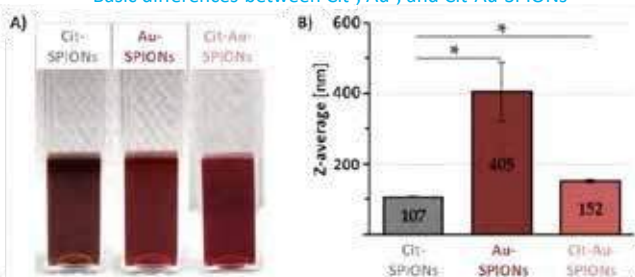
Fig. 1: (A) Color changes along the different steps of synthesis ; (B) Hydrodynamic sizes changed during the synthesis steps. Adding citrate for surface coating of Cit-Au resulted in nanoparticles with a final size of 152 nm.

Magnetic Properties
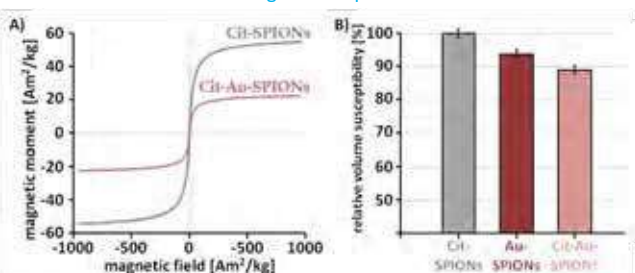
Fig. 2: Also the magnetic properties changed during the synthesis steps. (A) Cit-Au-SPIONs only had ca. 42% saturation magnetization of Cit-SPIONs, while magnetic volume susceptibility dropped only by 11%.

Influence of synthesis-parameters
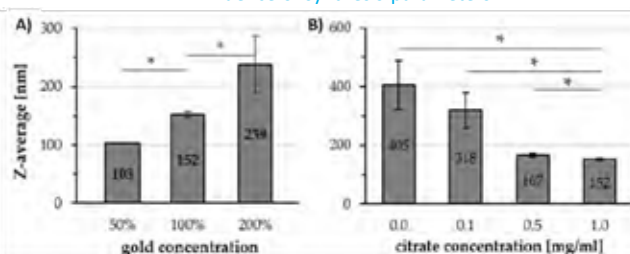
Fig. 3. Varying gold and citrate concentration had the most prominent influence on the final size of Cit-Au-SPIONs, while reaction time didn`t show major effects (not shown).

Gold-adsorption and substrate binding
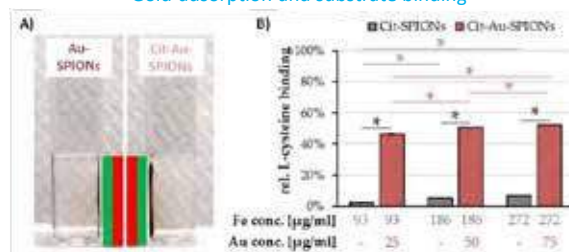
Fig. 4: (A) After exposure to a magnet, no residual single gold particles were visible. (B) Cit-Au-SPIONs revealed an efficient L-cystein-binding, while Cit-SPIONs did not.

Biocompatibility and Cell uptake
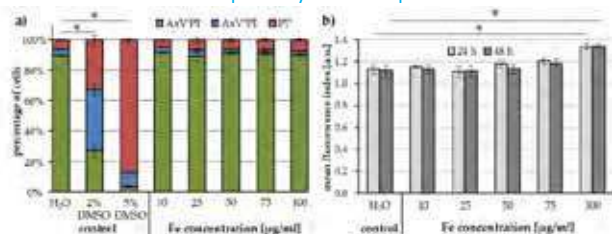
Fig. 5: (A) Up to 100 µg/ml, Cit-Au-SPIONs did not exhibit visible toxicity on Jurkat cells. (B) Zell-uptake measured with flow cytometry showed moderate uptake of Cit-Au-SPIONs in Jurkat cells, which was dependent on the particle concentration.

Conclusions

The physicochemical characterization and preliminary biocompatibility testing revealed the successful synthesis of bimetal particles with an iron core and a gold shell, that can be covalently coated via sulfide binding. Further investigations will show, if these particles proof capable of being used for imaging, drug delivery and by using AI be part of a future improved medicine.

* Contact: Section of Experimental Oncology and Nanomedicine, ENT-Department, University Hospital Erlangen, Glückstr. 10a, 91054 Erlangen, Germany, Email: rene.stein@uk-erlangen.de

Coupling ratiometric luminescence thermometry with hyperthermia for local intracellular heating as an advanced cancer hyperthermia therapy

Guillaume Maurin-Pasturel[1], Abelardo Martinez[2], Rafael Piñol[1], Rafael Cases[1], Yuanyu Gu[1], Pedro Téllez[1], Carlos D.S Brites[3], Luis D. Carlos[3], Nuno J. O. Silva[3], Ángel Millan[1]*.

[1] Instituto de ciencia de materiales de Aragón, ICMA-CSIC/University of Zaragoza, C/ Pedro Cerbuna, 10, 50006, Zaragoza (Spain).
[2] Departamento de Electónica de Potencia, I3A, Universidad de Zaragoza, 50018 Zaragoza (Spain).
[3] Departemento de Física and CICECO, Universidade de Aveiro, 3810-193 Aveiro (Portugal).
E-mail amillan@unizar.es

Introduction: Nowadays, nanoparticles for magnetic localized imaging, as iron oxide nanoparticles, appear as promising and powerful noninvasive techniques for biomedical applications, such as particularly for hyperthermia therapy of cancer. Such treatment is already approved and available in several hospitals in Europe. However, its actual performance is still far from the ideal non-invasiveness and no-secondary effects to become a primary choice for cancer therapy. Among all inconveniences, the main ones arise form the concept itself. Indeed, as the heat power of magnetic nanoheaters (MNHs is relatively low, the process required a direct and massive injection into the tumor, and the temperature control is achieved using inserted thermocouples. It is consequently not exactly non-invasive, and the elimination of such amount of nanoparticles may provoke side effects.

The current HYPTEMPCELL project proposes a much softer approach based on local intracellular heating. The idea consists in 1) to produce a magnetic heating at the intracellular level to provoke apoptosis, using less amount of MNHs and 2) control the temperature using a molecular luminescent thermometer, able to sense the temperature gradient at the vicinity of the cells with high-precision and fast response.

Objectives:
- To develop a 2D temperature imaging/magnetic induction system
- To determine the temperature gradient in MNHs internalized in cancer cells and cell heat conductivity
- To determine if local temperature gradient can provoke cell apoptosis

Hyperthermia using iron oxide NPs

AC magnetic field

Neel mechanism

Brown mechanism
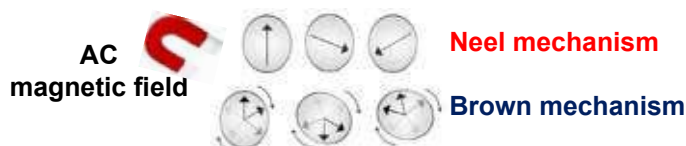
Depending of parameters such as frequency, NPs' size, type of iron oxide, concentration, medium, etc.…

ε-Fe$_2$O$_3$
19.1 ± 5.3 nm

γ-Fe$_2$O$_3$
18.3 ± 7.3 nm

100 nm   100 nm
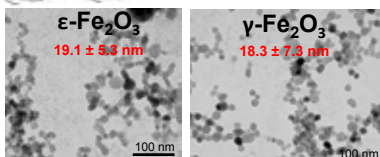
Development of an Hyperthermia equipment

Temperature control

Air cooled magnet camera

AC magnet

Water cooled sample camera

LC circuit

RF generator and Amplifier
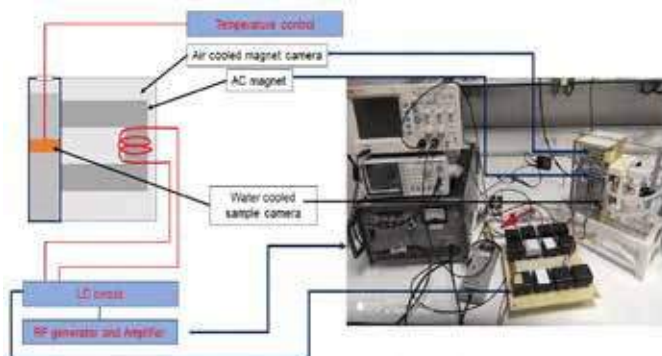
Heating of cell cultures under controled conditions

Study of the effect of the various parameters on the local hyperthermia treatment

Lanthanide luminescence thermometry

Luminescent thermometers

Peak position | Intensity | Lifetime

Lanthanide   Oxygen
Carbon   Fluor

Ratiometric thermometry
Self-referenced thermometry

Eu(L1)$_3$ (Complex 1)
Sm(L1)$_3$ (Complex 2)
L2 Ancillary Ligand (PhenA) attached to the Polymer Chain

R. Piñol and al., *ACS Nano*, **2015**, Vol. 9, NO. 3, 3134.

Microscope Images

Sm   Ro

Determination of temperature gradient and cell heat conductivity
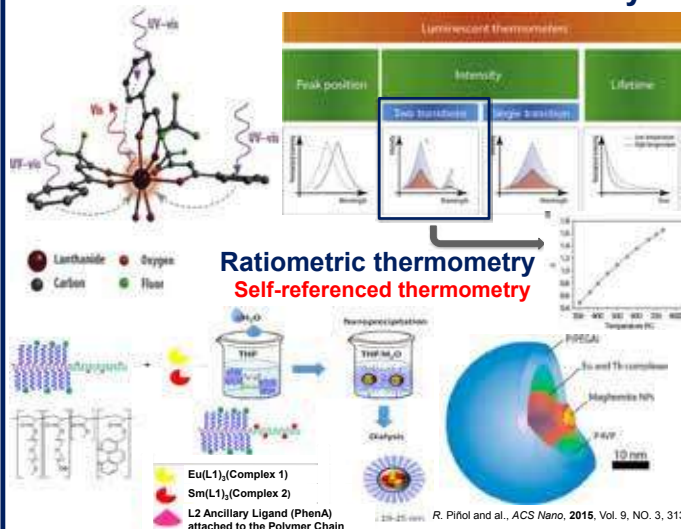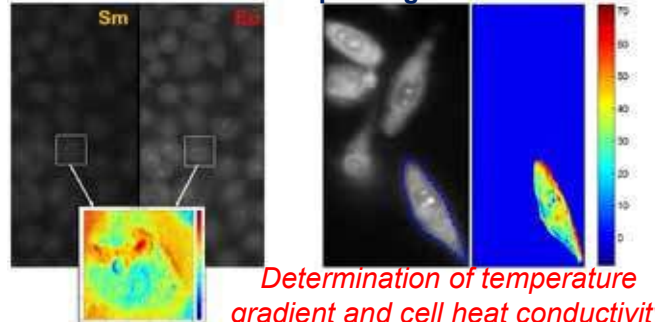
Conclusions
Study of the local hyperthermia treatment currently in progress
Study of the mechanic effect of MNHs exposed to AC magnetic field (Brown mechanism) on the cells' mortality
Improvement of the luminescent thermometer for the determination of the temperature gradient in cells

Sometimes less is more: Antibody amount determines the biodistribution and dendritic cell uptake of peptobrushes *in vivo*

Cinja Kappel,[1] Meike Schinnerer,[2] , **Carolina Medina-Montano**, [1] Irina Alberg, [2] Christian Leps, [3] Christine Seidl,[2] Gabor Kuhn,[1] Ingrid Tubbe,[1] David Paßlick,[1] Dominika Hobernik,[1] Rebekka Bent, [1] Katharina Haas, [1] Evelyn Montermann,[1] Kerstin Walzer, [5] Mustafa Diken, [5,7] Manfred Schmidt, [4] Volker Mailänder, [1,6] Rudolf Zentel, [2] Stefan Tenzer,[3] Matthias Barz, [2] Matthias Bros,[1] Stephan Grabbe[1]

1. Department of Dermatology, UMC of the JGU Mainz, Germany. 2. Institute for Organic Chemistry, JGU, Mainz, Germany. 3. Institute for Immunology, UMC of the JGU Mainz, Germany. 4. Institute for Physical Chemistry, JGU, Mainz, Germany. 5. TRON–Translational Oncology at the UMC of the JGU, Mainz, Germany. 6. Max Planck Institute for Polymer Research, Mainz, Germany. 7. Biontech AG, Mainz, Germany

Introduction

Despite considerable progress in the design of multi-functionalized nanoparticles (NP) to deliver drugs in a cell type-focused manner, their systemic application still often results in unwanted liver accumulation. The exact mechanisms contributing to this general observation have not been fully elucidated yet.

Here we asked for the role of cell targeting antibody density per NP as a determinant of NP liver accumulation. We used sarcosine-based peptobrushes (PB) which in an unconjugated form remain in the circulation for a long time (>24h) due to low unspecific cell binding. PB were labeled with a near infrared dye, and were conjugated with average numbers (2, 6 and 12) of antibodies specific for the dendritic cell (DC) selective surface receptor DEC205. We assessed the time-dependent biodistribution of PB-antibody conjugates by *in vivo* imaging and flow cytometry.

Results

Synthesis and characterization of PB-antibody conjugates

PB bind DCs when conjugated with aDEC205-Ab

Binding of aDEC205-NP in BMDCs
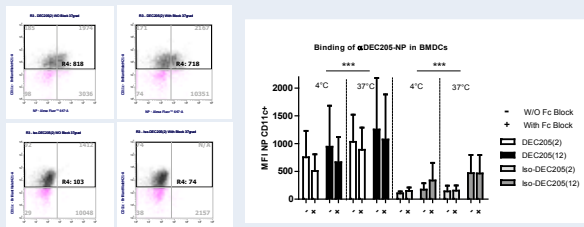
Quantification of PB-aDEC205(12) internalization by DCs

FACS Measure

Fluorometer Measure

~50.000 PB/DC
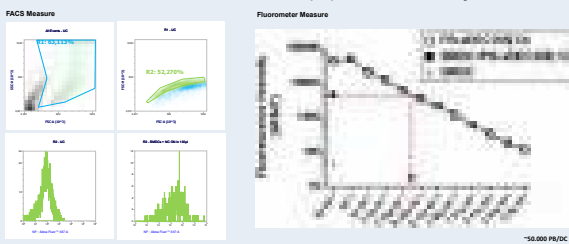
Results

The antibody number of PB correlates with their accumulation in the liver, and inversely correlates with their blood circulation time

Blood

Biodistribution

LSEC internalize PB-aDEC205(12)
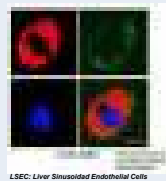
LSEC: Liver Sinusoidal Endothelial Cells

Blockade of FcγII receptors reduces accumulation of PB-antibody conjugates in the liver
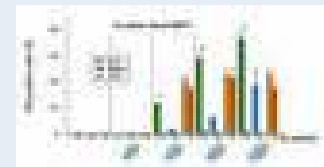
in vivo imaging

ex vivo imaging

Ganesan, L., 2012

Blocking FcγII receptors reduces binding to LSECs
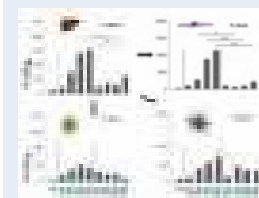
Efficacy of DC targeting inversely correlates with PB-antibody numbers
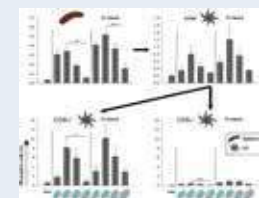
Discussion

We observed that PB-antibody conjugates were trapped in the liver. The extent of liver accumulation of PB-antibody conjugates correlated with the number of attached antibodies. In addition, liver endothelial cells via their Fc receptors are mostly responsible for retaining aDEC205 coated PB.

Accordingly, PB-antibody conjugates with an average of only two antibodies per PB showed lowest liver entrapment, and engaged DC in spleen and lymph nodes at highest extent. Altogether, our study underlines that liver endothelial cells play a yet scarcely acknowledged role in liver entrapment of antibody-coated PB, and that low antibody numbers on synthetic PB are both necessary to minimize liver accumulation and sufficient for specific cell targeting in other organs *in vivo*.

Conclusion and Summary

We generated sarcosine-based PB with defined average antibody numbers reaching from a "low" amount (2 molecules), over "intermediate" amount (6 molecules) to a high amount (12 molecules). These conjugates were similar in size and free of unbound antibodies. We were able to show that two antibodies are sufficient to reach an acceptable percentage of target cells (CD8a+DC) in lymphoid organs while bypassing the liver. PBs decorated with more than two antibodies accumulate rapidly in the liver. We demonstrate that liver accumulation of antibody-coated PB is largely due to binding of the Fc part of PB conjugated surface antibodies to FcR expressed by LSEC. Most importantly, capture of antibody-coated PB by LSEC can be greatly reduced if antibody numbers per PB are kept low, thus preventing liver accumulation while retaining effective target-specific binding in secondary lymphatic organs. Since LSEC are potent inducers of antigen-specific tolerance, nano-vaccines intended to induce immunity should minimize uptake by LSEC and other FcR-expressing cells in order to prevent tolerance induction.

Contact: gmedinam@students.uni-mainz.de

References

1. Shen, L.; Tenzer, S.; Storck, W.; Hobernik, D.; Raker, V. K.; Fischer, E.; Decker, S.; Dzionek, A.; Krauthauser, S.; Diken, M.; Nikolaev, A.; Maxeiner, J.; Schuster, P.; Kappel, C.; Verschoor, A.; Schild, H.; Grabbe, S.; Bros, M., Protein corona-mediated targeting of nanocarriers to B cells allows redirection of allergic immune responses. The Journal of allergy and clinical immunology 2018, 142 (5), 1558-1570.

2. Bros, M.; Nuhn, L.; Simon, J.; Moll, L.; Mailander, V.; Landfester, K.; Grabbe, S., The Protein Corona as a Confounding Variable of Nanoparticle-Mediated Targeted Vaccine Delivery. Frontiers in immunology 2018, 9, 1760.

3. Mohr, N.; Kappel, C.; Kramer, S.; Bros, M.; Grabbe, S.; Zentel, R., Targeting cells of the immune system: mannosylated HPMA-LMA block-copolymer micelles for targeting of dendritic cells. Nanomedicine (London, England) 2016, 11 (20), 2679-2697.

4. Shen, L.; Krauthauser, S.; Fischer, K.; Hobernik, D.; Abassi, Y.; Dzionek, A.; Nikolaev, A.; Voltz, N.; Diken, M.; Krummen, M.; Montermann, E.; Tubbe, I.; Lorenz, S.; Strand, D.; Schild, H.; Grabbe, S.; Bros, M., Vaccination with trifunctional nanoparticles that address CD8(+) dendritic cells inhibits growth of established melanoma. Nanomedicine (London, England) 2016, 11 (20), 2647-2662

5. Ganesan, L. P.; Kim, J.; Wu, Y.; Mohanty, S.; Phillips, G. S.; Birmingham, D. J.; Robinson, J. M.; Anderson, C. L., FcgammaRIIb on liver sinusoidal endothelium clears small immune complexes. Journal of immunology 2012, 189 (10), 4981-8.

Multi-Detector Field-Flow Fractionation for the Characterization of Liposomal Drug Formulations

Florian Meier, Roland Drexel, Evelin Moldenhauer, Robert B. Reed, Soheyl Tadjiki, Thorsten Klein

POSTNOVA

Introduction

Field-Flow Fractionation (FFF) belongs to the flow-based separation techniques, where separation of dissolved, suspended or dispersed sample constituents in the size range of 1 nm to 50 µm is achieved within a thin, ribbon-like channel without a stationary phase [1]. Based on the applied force field, a variety of FFF subtechniques have been commercialized such as Asymmetrical Flow FFF, Thermal FFF, Centrifugal FFF and, very recently, Electrical Asymmetrical Flow FFF. In recent years, FFF has gained increasing popularity as a powerful analytical tool in the field of nano- and biomedicine [2] including, for example, the characterization of liposomes [3,4].

In a first study, we present the application of Electrical Asymmetrical FFF for the determination of the size distribution as well the as Zeta potential of Liposomal Doxorubicin HCl under physiological conditions.

In a second study, Centrifugal FFF was used for the quantification of free drug content in a liposomal drug formulation.

Electrical Asymmetrical Flow FFF - EAF4

- Simultaneous flow and electrical field as separation force
- Separation based on hydrodynamic size and surface charge
- Access to size distribution and electrophoretic mobility / Zeta potential of sample constituents

Fig. 2: Postnova EAF2000

Fig. 1: Separation principle of EAF4.

Centrifugal FFF - CF3

- Centrifugal field as separation force
- Separation based on buoyant mass
- Access to size distribution and mass / density of sample constituents

Fig. 4: Postnova CF2000
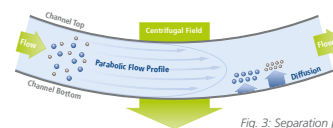
Fig. 3: Separation principle of CF3.

Analysis of Liposomal Doxorubicin HCl using EAF4

Sample
- Liposomal Doxorubicin HCl
  - 2 mg mL^{-1}
  - Sample diluted 1:8 in EAF4 eluent

Separation
- EAF4 coupled to UV-, MALS- and DLS detectors (EAF4-UV-MALS-DLS)
- Applied separation fields
  - Cross flow field: 0.90 mL min^{-1} to 0 mL min^{-1} via power, constant and linear decay
  - Electrical field: 0-4 mA, positive top plate
- Eluent: 10 mM phosphate buffer (pH = 6.9)

Results
- Diameter of gyration D_g (MALS): 32-58 nm
- Hydrodynamic diameter D_h (DLS): 56-125 nm
- Electrophoretic mobility: -1.88 µm cm V^{-1} s^{-1} ± 0.18 µm cm V^{-1} s^{-1}
- Zeta potential: -24 mV ± 2 mV (Smoluchowski approximation)

Fig. 5: EAF4-UV-MALS-DLS fractogram of the Liposomal Doxorubicin HCl sample.
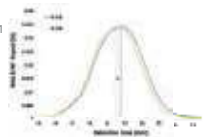
Fig. 6: Observed shifts in retention times in presence and in absence of an electrical field.

Fig. 7: Diagram of total drift velocity over applied electrical field in order to derive the electrophoretic mobility and eventually the Zeta potential of the sample.
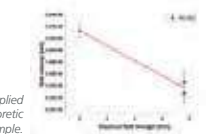
Quantification of free drug content using CF3

Sample
- Liposomal drug product containing
  - Free drug crystals (black specks)
  - Empty liposomes (bubbles)
  - Encapsulated liposomes
- 25 µm average particle size

Separation
- CF3 coupled to UV-detector (CF3-UV)
- Constant centrifugal field at 400 rpm
- Eluent: 1% Dextran (40 kDa) + 0.9% NaCl
- Fraction collection every 15 s

Results
- Clear separation of two populations
  - Peak 1 free drug
  - Peak 2: encapsulated drug and empty liposomes
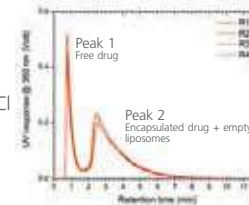- Amount of free drug calculated at 29.0% ± 1.6% of total UV-peak area
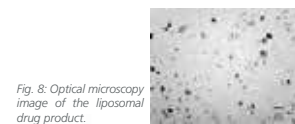
Fig. 8: Optical microscopy image of the liposomal drug product.

Peak 1 Free drug

Peak 2 Encapsulated drug + empty liposomes

Fig. 9: CF3-UV fractograms of the liposomal drug product (n = 4).

Peak 1   Peak 2

Fig. 10: Optical microscopy images of CF3 fractions collected from peak 1 (only free drug) and peak 2 (encapsulated drug and empty liposomes).

Conclusions

Both presented studies clearly highlight the capabilities of multi-detector FFF-techniques for the comprehensive physico-chemical characterization of liposomal drug formulations as they give valuable insights into crucial sample properties such as size distribution, Zeta potential and drug loading efficiency. This not only allows for a better understanding of the behavior of such promising drug delivery systems especially under physiological conditions, but can furthermore facilitate more rational synthesis approaches toward tailor-made liposomal formulations for particular biomedical applications.

References

[1] C.J. Giddings, *Science*, **1993**, 260(5113), 1456-1465.
[2] X. Zhang, Y. Li, et al., *TrAC Trends in Analytical Chemistry*, **2018**, 108, 231-238.
[3] S. Holzschuh, K. Kaeß et al., *Pharmaceutical Research*, **2016**, 33(4), 842-855.
[4] L.O.F. Monteiro, A. Malachias et al., *Langmuir*, **2018**, 34(20), 5728-5737.

Acknowledgements

contactpointnano.ch

Ana Milosevic[1], Christine D'Anna-Huber[2], Sergio Bellucci[3], Peter Wick[1]

[1] Empa, Swiss Laboratories for Material Science and Technology, Laboratory for Particles Biology Interactions, Lerchenfeldstrasse 5, St. Gallen
[2] cdh texte & kommunikation, Alter Markt 2, 3400 Burgdorf
[3] Bellucci Innovation Consulting, In der Looren 58, Zurich

| Email: contactpointnano@empa.ch |

Our mission

The independent, national contact point combines the scientific and regulatory expertise available in Switzerland on the safe handling of synthetic nanomaterials – from production and application to disposal – and conveys high-quality information to companies (established companies, SMEs and start-ups) in an efficient way. The aim is to accelerate the transfer from invention to innovation, so that Swiss companies remain competitive in the international environment. The contactpointnano.ch relies on a broad network of proven experts and is thus able to ensure a qualified and independent transfer of knowledge. It anticipates topics for regular workshops, organizes trainings and events for the exchange of information and experience in the area of nano-innovation, nano-safety as well as updates on the evolution of Swiss and international regulation requirements etc.

Challenges in nano-science translation activities

- Uncertainty about regulatory procedures
- Lack in overall standardized and generally accepted regulatory strategies
- Uncertainty about the involved cost and time
- Uncertainty on the return on investment

Collect ➡ Triage ➡ Connect
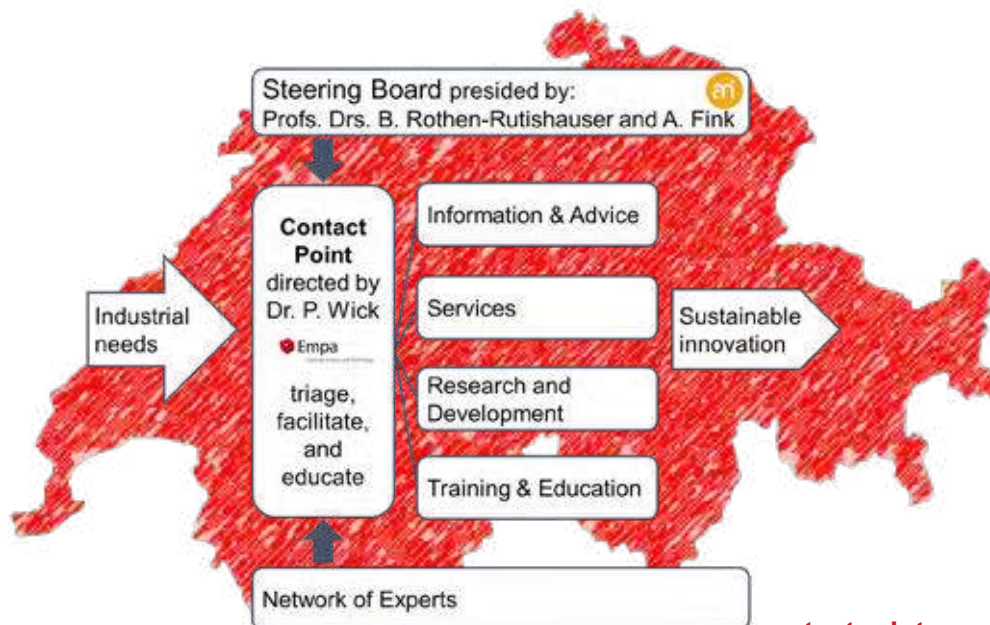
Impact

- **contactpointnano.ch** performs a central key function not carried out by any other institution in Switzerland.
- It transfers knowledge and expertise from cutting-edge research to the economy, thus promoting innovation and boosting Switzerland's competitiveness.
- It encourages novel nanomaterial applications which are safe for human health and for the environment.

contactpointnano.ch has been given its mandate by:

In vivo assessment of the Metal-Organic Framework Formulation Sil@nanoMIL-89 in a Monocrotaline Model of Pulmonary Arterial Hypertension.

Nura A. Mohamed[a,c] , Yu Kameno[b] , Ali Ashek[d] , Gilberto de Nucci[e,f] , Nicholas S.Kirkby[c] , Robert P. Davies[b] , Paul D. Lickiss[b], Haissam Abou Saleh[a], Lan Zhao[d] and Jane A. Mitchell[c]

[a]Department of Biological and Environmental Sciences, College of Arts and Sciences,Qatar University, Doha, Qatar.
[b]Department of Chemistry, White City Campus, Imperial College, London, UK.
[c]Department of Cardiothoracic Pharmacology, National Heart and Lung Institute, Imperial College, London, UK.
[d]Department of Medicine, Imperial College London, London, United Kingdom.
[e]Department of Pharmacology, Faculty of Medical Sciences, State University of Campinas (UNICAMP), Campinas, SP, Brazil.
[f]Department of Pharmacology, Institute of Biomedical Sciences, University of São Paulo, São Paulo, SP, Brazil.

Introduction

Nanomedicine is an attractive, promising and fast growing field that uses nanoparticles to serve as drug carriers for targeted drug delivery. We are working on the idea that targeted drug delivery could be therapeutically useful in the treatment of pulmonary arterial hypertension (PAH) and have focused on the highly porous, imageable iron-based metal-organic framework (MOF); nanoMIL-89 as a platform. PAH is an aggressive and incurable disease with high morbidity/mortality rates. Currently available PAH drugs work by either promoting vasodilation or inhibiting vasoconstriction however, they are limited by the systemic side-effects[1]. We have prepared nanoMIL-89 and found it to be relatively non-toxic when tested in cells in vitro and in control rats in vivo[2]. In this study we charged the nanoMIL-89 with the PAH drug sildenafil to produce Sil@nanoMIL-89 and test its effect on the monocrotaline PAH rat model.

Aims:
- To load sildenafil into the nanoMIL-89 creating Sil@nanoMIL-89.
- To determine Sil@nanoMIL-89 in vivo effects.

Methods

A-Loading nanoMIL-89 with sildenafil

Incubated at RT for 16-18 hours

5ml of 1000µg/ml Sildenafil in PBS

- Centrifuge at 12000rpm.
- Remove the supernatant.
- Re-suspend the pellet in 5ml PBS to be used for the in vivo experiments.

200mg of the nanoMIL-89 is added to the sildenafil solution
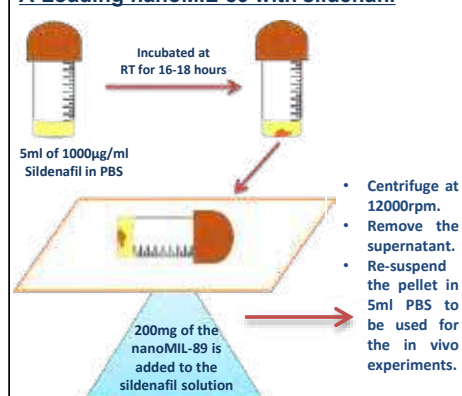
Figure 1. (A) Preparation of Sil@nanoMIL-89.

B- in vivo Effect of Sil@nanoMIL-89

After injections these tissues are collected

MCT Rats

Intravenous injection of nanoMIL-89 (50mg/kg) or sil@nanoMIL-89 (50mg/kg) twice a week for two weeks

- Sildenafil plasma level is measured by ELISA.
- ET-1 plasma level is measured by ELISA.
- Histological studies for iron measurements is done using Perls Stain.
- Iron measurement is done following previously described procedures.
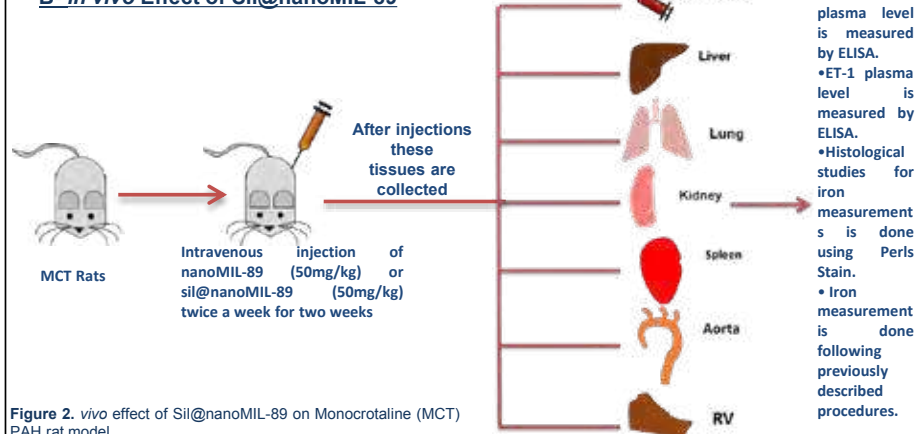
Figure 2. vivo effect of Sil@nanoMIL-89 on Monocrotaline (MCT) PAH rat model.

Results
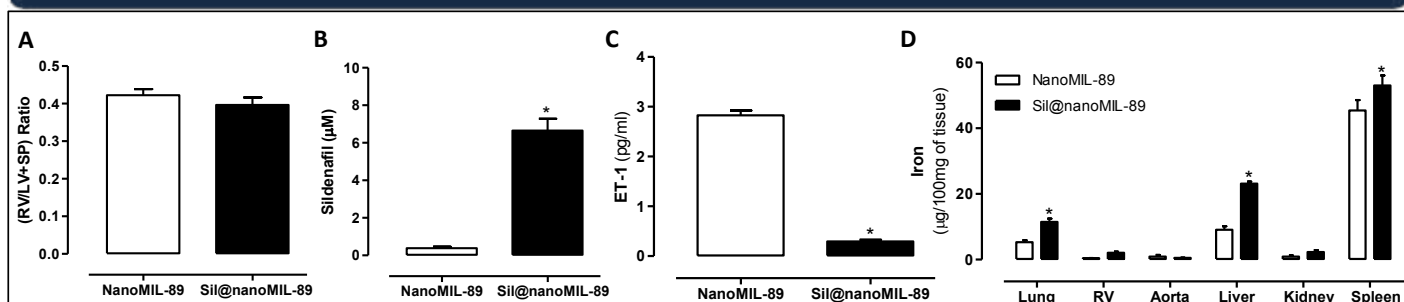
Figure 3. In Vivo effect of the Sil@nanoMIL-89 on the MCT rat model. A. RV/LV+SP ratio. B. Sildenafil levels from the plasma of the two groups after two weeks of treatment with either nanoMIL-89 or Sil@nanoMIL-89. C. ET-1 levels from the plasma of the two groups after two weeks of treatment with either nanoMIL-89 or Sil@nanoMIL-89. D. Measurement of iron (i.e. nanoMIL-89 or Sil@nanoMIL-89) deposition and accumulation in tissues and organs of the MCT rat models. Data presented as mean ± SEM for n=3 animals from one experiment. Statistical significance was determined by t test followed by Mann Whitney test for A, B and C, and by two-way ANOVA followed by Bonferroni posttest for D. Statistical significance was assumed where *p<0.05.

Conclusion

Sil@nanoMIL-89, the first imageable metal-PAH nano-drug passively accumulates in the lung, releases sildenafil and reduces endothelin-1 levels in vivo. Whilst these results are promising, they are at the pilot stage and higher powered studies are required to assess the efficacy of Sil@nanoMIL-89 in this and other models of PAH.

Acknowledgment

References

1.Archer SL, et.al,. Basic science of pulmonary arterial hypertension for clinicians: new concepts and experimental therapies. *Circulation*. 2010;121:2045-66.
2.Mohamed NA, et.al,.Chemical and biological assessment of metal organic frameworks (MOFs) in pulmonary cells and in an acute in vivo model: relevance to pulmonary arterial hypertension therapy. *Pulm Circ*. 2017;7:643-653.
3.Mohamed NA, et.al Metal-organic framework (MOF) nanomedicine preparations ofsildenafil designed for the future treatment of pulmonary arterial hypertension. *bioRxiv* 718478; doi: https://doiorg/101101/718478. 2019.

Composite scaffold made of hydroxyapatite coated PLA nanofibers containing BMP-2 loaded liposomes to improve bone regeneration

Marzieh Mohammadi 1, Mahmoud Reza Jaafari 2* , Mohammad Ramezani3*

1Department of pharmaceutics, School of Pharmacy, Mashhad University of Medical Sciences, Mashhad , Iran
2Nanotechnology research center, School of Pharmacy, Mashhad University of Medical Sciences, Mashhad, Iran
3 Pharmaceutical Research Center, School of Pharmacy, Mashhad University of Medical Sciences, Mashhad, Iran

Introduction

Current clinical treatment of critical bone defects is associated with considerable limitations and complications. The goal of the present study is to develop a simple biomimetic scaffold platform to provide a 3D microenvironment with controlled release property of an osteogenic peptide to enhance osteogenesis of mesenchymal stem cells (MSCs) and improve the healing process of the defected tissue. To this aim, we fabricated electrospun scaffolds conjugated to nanoliposomes encapsulating BMP-2 peptide. After physicochemical characterization of the designed nanoliposomal formulation and the scaffold, we evaluated osteogenic differentiation of the MSCs in vitro and in vivo.

Methods

Preparation and characterization of liposomes
eight different liposomal formulations were produced by the film rehydration method. Hydrodynamic diameter and ζ-potential of the liposomes were determined using Malvern ZS Nano Instrument in PBS.

Release assay
Liposomes were put into a dialysis bag (cut off 30KDa) in a solution of PBS supplemented with 10% FBS containing 0.02% sodium azide. The samples were withdrawn at 1day intervals and replaced with equal volume of fresh medium. The fluorescence intensity of the samples were monitored at different time points.

Scaffold preparation
Electrospun scaffolds made of PLLA-nanohydroxyapatite were prepared and conjugated to liposomes through thiol-maleimide conjugation method.

Biological studies
To study the effect of the released BMP-2 on osteogenic differentiation, human adipose- derived mesenchymal stem cells (hADSCs) were cultured. The osteogenic potential of the cells incubated with liposomal BMP-2 was assessed and compared to the free peptide by quantifying alkaline phosphatase (ALP) activity and the amount of mineralization7 days post-seeding.
the expression of osteogenic genes (Runtrelated transcription factor 2 (*RUNX2*) and Osteocalcin (*OCN*) was evaluated using real-Time Quantitative Polymerase Chain Reaction. *GAPDH* was used as the endogenous house keeping gene.

Invivo studies
Ectopic bone formation analysis was performed through Subcutaneous implantation of H-liposomal formulation lipo-scaffolds and free BMP-2 peptide loaded scaffolds as the control group to 4 weeks old wistar rats. Four weeks post implantation, the animals were sacrificed and the skin flaps at the implantation site were harvested for analysis.

Conclusion

The use of nanoHA coating greatly improved cellular attachment and proliferation. After immobilization of BMP-2 loaded liposomes, the liposcaffolds exhibited excellent properties in inducing osteogenesis in vitro and in vivo. The obtained results suggest that our designed efficient, simple nanoplatform could be a promising candidate in promoting bone regeneration although further in vivo studies are needed.
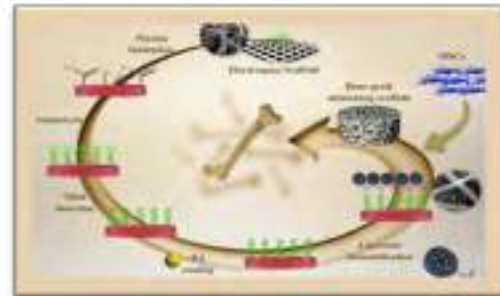
Results

Table 1. Liposome formulations, particle size, surface charge and encapsulation efficiency of each formulation (values expressed as molar ratios).

| Formulations	% Molar ratio	Z Average size (nm)	Poly dispersity index (PDI)	Zeta potential (mv)	% Encapsulation efficiency
A(HSPC/Cholesterol/mPEG-DSPE-maleimide)	84/15/1	139	0.23	−4.5	66
B(HSPC/Cholesterol/mPEG-DSPE-maleimide)	89/10/1	95	0.22	-4.9	53
C(HSPC/Cholesterol/mPEG-DSPE-maleimide)	94/5/1	99	0.24	-2.6	70
D(HSPC/Cholesterol/mPEG-DSPE-maleimide)	96.5/2.5/1	156	0.42	-1.0	76
E(DPPC/Cholesterol/mPEG-DSPE-maleimide)	84/15/1	109	0.30	-3.4	11
F(DPPC/Cholesterol/mPEG-DSPE-maleimide)	74/25/1	141	0.34	-2.6	24
G(DPPC/Cholesterol/mPEG-DSPE-maleimide))	69/30/1	108	0.11	-2.1	30
H(DPPC/Cholesterol/mPEG-DSPE-maleimide)	64/35/1	129	0.17	-2.8	28
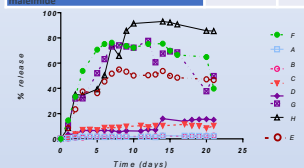
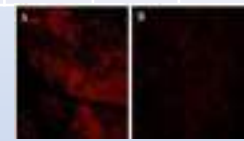Figure 1. Release profiles of different BMP-2 encapsulated liposomal formulations

Figure 2. Confocal microscopy images of fluorescent-labeled liposomes covalently and physically (A & B, respectively) attached to the electrospun nanofibrous scaffolds.
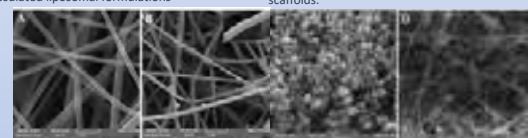
Figure 3. SEM image of (A) electrospun nanofibers, (B) nanoHA-coated nanofibers, (C) HA nanoparticles and (D) SEM image of liposome-loaded scaffolds (liposcaffolds).

Figure 5. Relative expression of OCN and RUNX2 by MSCs cultured on scaffolds containing liposcaffold-HA and scaffold-HA-peptide for 14 days (** indicative of P value b0.01).

Figure 4. ALP evaluation after 7 and 14 days from MSCs seeded on to lipo-scaffolds-HA, scaffold-HA-peptide, scaffold-HA and scaffold

Table 1. Quantification of calcium concentration after 28 days of MSCs seeded on to the scaffold coated and non-coated with nanoHA, loaded and non-loaded with liposomal formulations using ICP-OES method.

	Liposcaffold-HA	Scaffold-HA-Peptide	Scaffold	Scaffold-HA
Calcium content (mg/ml)	1071±18.3	763±9.5	216±2.4	113±0.1

Figure 6. H&E staining of subcutaneously implanted scaffolds. (A) Liposcaffolds-HA (B) scaffold-HA-peptide.

References

López-Noriega, A., et al., *Thermally triggered release of a pro-osteogenic peptide from a functionalized collagen-based scaffold using thermosensitive liposomes.* Journal of Controlled Release, 2014. **187**: p. 158-166.

Normalization of Tumor Microenvironment with Dexamethasone Increases Cisplatin-Loaded Nanocarrier Delivery and Efficacy in Metastatic Breast Cancer

Fotios Mpekris[a], John D. Martin[b], Myrofora Panagi[a], Thahomina T. Khan[b], Margaret R. Martin[b], Chrysovalantis Voutouri[a], Panagiotis Papageorgis[a], Christiana Polydorou[a], Jumpei Norimatsu[b], Triantafyllos Stylianopoulos[a], Kazunori Kataoka[c] and Horacio Cabral[b]

a: Cancer Biophysics Laboratory, Department of Mechanical Engineering, University of Cyprus, Cyprus
b: Department of Bioengineering, Graduate School of Engineering, The University of Tokyo, Bunkyo, Tokyo, Japan
c: Innovation Center of NanoMedicine, Kawasaki Institute of Industrial Promotion, Kawasaki, Kanagawa, Japan

Introduction

Nanocarriers (NCs) accumulate in tumors through the enhanced permeability and retention (EPR) effect. As NCs and other nano-sized therapies are in clinical practice, translatable strategies that increase the magnitude of their accumulation and penetration while reducing heterogeneity of microdistribution may improve treatment outcomes. One such strategy to increase and conform NC penetration and accumulation involves normalizing the non-cancerous components of the tumor, which collectively are known as the tumor microenvironment (TME)[1]. Without normalization, tumor vessel function is compromised because the TME promotes vessel leakiness and compression. Dexamethasone is a glucocorticoid steroid with anti-inflammatory properties used to treat many diseases, including cancer, in which it helps manage various side effects of chemo-, radio-, and immunotherapies. Here[2], we investigated the tumor microenvironment -normalizing effects of dexamethasone in metastatic murine breast cancer (BC). We found that low dose dexamethasone normalizes vessels and the extracellular matrix, thereby reducing interstitial fluid pressure, tissue stiffness, and solid stress. Also, dexamethasone increases the tumor accumulation and efficacy of ~30 nm polymeric micelles containing cisplatin (CDDP/m) against murine models of primary BC and spontaneous BC lung metastasis, which also feature a TME with abnormal mechanical properties.

Methods

Orthotopic models for murine mammary tumors were generated by implantation of 5×10^4 4T1 and 1×10^7 MDA-MB-231 mouse mammary cancer cells into the third mammary fat pad of 6-8 week old BALB/c or BALB/c nu/nu female mice, respectively. Treatment was initiated when tumors reached ~90mm³. Dexamethasone at 3mg/kg was administered daily from days 0 through 8. CDDP/m at 1mg/kg was administered by retro-orbital injection during sedation with isoflurane on days 2, 5, and 8.

Results

Dexamethasone normalizes tumor vessels dose-dependently

- Vascular endothelial growth factor (VEGF) is the major driver of the pathophysiology of tumor vessels and blocking it promotes vascular normalization. Dexamethasone reduces VEGF expression in murine models of brain cancer, so we hypothesized it would do so in BC. We treated BALB/c mice daily for 4 days.
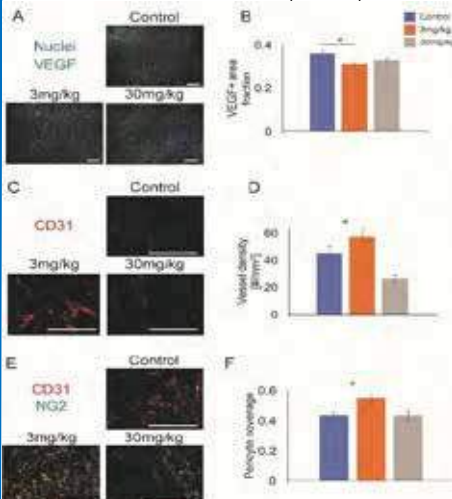
- Dexamethasone reduced the levels of VEGF. (A) Representative images of VEGF (green) with nuclear counterstain (blue) immunofluorescence. (B) Quantification of area fraction positive for VEGF immunofluorescence staining.
- Dexamethasone at 30 mg/kg reduced the microvessel density. (C) Representative images of CD31 (red) immunofluorescence marking tumor vessels. (D) Quantification of tumor vessel density.
- Dexamethasone at 3 mg/kg avoided pruning yet increased vessel maturity, as indicated by the association of NG2+ pericytes with CD31+ endothelial cells. (E) Representative images of CD31 (red) and NG2 (green) immunofluorescence marking endothelial cells and pericytes, respectively. (F) Quantification of the pericyte coverage of microvessels.

Dexamethasone Normalizes the ECM and Mechanical TME

- Collagen I and hyaluronan have been identified as matrix components that contribute to solid stress and vessel compression. With histological staining we found that dexamethasone reduced levels of hyaluronan and not collagen I in the tumors. (A) Representative images of hyaluronan (red) and collagen I (green) immunofluorescence. Yellow areas indicate colocalization of both ECM components. (B) Quantification of area fraction positive for hyaluronan. (C) Quantification of area fraction positive for collagen.
- Dexamethasone 30 mg/kg reduced tissue stiffness, as measured by the elastic modulus, whereas 3 mg/kg only produced a trend. (D) Tumor tissue elastic modulus, which is a measure of stiffness.
- (E) Using the tumor-opening assay, which indicates the amount of residual solid stress held within the tumor tissue by the amount it opens after cutting, we confirmed that both doses reduced solid stress. A larger opening is associated with more solid stress.
- (F) Dexamethasone reduces Interstitial Fluid Pressure.

Dexamethasone increases the transvascular transport of nanocarriers

- Dexamethasone increases the transvascular transport of nanocarriers. Representative confocal intravital microscopy images of 4T1 tumors treated with (A) control, (B) 3 mg/kg, or (C) 30 mg/kg dexamethasone after co-injection of 70 kDa (13 nm, red) and 500 kDa (32 nm, green) fluorescent dextrans. (D) Quantification of effective permeability, with dexamethasone 3 mg/kg (orange), 30 mg/kg (gray), and control (blue).

Dexamethasone Increases Efficacy of NCs in Metastatic BC
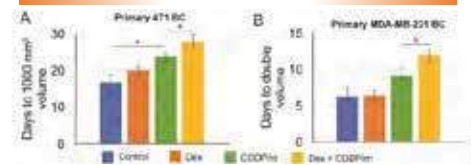
- (A) After confirming that dexamethasone normalizes vascular structure, ECM, and vessel function, we next hypothesized that dexamethasone would affect the rate of NCs transport across tumor vessels and penetrate toward cancer cells. Thus, we used CDDP/m, which are ~30 nm. We tested the therapies in a primary tumor growth delay study against orthotopic 4T1 tumors, with an end point of days until 1000 mm³ tumor volume. We found that CDDP/m (1 mg/kg) monotherapy increased the number of days for the tumors to reach 1000 mm³ compared to control. Combining dexamethasone (3mg/kg) with CDDP/m significantly increased this time period compared to that with CDDP/m monotherapy.
- (B) In mice bearing orthotopic MDA-MB-231 BC, the combination of dexamethasone and CDDP/m significantly extended the time to double the volume compared to CDDP/m alone.

Dexamethasone Increases Efficacy of NCs in Pulmonary BC Metastases
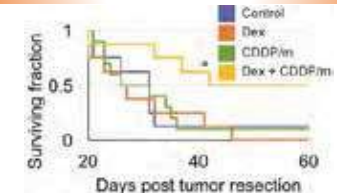
- We investigated the effects of the combination of dexamethasone and CDDP/m on lung metastases. To mimic the clinical treatment protocol of metastatic disease we surgically removed 4T1 primary BC tumors when they reached ~300 mm³.
- Animal survival in mice with spontaneous metastases. We administered two cycles of CDDP/m with daily dexamethasone and we found that only the combination of dexamethasone (3mg/kg) and CDDP/m (1mg/kg) provided a survival advantage. Thus, dexamethasone increases the efficacy of CDDP/m against BC pulmonary metastasis.

Discussion

- Dexamethasone normalizes the tumor microenvironment vessels and matrix and increases the efficacy of nanocarriers against primary breast tumors and their metastases.
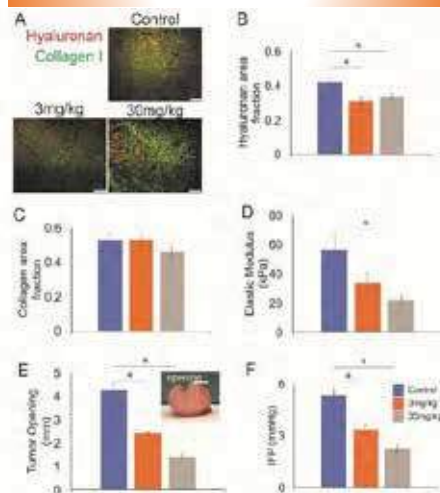
References

1. Stylianopoulos, T., et. al., Reengineering the Physical Microenvironment of Tumors to Improve Drug Delivery and Efficacy: From Mathematical Modeling to Bench to Bedside, Trends in cancer, 2018. 4(4): p. 292-319.
2. Martin, J.D. et. al., Dexamethasone Increases Cisplatin-Loaded Nanocarrier Delivery and Efficacy in Metastatic Breast Cancer by Normalizing the Tumor Microenvironment, ACS Nano, 2019. 13(6): p. 6396-6408.

ETH zürich

Empa — Materials Science and Technology

Cancer Microtissues for Rationalized Nanoparticle-Based Radiotherapy

Anna Lena Neuer[1,2], Lukas RH Gerken[1,2], Kerda Keevend[1], Alexander Gogos[2] and Inge K Herrmann[1,2]

[1] Nanoparticle Systems Engineering Lab, Department of Mechanical and Process Engineering, **ETH Zürich**, Sonneggstrasse 3, CH-8093 Zürich, Switzerland

[2] Particles 4D, Laboratory for Particles Biology Interactions, Swiss Federal Laboratories for Materials Science and Technology (**Empa**), Lerchenfeldstrasse 5, CH-9014, St. Gallen, Switzerland

INTRODUCTION

Radiotherapy is next to surgery and chemotherapy a first line treatment for cancer. However, radiation therapy is non-specific, potentially damaging to surrounding tissue and bears the risk of secondary tumor development.[1]

Atoms with high atomic number interact strongly with ionizing radiation. High-z nanoparticle-based radio-enhancement[2] takes advantage of these strong interactions to amplify radiation damage in close proximity of the nanoparticles.[3,4] Gold nanoparticle (AuNP) hold great promise,[5] however, clinical translation is challenged by the absence of human representative and clinically relevant 3D models. Here, we developed an advanced 3D tumor model exhibiting tissue-like features. This model, along with label-free nanoanalytical imaging based on elemental analysis and density dependent electron microscopy[6] offers a route to overcome the disconnect between 2D *in vitro* data and *in vivo* data and allows pre-selection of promising nanoparticle-based radioenhancers or combination therapies.
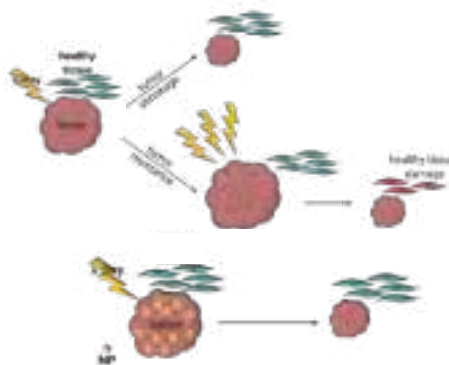
RESULTS

Development of an advanced human tumor model with tissue-like characteristics. Microtissues (MT) show linear growth behaviour up to 20 days after seeding for both mono-cultured (HeLa) and co-cultured (HeLa/fibroblasts) microtissues (n=3).
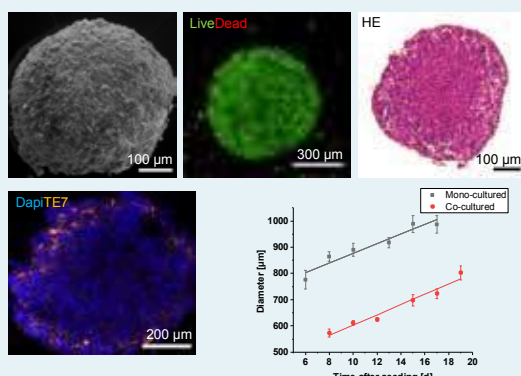
NP intratissural distribution and cytotoxicity after 24h exposure to nanoparticles (NP). NP administration of 5 µg/MT (5000 cells) correspond to 1 ng/cell. Microtissue exhibit higher cytotoxic resistance than conventional 2D cell culture (n=3). NP were administered either pre-MT-formation or post-MT-formation.
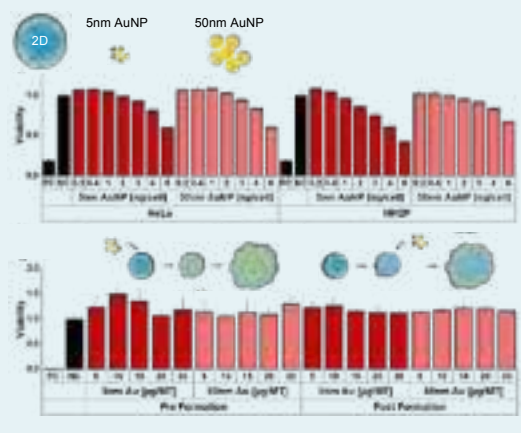
Total AuNP uptake was measured by ICP-MS (n=2) for 2D and 3D cell cultures. Measured NP/cell was 20-30-fold higher for 5 nm compared to 50 nm AuNP.
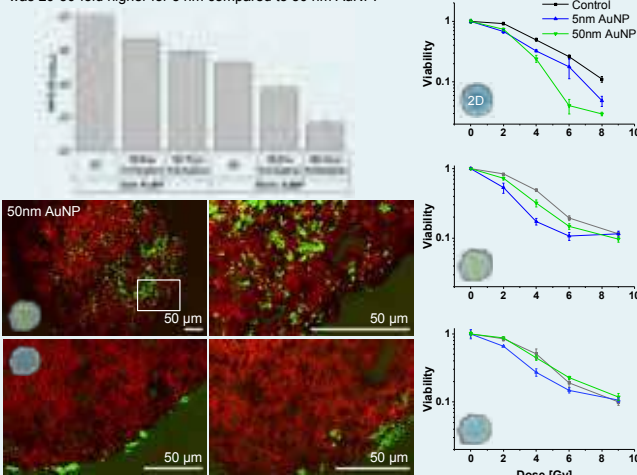
Intratissural distribution of AuNP was assessed by density dependent colour scanning electron microscopy (DDC-SEM) with resolution sufficient to identify individual 50 nm AuNP in histology sections. As expected, NP distributions are more uniform for pre-MT-formation tissues and of shell-like nature in post-MT-formation tissues.

Comparison of nanoparticle-based radio-enhancement effect showed higher resistance of 3D microtisse for x-ray radiation than 2D. While in 2D cell cultures, 50 nm AuNP showed the strongest enhancement, in 3D cultures, more pronounced radioenhancement was observed for 5nm nanoparticles, in line with the enhanced tissue penetration of 5 nm compared to 50 nm AuNP in 3D cell cultures.

CONCLUSION

- Successful development of a tumor spheriod model to assess radio-enhancement effects as a function of nanoparticle uptake, penetration, exocytosis and retention.

- Cells in 3D *in vitro* environments show higher resistance to chemotherapeutic drugs, NP treatment and x-ray radiation.

- Microtissue model accurately accounts for reduced tissue penetration of larger NP in line with *in vivo* findings[7], leading to reduced therapeutic efficacy and hence (partially) explains mismatch between 2D cell culture and *in vivo* findings.

- Model offers rapid and robust pre-selection strategy for promising NP candidates and combination therapies prior to in vivo studies

REFERENCES
1. Chung C.S. et al., Int. J. Radiat. Oncol.,, Biol., Phys., 2013
2. Kuncic Z. and Lacombe S., Phys. Med. Biol., 2018
3. Pottier A et al., Biochem Biophy Res Comm, 2015
4. Howard D. et al., Int. J. Mol. Sci., 2020
5. Butterworth K.T. et al. Nanoscale, 2012
6. Neuer A et al., Nanoscale Adv., 2020
7. Huang K. et al., ACS Nano, 2012

D MAVT

CONTACT
annalena.neuer@empa.ch
www.nse.ethz.ch

Nanoparticle Systems Engineering Laboratory

MULTIFUNCTIONAL BLOCK-COPOLYMERS FOR THE ASSEMBLY OF WELL DEFINED pDNA POLYPLEXES

Nicolas Ritt[1], Simone Hager[2], Ernst Wagner[2], Rudolf Zentel[1]

[1] Johannes Gutenberg-Universität Mainz. Department of Chemistry. Duesbergweg 10-14, 55128 Mainz, Germany
[2] Ludwig-Maximilians-Universität Munich. Department of Pharmacy. Butenandtstraße 5-13. Haus D. 81337 Munich, Germany

INTRODUCTION

Manipulation of the genome is a promising approach for many therapeutic applications

Because of rapid degradation in the blood stream and diverse physiological barriers, nucleinic acids can't be used as stand-allone transfection agents in an in-vivo system.
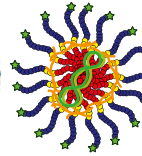
Polymer based DNA/RNA complexes (polyplexes) as transfection systems are a promising way to protect the genetic information. In addition to shielding, the system has to release the payload on target. Hence, a reversible stabilization and destabilization of the transfection agent is advantageous.

CONCEPT

We wanted to synthesize a Triblock-Copolymer with three orthogonal reactive functionalities:

1. A reactive end group, for post polymerization modification via azide-alkyne ,click' reactions → incooporation of targeting- or imaging agents.
2. A short block, bearing reactive disulfide groups (sensible to soft nucleophiles) → reversible crosslinking / codelivery of drugs.
3. A reactive ester block (reactive to hard nucleophiles) → incooporation of assymetric diamines for pDNA complexation, tuning of initial polyplex stability.

POLYMER SYNTHESIS

MEO₃MA
PDSM
PFPMA

Synthesis via RAFT-Process in a 5 step synthesis.

- CTA:1-azido-16cyano-13-oxo-3,6,9-trioxa-12-azaheptadecan-16-yl benzothioate (azide-CTA)
- Initiator: 2,2'-azobis(4-methoxy-2,4-dimethyl-valeronitrile) (AMDVN)
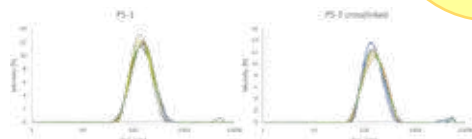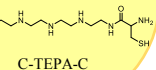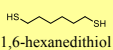- Solvent: 1,4-dioxane; temperature: 40°C

DMEDA
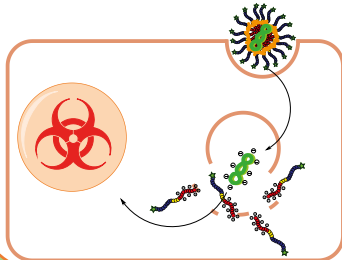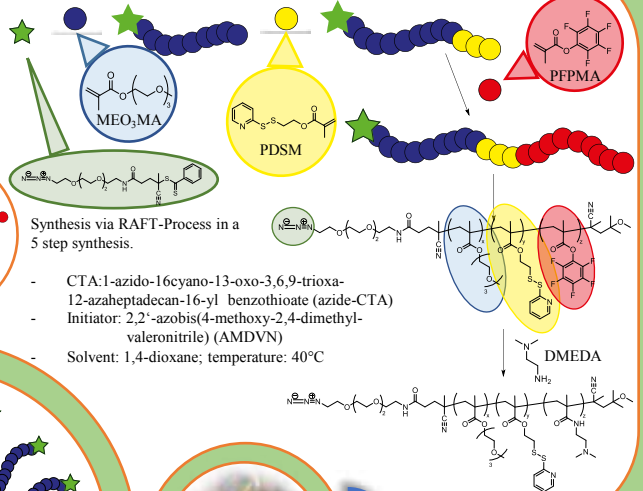
POLYPLEX CHARAKTERIZATION
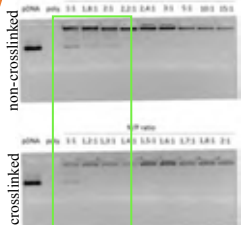
Stable, non crosslinked polyplexes are formed at low N/P-ratios

Crosslinking with either, 1,6-hexanedithiol or C-TEPA-C both improves polyplex stability

Crosslinkers:
HS   SH
1,6-hexanedithiol

C-TEPA-C

Dynamic light scattering (DLS): Formed polyplexes meet targeted sizes with low size distribution (d = 113-136 nm; PDI = 0,15-0,17). Crosslinking only slightly increases size.
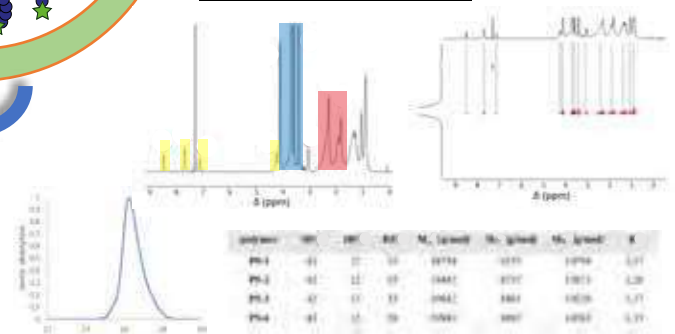
Cell viability essay on N2a cells: No extensive toxicity detectable for a broad range of N/P-ratios for non-crosslinked and crosslinked polyplexes

POLYMER CHARAKTERIZATION

The products of every reaction step are characterized via NMR Spectroscopy and SEC. Good accordance of calculated and measured polymer compositions.
→ High control over molecular weight and narrow weight distribution.

Proof of concept:

,Click'-Reaction with IR dye CW800-DBCO proves conservation of azide-functionalities

Co-amidation of Texas Red®-cadaverine

UV-Vis spectroscopy: 2-Thiopyridine is cleaved during crosslinking detected in the filtrate after precipitation
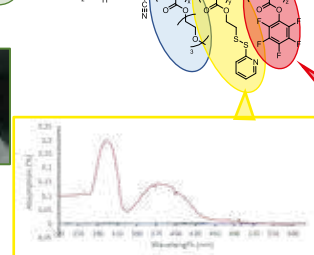
CONCLUSION

- A multifunctional, versatile polymer system was established.
- Three orthogonally reactive functional groups for postpolymerization reactions
- Effective pDNA complexation
- Reversibly crosslinkable.
- Incooporation of targeting- and imaging-agents or codelivery of drugs possible
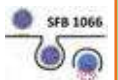- Non-toxic

LITERATURE:

1. Ritt, N.; Hager, S.; Wagner, E.; Zentel, R. *submitted*
2. Heller, P.; Hobernik, D., Laechelt, U. et al.; *J. Control. Release* **2017**, 258, 146-160
3. Nuhn, L. et al.; *Macromol. rapid commun.* **2014**, 35, 2057–2064

CONTACT
niritt@uni-mainz.de,
www.ak-zentel.chemie.uni-mainz.de,
simone.hager@cup.uni-muenchen.de,
www.cup.lmu.de/pb/aks/ewagner

Oxidative Toxicity in Diabetes Mellitus: Role of Nanoparticles and Future Therapeutic Strategies

Mohammadmahdi Sabahi[1] , Sara Ami Ahmadi[1], Reza Mahjub[2], Akram Ranjbar[3]

1. Student Research Committee, Hamadan University of Medical Sciences, Hamadan, Iran.
2. Department of Pharmaceutics, School of Pharmacy, Hamadan University of Medical Sciences, Hamadan, Iran.
3. Department of Toxicology and Pharmacology, School of Pharmacy, Hamadan University of Medical Sciences, Hamadan, Iran.
E-mail: m.sabahi@edu.umsha.ac.ir, mmsabahi1996@gmail.com.

Introduction

Oxidative stress (OS), an unbalance between the generation of reactive oxygen species (ROS) and antioxidants in the body, is involved in the pathogenesis of many diseases, including diabetes mellitus (DM). The destruction of pancreatic β-cells results from an OS-induced immune response and secondary apoptosis. In recent years, antioxidants have been considered as preventative, curative and most importantly, counteracting factors for OS. The main function of antioxidants is converting ROS and reactive nitrogen species (RNS) to non-reactive products. Since orally delivered antioxidants are destroyed by enzymes and gastric acid and only a small percentage of them are absorbed, they have a small bioavailability with low concentrations in target cells. Therefore, there is an instant need to develop efficient methods to deliver antioxidants to the target sites. For this purpose, advanced nanoparticles (NPs) carriers, such as liposomes, polymeric NPs, solid lipid NPs or self-emulsifying drug delivery systems have been used. NPs containing antioxidants have been suggested as high-performance therapeutic nanomedicines in attenuating OS with potential applications in treating and preventing DM.
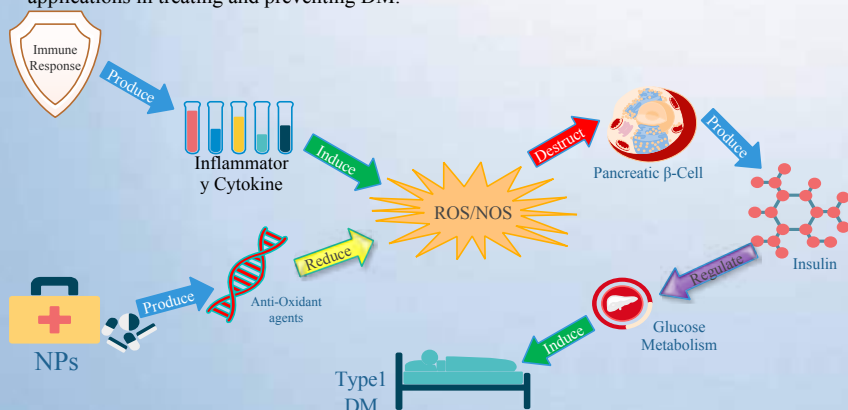

Figure 1. Schematic representation of nanoparticles as a vehicle for therapeutics and their innate antioxidant properties for the effective treatment of type 1 DM.

Discussion

Nanotechnology has provided a promising platform for engineering insulin carriers. The present brief review aims to analyse the effects of nanoparticles on oxidative stress in diabetes mellitus. Elevated levels of ROS are related to DM in the hyperglycaemic pathways. Some NPs are antioxidants and may improve DM disorders. However, some outstanding problems remain in diabetes care, such as the need for improved glucose sensing, oral insulin formulations, and transplantation of islets with enhanced survival are likely to have nanomedicine solutions and research is already very active in these areas. Many studies have contributed to the ability of colloidal NPs to increase insulin absorption in the colon; however, these drugs are limited due to the inability of NPs be safely transported through the intestine and stomach. There have been many new investigations and discoveries of potential NPs to oral administration of insulin, and these formulations are continuously being improved for OS reduction, the future of oral insulin looks promising. However, very few studies have focused on the effects of NPs on diabetes, and further research is needed to clarify the mechanism of these NPs.

Authors	Year of study	Location	Nanoparticle	Efficacy of NPs on DM
Crans et al.	1995	Colorado State University	Vanadium	Increases the release of insulin from the pancreatic β-cells
Pourkhalili et al.	2012	Pharmaceutical Sciences Research Center, Tehran, Iran.	Cerium oxide	increase in cells viability, secretion of insulin, and ATP/ADP ratio and reduction in ROS
Moridi et al.	2018	Hamadan University of Medical Sciences	Cerium oxide	Increases secretion of insulin
Anderson	2000	Beltsville Human Nutrition Research	Chromium	Increases the number of insulin receptors and sensitivity of β-cells
Vincent	2000	The University of Alabama	Chromium	Enhanced insulin binding
Afifi et al.	2015	University of Jeddah	Zinc oxide	increased of SOD, CAT, GRD, GPx and GSH mRNA expression levels
Alkaladi et al.	2014	King Abdulaziz University	Zinc oxide	Increased levels of insulin in serum and reduced levels of blood glucose
Richards-Williams et al.	2008	University of Alabama at Birmingham	Zinc oxide	Increase the insulin secretion from rat isolated pancreatic islets
Grama et al.	2013	University of Strathclyde	Curcumin	Causes significant delay in progression of diabetic cataract
Al-Quraishy et al.	2015	King Saud University	Selenium	Enhanced glycogen contents in the liver and kidney through the stimulation of glycogen synthase activity

ATP/ADP: Adenosine triphosphate/Adenosine diphosphate; CAT: catalase; DM: Diabetes mellitus; GPx: Glutathione peroxidase; GRd: Glutathione reductase; GSH mRNA: Glutathione messenger ribonucleic acid; ROS: Reactive oxygen species; SOD: Superoxide dismutase.

References

1. Eizirik DL, et al. The role of inflammation in insulitis and β-cell loss in type 1 diabetes. Nature Reviews Endocrinology. 2009 Apr;5(4):219.

2. Feuerer M, et al. Lean, but not obese, fat is enriched for a unique population of regulatory T cells that affect metabolic parameters. Nature medicine. 2009 Aug;15(8):930-9.

Anti-cancer activity of pH- and thermo-responsive silica nanoparticles (SiNPs) encapsulated doxorubicin and avocado (*Persea americana*) seed extract on 2D human liver tumour model

Arunsajee Sae-be[1], Piyaporn Plommaithong[1], Apichat Chatsukit[1], Rawinan Srisamanuwat[3], Orasa Suriyaphan[3], Khanit Sa-ngiamsuntorn[2], Jiraporn Leanpolchareanchai[1], Pongtip Sithisarn[4], Pakatip Ruenraroengsak[1*] (*corresponding author)

[1] Department of Pharmacy, [2] Department of Biochemistry, [3] Department of Food Chemistry and Department of Pharmacognosy, Faculty of Pharmacy, Mahidol University, Bangkok, Thailand, 10400

Introduction

Cancer has become the second leading cause of death globally. Chemotherapy is one of standard treatments for cancer. However, the limitations of chemotherapy including side effects and drug resistance lead to failure of cancer treatment. (1). The combined therapy between anti-cancer drugs and plant extracts or plant products may help to resolve such limitations. Therefore, It could be very interesting to study activity of the individual avocado (*Persea americana*) seed extract (PAX) (2) and its combined activity with an anti-cancer drug, doxorubicin, (DPAX) whether they have synergistic effect or not. Both doxorubicin (DOX) and PAX were encapsulated by SiNPs to achieve passive drug targeting. The anti-anticancer efficacy was then evaluated *in vitro* using 2D liver models.

Objectives

❑ To investigate secondary metabolites in PAX.
❑ To evaluate anti-cancer activity of DOX and PAX against 2D-human liver HepG2 cells *in vitro*.
❑ To evaluate the anti-cancer efficacy of DOX and PAX encapsulated pH- and thermo-responsive SiNPs against 2D human liver HepG2 cells.
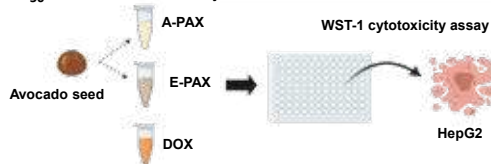
Methods

1. Determine polyphenol compounds in aqueous avocado seed extract (A-PAX) and ethanolic avocado seed extract (E-PAX, 2)

The polyphenol compounds of A-PAX and E-PAX were determined in both the qualitative method, thin layer chromatography (TLC) and the quantitative methods to analyze total phenolic and flavonoids.
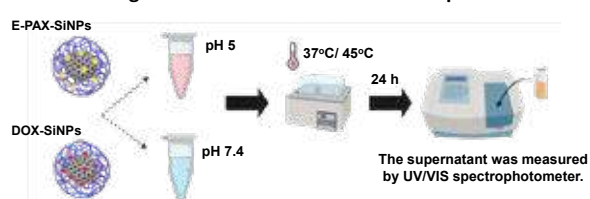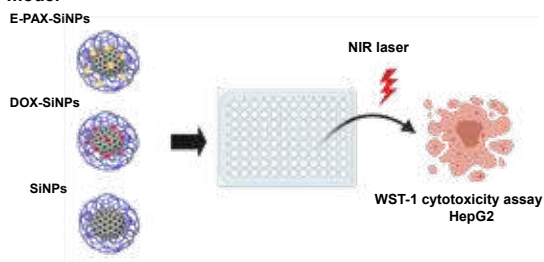
2. IC$_{50}$ of DOX and PAX by WST-1

3. DOX and E-PAX encapsulated by SiNPs (3)

$$\%Encapsulation\ (\%EE) = \left[\frac{Total\ drug - entrapped\ drug}{Total\ drug}\right] \times 100$$
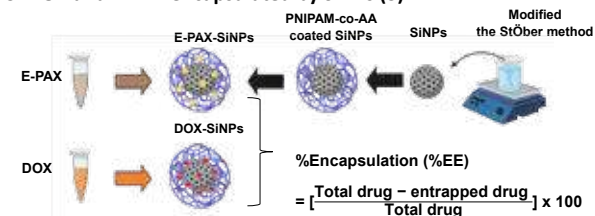
4. *In vitro* drug release from DOX- and PAX- encapsulated SiNPs

The supernatant was measured by UV/VIS spectrophotometer.

5. *In vitro* efficacy of DOX and PAX SiNPs in the 2D liver tumour model

Results

1. Determine polyphenol compounds in A-PAX and E-PAX[β]

Fig. 1 Thin layer chromatogram of PAX analyzed by UV 254 nm and 366 nm, respectively
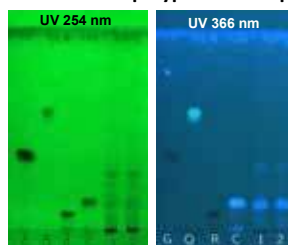
Table 1 Total phenolic and flavonoids content in PAX (n=3)

Avocado seed extract	Total phenolic compounds (%g, Gallic acid) (mean ± SD)	Total flavonoids (%g, Quercetin) (mean ± SD)
E-PAX (% yield = 11.12%)	13.38 ± 0.10	2.87 ± 0.56
A-PAX (% yield = 8.82%)	11.81 ± 0.18	7.96 ± 0.12

Noted[β] : G = standard Gallic acid, Q = standard Quercetin, R = standard Rutin, C = standard Chlorogenic acid, 1= E-PAX, 2 = A-PAX. TLC mobile phase = Chloroform: Methanol: Formic acid at ratio 7.5: 1.5: 1

2. IC$_{50}$ of individual DOX and PAX by WST-1

Table 2 Anti-cancer activity of PAX and DOX against HepG2 cells

Samples	IC$_{50}$ (μg/mL) (mean ± SD) (n=3)
E-PAX	75.69 ± 1.71
A-PAX	136.08 ± 4.48
DOX	20.76 ± 1.59

Table 3 Anti-cancer activity of the mixtures (E-PAX and DOX) at different ratios against HepG2 cells

E-PAX + DOX	% Cell viability
1:1	0.19%
2:1	0.13%

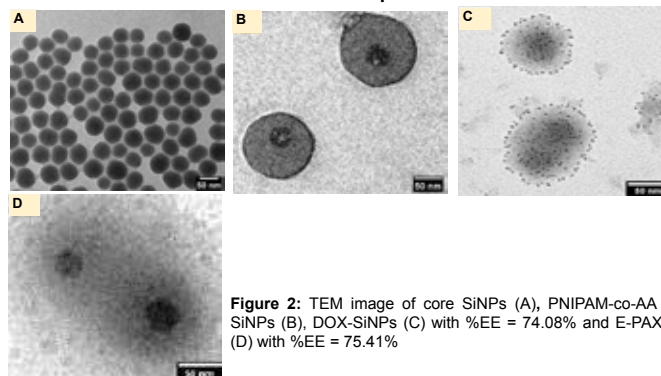### 3. Characterization of DOX and E-PAX encapsulated SiNPs

Figure 2: TEM image of core SiNPs (A), PNIPAM-co-AA coated SiNPs (B), DOX-SiNPs (C) with %EE = 74.08% and E-PAX-SiNPs (D) with %EE = 75.41%

4/5. *In vitro* drug release and the efficacy of DOX- and PAX- encapsulated SiNPs in the 2D liver tumour model

❑ After incubation at different pH and temperature, the drug release from DOX-SiNPs and E-PAX-SiNPs did not quantified.

Table 5 Anti-cancer activity of encapsulated SiNPs against HepG2 cells

Samples	% Cell viability
DOX-SiNPs (equi DOX 120 μg/mL)	71.94%
E-PAX-SiNPs (equi E-PAX 225 μg/mL)	79.00%
DP-SiNPs (equi DOX 40 μg/mL + E-PAX 150 μg/mL)	95.98%
SiNPs	104.6%

Conclusion

1. The major secondary metabolite of PAX is Chlorogenic acid. In addition, the different method of extraction such as type of solvents and to extraction temperature significantly impact on % yield, total phenolic and total flavonoids of extracts.
2. Both E-PAX and DOX exhibited anti-cancer activity and demonstrated the synergistic effect on HepG2 cells at ratio 1:1 and 1:2 (E-PAX:DOX).
3. The biocompatible SiNPs did not increase anti-cancer activity of DOX, E-PAX and DPAX as the encapsulated-SiNPs did not reduce % viability of HepG2 cells. This may be due to the strong electrostatic interaction between DOX and SiNPs resulting in the low release of DOX and E-PAX. Therefore, the further optimization on drug entrapment is needed. Consequently, the efficacy of DOX and PAX SiNPs will be evaluated both 2D- and 3D-liver tumour models.

References: 1. World health organization (WHO). All cancers: Fact sheet [Internet]. [cited 2020 Sep 20]. Available from: https://gco.iarc.fr/today/data/factsheets/cancers/39-All-cancers-fact-sheet.pdf; **2.** Abubakar ANF, Achmadi SS, Suparto IH. Triterpenoid of avocado (*Persea americana*) seed and its cytotoxic activity toward breast MCF-7 and liver HepG2 cancer cells. Asian pac J Trop Biomed 2017; 7(5): 397-400; **3.** Zhang Z, Wang J, Nie X *et al.* Near infrared laser-induced targeted cancer therapy using thermoresponsive polymer encapsulated gold nanorods. J. Am. Chem. Soc 2014; 136: 7317-26.

Site-specific nanobody conjugation for targeted drug delivery to protumoral tumor-associated macrophages

Maximilian Scherger,[1] Evangelia Bolli,[2] Sana Arnouk,[2] David Straßburger,[3] Moritz Urschbach,[3] Hans-Joachim Räder,[1] Hansjörg Schild,[4] Stephan Grabbe,[4] Pol Besenius,[3] Jo A. Van Ginderachter,[2] Lutz Nuhn[1]

[1] Max Planck Institute for Polymer Research Mainz, Germany
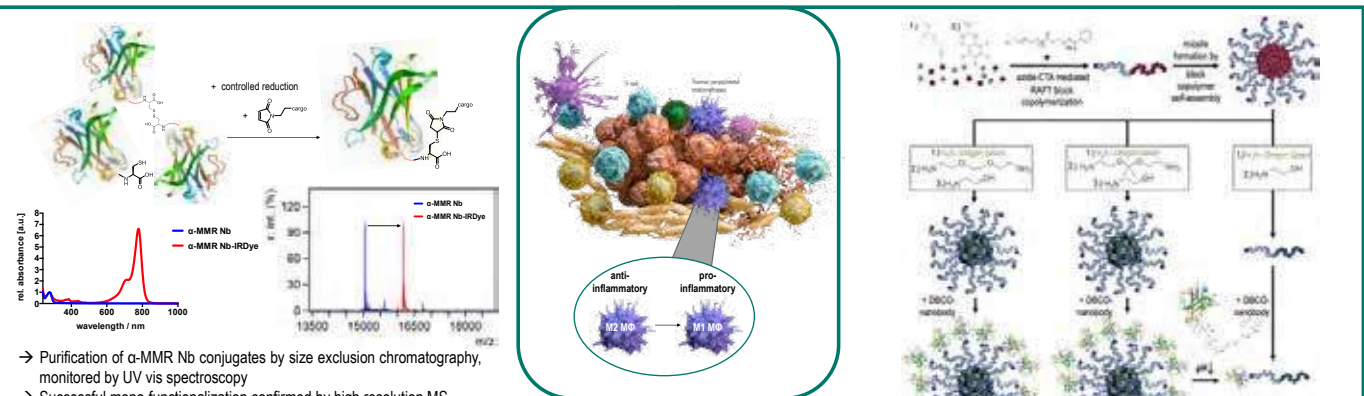[2] Lab of Cellular and Molecular Immunology, Vrije Universiteit Brussels, Belgium
[3] Department of Chemistry, Johannes Gutenberg-University Mainz, Germany
[4] University Medical Center, Johannes Gutenberg-University Mainz, Germany
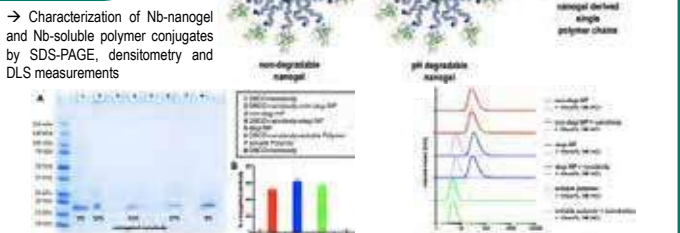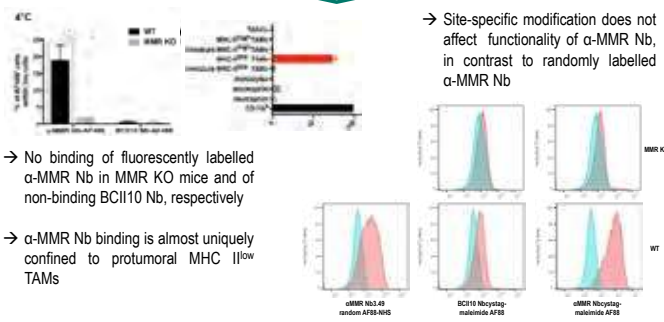
MAX-PLANCK-INSTITUT
FÜR POLYMERFORSCHUNG

Nanobodies are one of the smallest available single chain antigen binding fragments derived from camelid heavy chain-only antibodies. With a molecular weight of about 15 kDA they are 10 times smaller than conventional antibodies. They can be produced recombinantly and genetically engineered to provide chemical functionalities for site-specific protein modification. In this study, nanobodies were used to target the macrophage mannose receptor (MMR, CD206) overexpressed on tumor-associated macrophages (TAMs). Those type of immune cells govern chronic cancer-associated inflammations and establish immunosuppressive tumor micromilieus. Strategies to re-polarize TAMs and trigger an antitumoral activity can be followed by using the targeting potential of anti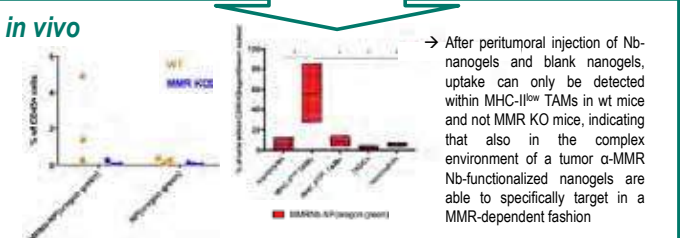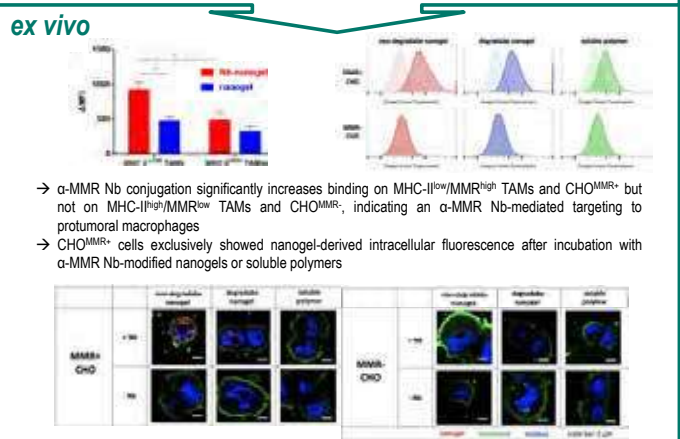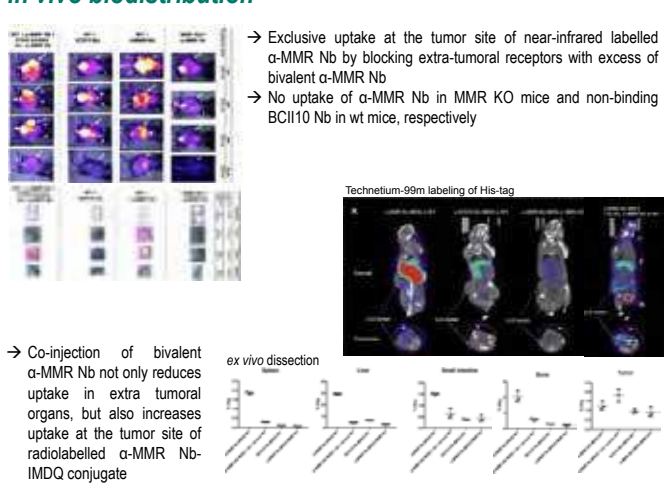-MMR/CD206 specific nanobodies engineered with a C-terminal cysteine. They can be site-specifically modified via maleimide chemistry under reducing conditions without interfering with their internal disulfides. Thus, one single fluorescent dye can be coupled to the nanobody, for instance, to monitor the recruitment of TAMs into immunosuppressive cancers. Additionally, immune modulating small molecules can be ligated to the nanobodies to stimulate the immune system of the tumor microenvironment after systemic injection. Alternatively, nanobodies can further be attached to the surface of nanogels loaded with multiple immune modulating molecules in order to trigger TAM repolarization after peritumoral injection. In summary, we believe that our nanobody approach may pave the road for targeted modulation of pro-tumoral TAMs during cancer immunotherapy.

→ Purification of α-MMR Nb conjugates by size exclusion chromatography, monitored by UV vis spectroscopy
→ Successful mono-functionalization confirmed by high resolution MS

→ Characterization of Nb-nanogel and Nb-soluble polymer conjugates by SDS-PAGE, densitometry and DLS measurements

ex vivo

→ Site-specific modification does not affect functionality of α-MMR Nb, in contrast to randomly labelled α-MMR Nb

→ No binding of fluorescently labelled α-MMR Nb in MMR KO mice and of non-binding BCII10 Nb, respectively

→ α-MMR Nb binding is almost uniquely confined to protumoral MHC II^{low} TAMs

in vivo biodistribution

→ Exclusive uptake at the tumor site of near-infrared labelled α-MMR Nb by blocking extra-tumoral receptors with excess of bivalent α-MMR Nb
→ No uptake of α-MMR Nb in MMR KO mice and non-binding BCII10 Nb in wt mice, respectively

Technetium-99m labeling of His-tag

→ Co-injection of bivalent α-MMR Nb not only reduces uptake in extra tumoral organs, but also increases uptake at the tumor site of radiolabelled α-MMR Nb-IMDQ conjugate

ex vivo dissection

ex vivo

→ α-MMR Nb conjugation significantly increases binding on MHC-II^{low}/MMR^{high} TAMs and CHO^{MMR+} but not on MHC-II^{high}/MMR^{low} TAMs and CHO^{MMR-}, indicating an α-MMR Nb-mediated targeting to protumoral macrophages
→ CHO^{MMR+} cells exclusively showed nanogel-derived intracellular fluorescence after incubation with α-MMR Nb-modified nanogels or soluble polymers

in vivo

→ After peritumoral injection of Nb-nanogels and blank nanogels, uptake can only be detected within MHC-II^{low} TAMs in wt mice and not MMR KO mice, indicating that also in the complex environment of a tumor α-MMR Nb-functionalized nanogels are able to specifically target in a MMR-dependent fashion

References

[1] K. Movahedi et al. Cancer Res. 2012, 72, 4165–4177.
[2] L. Nuhn et al. Bioconjugate Chem. 2018, 29, 2394–2405.
[3] M. Scherger et al. Cells 2020, in revision.
[4] modified from: Bristol-Myers Squibb. Revealing the Potential of the Immune System in Cancer. (2017). https://www.immunooncologyhcp.bmsinformation.com/antitumor-immunity, 01.03.2019.

maximilian.scherger@mpip-mainz.mpg.de

Fluorescence correlation spectroscopy studies of nanocarrier-based drug delivery systems

Sascha Schmitt, Jennifer Schultze[1], Inka Negwer[1,2], Hans-Jürgen Butt[1], Kaloian Koynov[1]

[1]Max Planck Institute for Polymer Research, Mainz, Germany
[2]Johannes Gutenberg University, Mainz, Germany

Physics at Interfaces

Principle of FCS

Introduction

Using nanoparticle-based carriers is an extremely promising way for the administration of therapeutic agents, such as drug molecules, proteins and polynucleotides. In order to get full advantage of this approach one needs a careful characterization of the nanocarrier systems at all stages of the drug delivery process: from their formation, to their stability all the way to the drug release in the cytoplasm of the target cells. In this regard, fluorescence correlation spectroscopy (FCS) offers a powerful and universal tool. [1]

$$G(\tau) = \frac{\langle I(t)I(t+\tau)\rangle}{\langle I(t)\rangle^2}$$
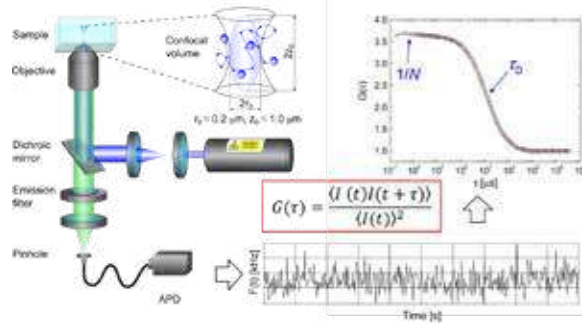
For simple Fickian diffusion:

$$G_{fit}(\tau) = 1 + \frac{1}{N}\frac{1}{\left(1+\frac{\tau}{\tau_D}\right)}\frac{1}{\sqrt{1+\frac{\tau}{S^2\tau_D}}}$$

where $\tau_D = \frac{r_0^2}{4D}$ $\quad S = \frac{z_0}{r_0}$ $\quad D = \frac{kT}{6\pi\eta R_H}$

The fitting yields:

- Diffusion coefficient D and hydrodynamic radius R_H → e.g. size of nanocarrier and payload
- Fluorescence brightness → Labeling and loading efficiency
- Concentration

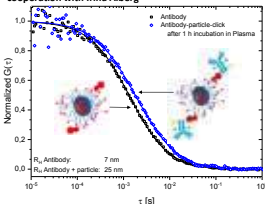## Nanocarriers' characterization in aqueous buffer or blood plasma

Bioorthogonal reaction

Formation of bioorthogonal click reaction compound from an core cross-linked HPMA-based micelle with an modified antibody
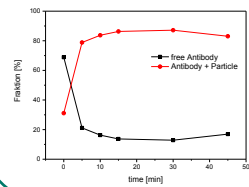[2] Kramer, et al. (2019)

SFB 1066 Barz, Zentel

cooperation with Irina Alberg

Monitoring of the different fractions of the bioorthogonal reaction.
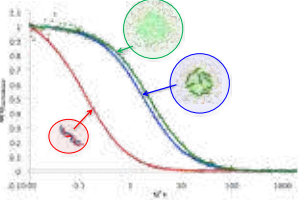

Loading efficiency

Complexation of cationic nanohydrogel particles with siRNA.
[4] Nuhn, et al. (2012)

SFB 1066 Schmidt, Helm, Zentel

Besides the determination of the hydrodynamic radius of the carrier system FCS can be used to estimate the number of siRNA molecules per particle. For this purpose the fluorescence brightness (FB) of the siRNA and the siRNA loaded particle were compared.


siRNA: R_H = 2 nm; FB = 9 kHz/molecule
siRNA + particle: R_H = 35 nm; FB = 370 kHz/particle
Loading efficiency: 370/9 ≈ 40 siRNA/particle

Stability of non cross-linked micelles

Block copolymer micelles are promising drug nanocarriers. We studied the stability of PeptoMicelles in blood plasma by analyzing the possess of unimers exchange. To this end unimers were labeld either with Oregon Green or Alexa 647 dye and "blue", "red" or "blue-red" (as positive control) micelles were prepared. With dual color fluorescence cross-correlation spectroscopy (FCCS), the distinct exchange tendency of the different labeled diblock-polymers between the PeptoMicelles were observed.

SFB 1066 Bartz, Zentel
Cooperation with Kerstin Johann
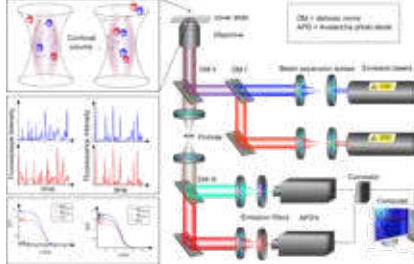
In FCCS the fluorescence intensity signals of the Oregon Green and Alexa647 are cross correlated. Hereby, simultaneous diffusion of double labeled micelles through the confocal volume is quantified by the increase of the amplitude of the cross-correlation curve as seen for the positive control sample (A). The fact that there is no cross-correlation in the mixture (B) indicates that the micelles show no exchange dynamic.
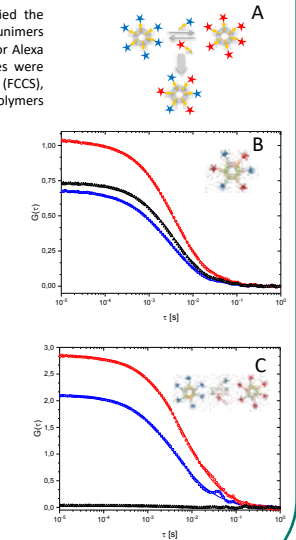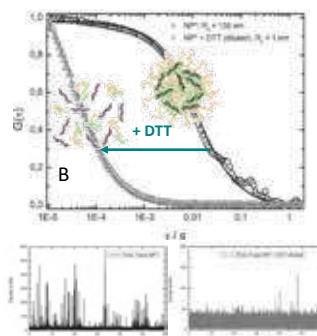

Release from nanocarriers

Degradation and release in buffer
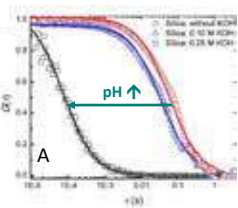
pH induced degradation of silica nanocapsules with sulforhodamine trapped in the shell (A).
[5] Hood, et al. (2015) **SFB 1066 Landfester**

siRNA-loaded cationic nanohydrogel particles containing a disulfide-modified spermine cross-linker. Degradation and release of fluorescently labeled siRNA after reduction with DTT (B).
[6] Nuhn, et al. (2014)
SFB 1066 Zentel

Nanocarriers' characterization in blood

Nanocarrier characterization with FCS in whole blood is difficult to execute, because blood is densely crowded with cells and posses a high absorption in the UV-Vis range. To overcome these obstacles, the measurement were performed with an continuous flow and nanocarrier labeled with an NIR dye that have excitation emission wavelengths in the range 700-1100 nm. The blood cell contribution to the autocorrelation function must be subtracted.
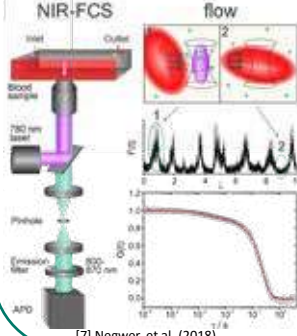
Stability measurements of core-crosslinked micelle nanocarriers in blood (B). The IRDye®800CW were either covalently or noncovalently loaded to the micelle nanocarrier. The blood measurements was done in an continuous flow. The noncovalently loaded IRDye®800CW were fully released from the core-crosslinked micelle nanocarrier in blood, whereas the covalently loaded dye remain inside the micelle nanocarrier.

Blue: covalently loaded IRDye
green: noncovalent loaded IRDye

[7] Negwer, et al. (2018)
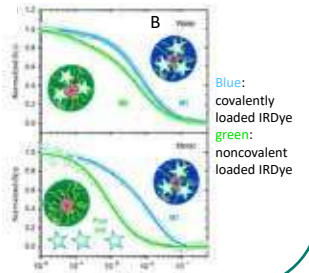
References

[1] K. Koynov, H.-J. Butt, *Current Opinion in Colloid & Interface Science* **2012**, *17*, 377-387.
[2] S. Kramer, D. Svatunek, I. Alberg, B. Grafen, S. Schmitt, L. Braun, A. H. A. M. van Onzen, R. Rossin, K. Koynov, H. Mikula, R. Zentel, *Biomacromolecules* **2019**, 20, 10, 3786-3797
[3] I. Tabujew, C. Freidel, B. Krieg, M. Helm, K. Koynov, K. Mullen, K. Peneva, *Macromolecular rapid communications* **2014**, *35*, 1191-1197.
[4] L. Nuhn, M. Hirsch, B. Krieg, K. Koynov, K. Fischer, M. Schmidt, M. Helm, R. Zentel, *ACS nano* **2012**, *6*, 2198-2214.
[5] M. A. Hood, U. Paiphansiri, D. Schaeffel, K. Koynov, M. Kappl, K. Landfester, R. Muñoz-Espí, *Chemistry of Materials* **2015**, *27*, 4311-4318.
[6] L. Nuhn, L. Braun, I. Overhoff, A. Kelsch, D. Schaeffel, K. Koynov, R. Zentel, *Macromolecular rapid communications* **2014**, *35*, 2057-2064.
[7] I. Negwer, A. Best, M. Schinnerer, O. Schäfer, L. Capeloa, M. Wagner, M. Schmidt, V. Mailänder, M. Helm, M. Barz, H.-J. Butt, K. Koynov, *Nat Commun* **2018**, 9, 5306.

Max Planck Institute for Polymer Research

Stimulation of Immune Cells with adjuvant-loaded protein-based Nanoparticles in the Context of Melanoma Therapy

Jenny Schunke, David Paßlick, Natkritta Hüppe, Katharina Landfester, Volker Mailänder

UNIVERSITÄTSmedizin.
Department of Dermatology

MAX PLANCK INSTITUTE FOR POLYMER RESEARCH

Introduction

In the context of medical applications, nanoparticles (NPs) are developed as versatile delivery systems for the treatment of tumors and infectious diseases. With their adjustable properties, nanoparticles enable protected drug transport and targeting of cells and tissues. Here, we have introduced novel protein-based nanocapsules (NCs) for effective, simultaneous delivery of antigen and adjuvant combinations to dendritic cells (DCs). The targeting of these professional antigen-presenting immune cells with NCs is of particular interest, since it allows guiding the immune response in a desired direction. Our aim is to develop an efficient treatment tool for melanoma therapy based on NPs. Therefor, we encapsulate combinations of common adjuvants to induce a strong and directed immune response by targeting DCs, which can then activate T cells for a specific anti-tumor response.

Material and Methods

Nanocapsules:

OVA/HSA

MDP, R848, (Poly I:C)

Mice:
Wildtype C57BL/6 and transgenic OT-I and OT-II (both C57BL/6 background) mice were bred and maintained in the Translational Animal Research Center of the University Medical Center Mainz under pathogen-free conditions on a standard diet. CD8^{+} OT-I T cells recognize OVA$_{257-264}$ peptides in the context of H-2K^b, and CD4^{+} OT-II T cells are specific for OVA$_{323-339}$ peptide in the context of H-2 I-A^b and I-A^d.

Primary immune cells of bone marrow and spleen:
All primary immune cells were obtained from mice. They were grown and treated in specific cell culture media and maintained at 37 °C and 10 % CO_2. In all experiments the cells were handled under sterile conditions. Splenic T Cells were isolated using the MACS Miltenyi Biotec CD4^{+} or CD8^{+} T Cell Isolation Kit mouse.

Flow cytometric analysis:
Single cell suspensions were incubated with Fc-block (2.4G2) for 10 min at 4°C and incubated with monoclonal Abs (eBioscience: αCD11c-PE-Cy7, αMHC-II-eFl450, αCD80-PE, αCD86-FITC). Data were acquired with Attune NxT (Life Science) and analyzed using AttuneNxT software.

Results

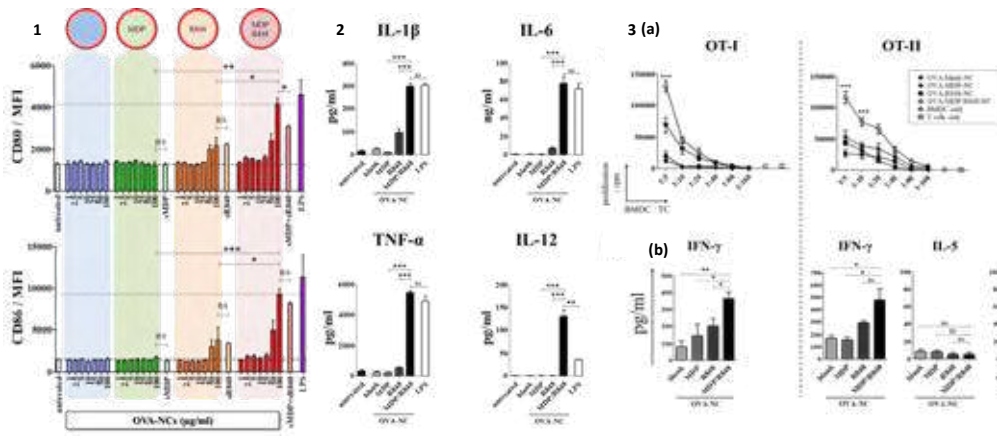### 1) Superadditive DC stimulation with double adjuvant-loaded OVA-NCs

Fig. 1 Stimulation of BMDCs with MDP/R848-OVA-NCs leads to maturation, increased secretion of proinflammatory cytokines and T cell proliferation. (1) BMDCs (2 x 10^5 cells/ml) were treated with OVA-blank- (blue), OVA-MDP- (green), OVA-R848 (orange) or OVA-MDP/R848-NCs (red) as indicated for 24 h. For comparison, equimolar amounts of sMDP (383 ng/ml) and sR848 (111 ng/ml) alone or in combination were used as stimulants. LPS (100 ng/ml) treated BMDCs were used as positive control. Surface expression of CD80 and CD86 on BMDCs was measured by flow cytometry based on MFIs. Dashed lines indicate expression levels of the untreated control, dotted lines those induced by the highest concentration of OVA-MDP-R848-NCs (mean ± SD; n=3). *p < 0.05, **p < 0.01, ***p < 0.001. (2) Cytokine contents in supernatants of BMDCs (1 x 10^6 cells/ml) treated with adjuvant-loaded OVA-NCs (100 µg/ml) for 24 h were analyzed by CBA. LPS treated BMDCs were used as positive control (mean ± SD; n=3). **p < 0.01, ***p < 0.001. (3) BMDCs (1 x 10^6 cells/ml) were incubated with OVA-blank-, OVA-MDP-, OVA-R848- or OVA-MDP/R848-NCs (each 100 µg/ml) for 24 h. (a) For proliferation measurement, titrated numbers of pre-treated BMDCs (starting with 10^5 cells) were co-cultured with OVA peptide-specific OT-I and OT-II T cells (each 5 x 10^5 cells) in triplicates in 96 well plates. Proliferation was recorded in cpm by ^3H-thymidine incorporation, applied after three days of BMDC/T cell co-culture for 16 h. Proliferation of BMDCs and T cells without treatment was used as control (n=3). (b) Supernatants of BMDC/T cell co-culture were collected after 3 days, and cytokines of interest were measured by CBA (mean ± SD, n=3). *p < 0.05, **p < 0.01, ***p < 0.001, OVA-MDP/R848-NC vs. OVA-R848-NC, unless otherwise indicated.

2) The triple combination of MDP, R848 and Poly I:C in HSA-NCs leads to strong stimulation of splenic DCs and BMDCs
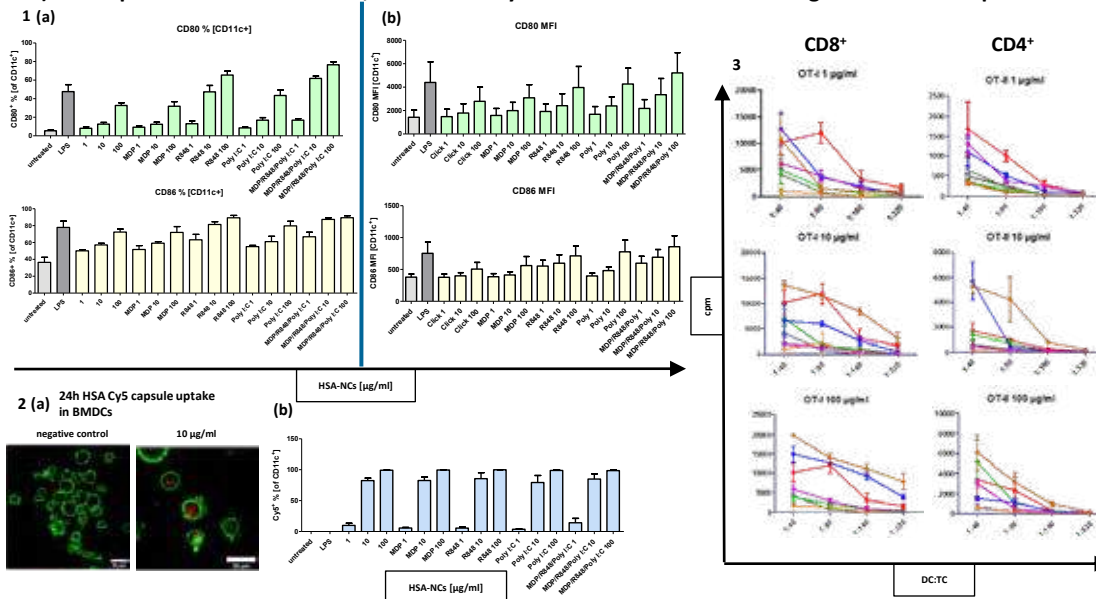

Fig. 2 Stimulation of DCs with MDP/R848/Poly I:C-HSA-NCs enhances the expression of maturation markers and induces strong T Cell proliferation in vitro. (1) (a) BMDCs (1 x 10^5 cells/ml) and (b) whole spleen suspension (2,5 x 10^6 cells/ml) were treated with HSA-blank-, HSA-MDP-, HSA-R848-, HSA-Poly I:C- or HSA-MDP/R848/Poly I:C-NCs for 24 h. LPS (100 ng/ml) treated BMDCs/splenic cells were used as positive control. Surface expression of CD80 and CD86 on BMDCs/ splenic DCs was measured by flow cytometry based on MFIs or %. (2) (a) BMDCs (8 x 10^5 cells/ml) were treated with HSA-MDP/R848/Poly I:C-NCs [10 µg/ml] for 24 h in 15 µ slides. The Uptake of the NCs was evaluated by fluorescence microscopy. (b) BMDCs (1 x 10^5 cells/ml) were treated with HSA-blank-, HSA-MDP-, HSA-R848-, HSA-Poly I:C- or HSA-MDP/R848/Poly I:C-NCs for 24 h. NC-Uptake was measured by flow cytometry based on %. (3) BMDCs (1 x 10^6 cells/ml) were incubated with HSA-blank-, HSA-MDP-, HSA-R848-, HSA-Poly I:C- or HSA-MDP/R848/Poly I:C-NCs [1/10/100 µg/ml] for 24 h. For proliferation measurement, titrated numbers of pre-treated BMDCs (starting with 10^5 cells) were co-cultured with OVA peptide-specific OT-I and OT-II T cells (each 5 x 10^5 cells) in triplicates in 96 well plates. Proliferation was recorded in cpm by ^3H-thymidine incorporation, applied after three days of BMDC/T cell co-culture for 16 h. Proliferation of BMDCs and T cells without treatment was used as control (n=3).

Outlook

- *In vivo* T Cell proliferation
- Establishment of B16-Ova-Luc-melanoma model *in vivo* and application of OVA-NCs
- OVA-independant B16-model: application of antigen- and adjuvant-loaded NCs

Summary

We could show supperadditive effects of R848/MDP and R848/MDP/Poly I:C encapsulated in OVA- and HSA-NCs concerning the maturation and cytokine secretion of DCs as well as a stronger T cell proliferation compared to treatments with single adjuvants.

References

D. Paßlick et al.: Delivering all in one: Antigen-nanocapsule loaded with dual adjuvant yields superadditive effects by DC-directed T cell stimulation. Journal of Controlled Release (2018), 289, 23-34.

CLINAM
European Foundation for Clinical Nanomedicine
BASEL, SWITZERLAND

12/2020
Basel, October 25~28

جامعة الإسراء
Isra University
Amman - Jordan

Shield and Sword against SARS-CoV-2

Andrei P. Sommer, Faculty of Science, ISRA-University, Amman, Jordan
andrei.sommer@alumni.uni-ulm.de

BRIDGING BETWEEN LLLT AND NANOMEDICINE

Low level light therapy (LLLT) uses moderate light intensities delivered by red to near infrared (R-NIR) lasers or light emitting diodes (LED) operating in the 1- 4 J/cm² dose window, effective in vitro and in vivo. Pulsed LLLT forces cells and tissues to uptake nanoparticles (1).
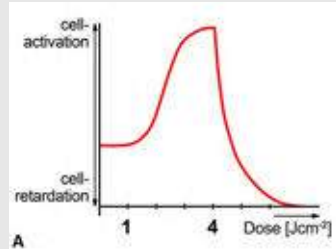
A: Classical biostimulatory dose window in LLLT, where light intensities are comparable to the solar constant (ca. 1 kW/m²).


B: Rapid wound healing and minimal scar formation after cosmetic surgery.

APPLICATIONS: treatment of diabetic ulcers, dementia, depression, stroke, TBI, peripheral neuropathy, retinal disorders, oral mucositis, burns, inflammatory processes, infertility, cosmetic surgery. In viral infections LLLT can be used to upregulate the immune system, kill viruses and help cells to get rid of internal amyloid-β deposits (2). Except for the antiviral action, the therapeutic effects are explicable via ATP upregulation in mitochondria (3).

MITOCHONDRIAL PHOTO FIELD-EFFECT TRANSISTOR: The biological photo-FET model provides an intuitive explanation to the discovery that the frequencies 750 and 950 nm reduced the activity of COX (via inhibition of the reaction of CYTc and COX) and limited ROS generation in irradiated brains. The model explains the recovery of pigs 13.5 minutes post cardiac arrest, resuscitation and irradiation of the foreheads for 2 hours with an intensity of 2W/m² distributed on 10 powerful LEDs – 5 operating at 750 and 5 at 950 nm (Mike Hüttemann, personal communication). What is so special about the wavelengths 750 and 950 nm?

MITOCHONDRIAL SOLAR SENSITIVITY: There are 2 pronounced minima in the R-NIR sector of the spectral solar irradiance, at 750 and 950 nm (**C**). During evolution mitochondria were not exposed to light except the sun. The simplest argument is that the mitochondrial photo-FET apparatus had no opportunity to adapt to these wavelengths. It is plausible that lack of adaptation to 750 and 950 nm results in a stronger perturbation of the H_2O barrier than for other wavelengths of the solar spectrum, inhibiting electron tunneling from CYTc to COX (6). Together with the findings of the Hüttemann group (7) this holds the promise to change the accepted brain death dogma.
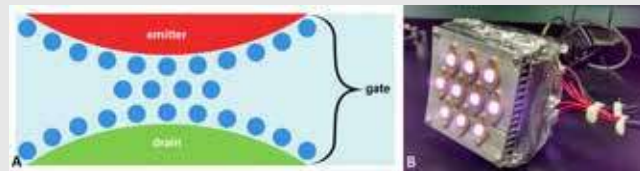
A: Biological photo-FET. Tunneling of electrons across 3 monolayers of H_2O between CYTc and COX is controlled by R-NIR light. Image: ref. 4. Probability for an electron incident on a potential U-E to cross a barrier of width L is $T=e^{-kL}$, where $k=\sqrt{(2m(U-E))}/\hbar$, with m and ħ standing for the electron mass and Planck constant h divided by 2π respectively.
B: Powerful LEDs used to rescue pigs from terminal brain damage 13.5 minutes post cardiac arrest. Courtesy: Maik Hüttemann.
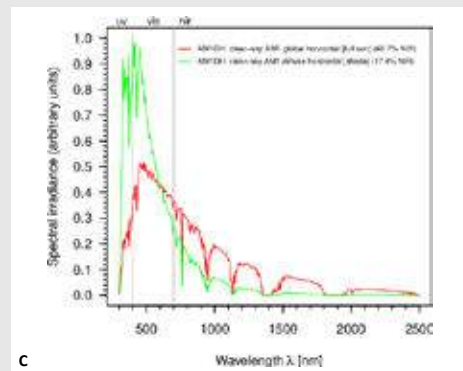
C: Solar spectral irradiances incident on a horizontal terrestrial surface in full sun (red) or shade (green) (5). Courtesy: Ronnen Levinson, Heat Island Group, Lawrence Berkeley National Laboratory.

HERPES LABIALIS: NO MORE CREAMS

A: Herpes labialis treated with Acyclovir, 8 days after manifestation of first symptoms. B: Herpes labialis treated with red laser light, 4 days after manifestation of first symptoms. Laser intensity ca. 15 times that of the solar constant. No inflammation, no pain, no bleeding, only a mild warm sensation.

Infection with HSV-1 is suspected to be a risk factor in the formation of Alzheimer's disease. Irradiation of the affected area at the time of the manifestation of the first symptoms with 650 nm laser light (2 W/cm2) for 5 min, twice a day for 2 consecutive days, prevented the outbreak. Assumption: the virus was killed by mitochondrial ROS, triggered by the high laser intensity.
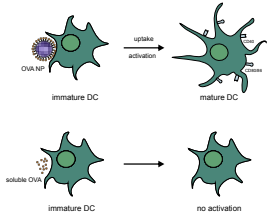
COVID-19 COULD TRIGGER ALZHEIMER'S

During a severe infection with all the lead symptoms of Covid-19, LLLT has been used to treat a painful frontal sinusitis (8). Could LLLT be extended to treat further manifestation of Covid-19? Recently, Ezzat et al. identified the viral protein corona as a critical factor for viral–host interactions and showed that that respiratory syncytial virus (RSV) and HSV-1 accumulate a protein corona in biological fluids, and that HSV-1 triggers amyloid-β aggregation (9). Possible involvement of SARS-CoV-2 in the etiology of Alzheimer's disease is sufficient motivation for further research efforts: While the moderate light doses used in LLLT are instrumental to support the immune defense via ATP upregulation – as could be useful in Covid-19 – ROS generation via higher light doses based on higher intensities could be used to destroy the coronavirus, in this case using pulsed light to prevent overheating and by avoiding the wavelengths 750 and 950 nm – shield and sword against SARS-CoV-2.

1. Sommer AP, Zhu D, Scharnweber T. J Control Release 2010;148:131-134.
2. Sommer AP, et al. Photomed Laser Surg 2012;30:54-60
3. Sommer AP, Haddad MKh, Fecht HJ. Sci Rep 2015;5:12029.
4. Shimada S, et al. EMBO J 2017;36:291-300.
5. Levinson R, Akbari H, Berdahl P. Solar Energy 2010;84:1717-1744.
6. Sommer AP. Ann Transl Med 2020;8:161.
7. Strubakos CD, et al. J Cereb Blood Flow Metab 2020;40:833-844.
8. Sommer AP, Försterling HD, Naber KG. Precis Nanomed 2020;3:541-548.
9. Ezzat K, et al. Nat Commun 2019;10:2331.

Polymer nanoparticles for delivering a model antigen to dendritic cells

Monika Stahl, Achim Goepferich
Department of Pharmaceutical Technology, University of Regensburg, Universitaetsstrasse 31, 93053 Regensburg, Germany.
✉Monika.Stahl@ur.de

Introduction

Delivering antigens to dendritic cells (DC) is a powerful approach in vaccine development, since dendritic cells are the most important and efficient antigen presenting cells in the body and are able to induce a strong and long-lasting T cell immunity efficiently protecting us against various pathogens [1].

Polymer nanoparticles offer an excellent platform for antigen delivery to dendritic cells. Due to their size, dendritic cells can easily capture and process them [2]. Additionally, they provide a broad range of possibilities to associate antigens with the nanoparticle, are biocompatible, non-toxic, and known to enhance the immune response towards antigens [3]. The goal of this study was to develop a nanoparticulate system capable of delivering the model antigen ovalbumin to dendritic cells and enhance immunogenicity.

## Results

Particle Preparation and Characterization

Ovalbumin (OVA) was covalently coupled to the surface of PEG-PLGA nanoparticles (NP) which were previously modified with a peptide linker.

Nanoparticles were characterized by dynamic light scattering (DLS).

The amount of ovalbumin on the nanoparticle surface was determined with a BCA assay, which was around 80 µg OVA per mg nanoparticle.
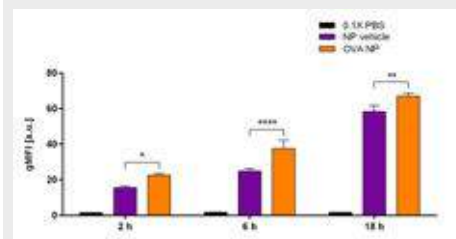
The absence of adsorbed OVA was verified by SDS PAGE.

For visualization purposes, the PLGA core was labeled with a fluorescent dye.
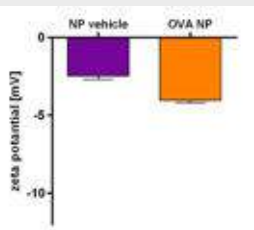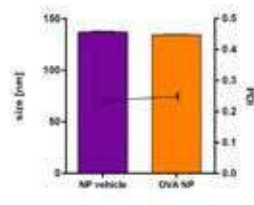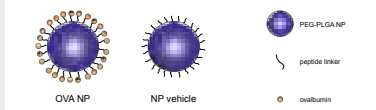

Cellular Uptake of Nanoparticles

Bone marrow derived dendritic cells (BMDCs) were incubated with fluorescently labeled nanoparticles and cellular internalization was determined by flow cytometry after different time points.

Antigen presenting and control nanoparticles were both internalized because their size (< 500 nm) is optimal for uptake by dendritic cells. OVA NP show at every time point a significantly higher uptake compared to the nanoparticles without antigen, suggesting that ovalbumin on the surface of nanoparticles enhances the internalization by addressing uptake mediating receptors like the mannose receptor CD206.

Stimulation of Bone Marrow derived Dendritic Cells
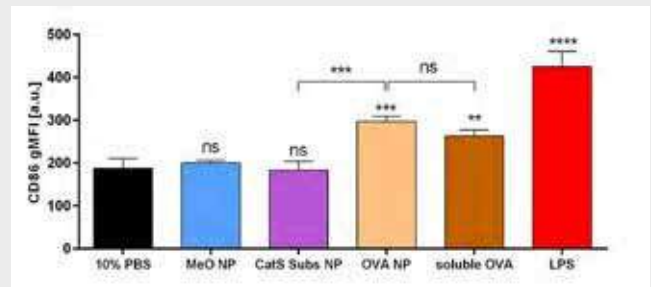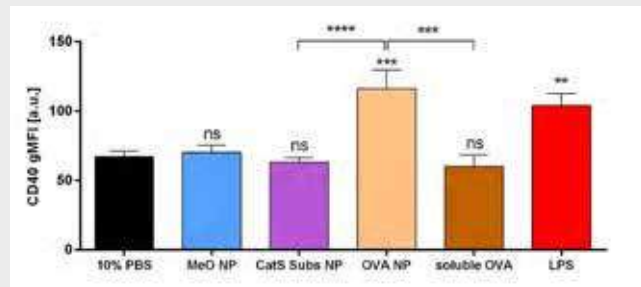
Stimulation potential of the nanoparticles was evaluated by incubating BMDCs for 18 h with OVA NP, soluble ovalbumin or NP vehicle adjuvanted with CpG ODN1826. The final stimulation concentration of OVA was 50 µg/ml and LPS was used as positive control. The stimulation pattern was analyzed by detecting different maturation markers on the surface of dendritic cells using flow cytometry.

The particle associated ovalbumin showed a higher degree of activation compared to the soluble antigen, suggesting that the nanoparticle system enhances the immunogenicity of ovalbumin. In contrast, the antigen-free nanoparticles did not show any activation of BMDCs, indicating that they are pyrogen-free and not immunogenic.

Conclusion

Here we show that we successfully developed a nanoparticle platform for delivering the model antigen ovalbumin to dendritic cells. The results confirm that the particle system is taken up by BMDCs and is able to activate them to a higher degree than the antigen in its soluble form. More so, this shows the potential of the technology to be used as a vaccine platform.

References

[1] Kastenmüller, Wolfgang; Kastenmüller, Kathrin; Kurts, Christian; Seder, Robert A. Dendritic cell-targeted vaccines-hope or hype?, Nature reviews. Immunology 14, 705–711 (2014).
[2] Foged, Camilla; Brodin, Birger; Frokjaer, Sven; Sundblad, Anne Particle size and surface charge affect particle uptake by human dendritic cells in an in vitro model, International journal of pharmaceutics 298, 315–322 (2005)
[3] Han, Jinyu; Zhao, Dandan; Li, Dan; Wang, Xiaohua; Jin, Zheng; Zhao, Kai Polymer-Based Nanomaterials and Applications for Vaccines and Drugs, Polymers 10 (2018)

Reduced magnetic coupling in ultra-small iron oxide T_1 MRI contrast agents

Fabian H. L. Starsich[1,2],

C. Eberhardt[3], K. Keevend[1,2], A. Boss[3], A.M. Hirt[4], I. K. Herrmann[1,2], S. E. Pratsinis[5]

[1]Nanoparticle Systems Engineering Laboratory (ETH Zurich, Switzerland)
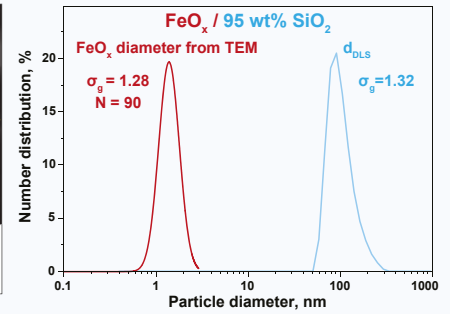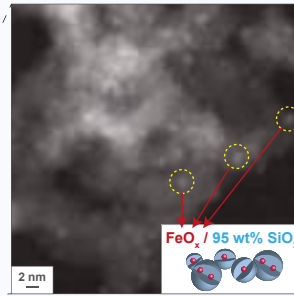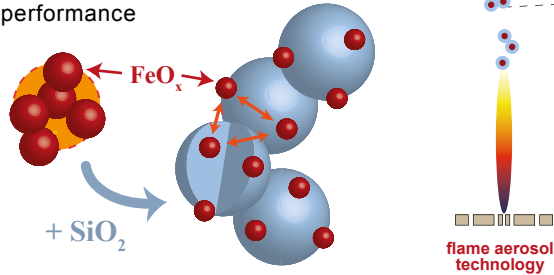[2]Particles-Biology Interactions (EMPA St. Gallen)
[3]Institute of Diagnostic and Interventional Radiology (University Hosptial Zurich), [4]Institute of Geophysics (ETH Zurich),
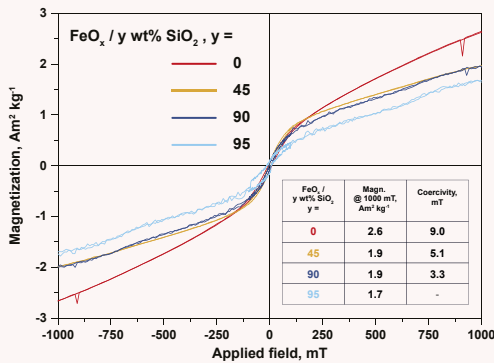[5]Particle Technology Laboratory (ETH Zurich),
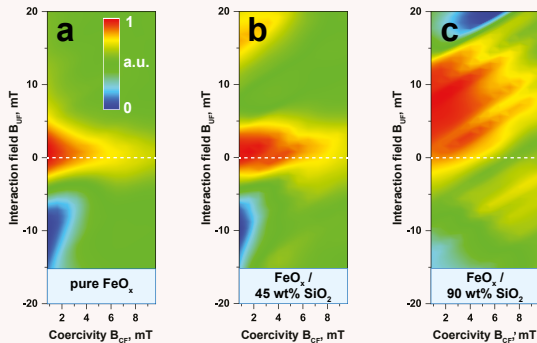
fabian.starsich@empa.ch - www.nse.ethz.ch

Everyday clinically applied MRI contrast agents are based on paramagnetic Gd-complexes. However, especially for patients with kidney failures the administration of such drugs can be life-threatening, as toxic Gd_{3+} ions have been shown to potentially leach out of these structures.[1] Here, flame-made ultra-small (< 4 nm) iron oxide (Fe_xO_y) nanoparticles supported on SiO_2 are investigated as a promising biocompatible alternative. Special emphasis is put on the interplay between morphology and MRI performance
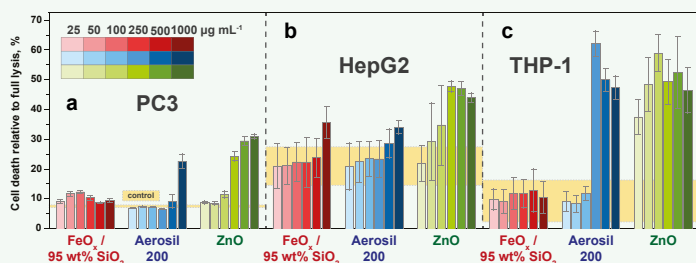

FeO$_x$

+ SiO$_2$

flame aerosol technology

FeO_x / 95 wt% SiO$_2$
FeO_x diameter from TEM
σ_g = 1.28
N = 90
d_{DLS}
σ_g = 1.32

FeO_x / 95 wt% SiO$_2$

Para-magnetic Properties

FeO$_x$ / y wt% SiO$_2$, y =

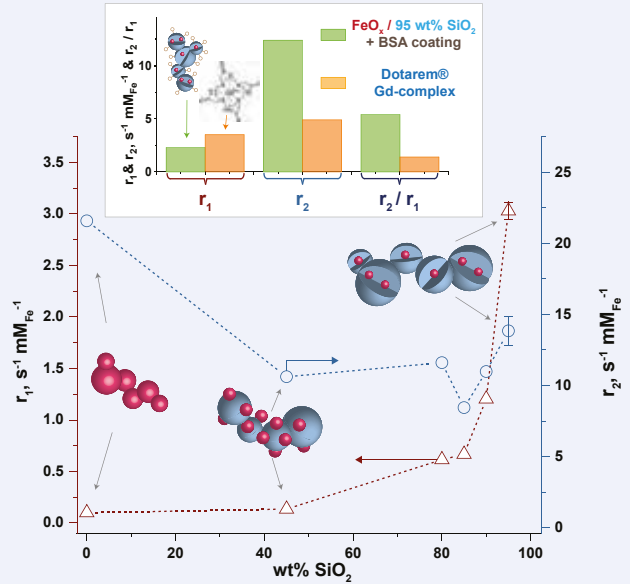| FeO$_x$ / y wt% SiO$_2$, y =	Magn. @ 1000 mT, Am^2 kg^{-1}	Coercivity, mT
0	2.6	9.0
45	1.9	5.1
90	1.9	3.3
95	1.7	-

Hysteresis curves **(top)** and first order reversal curves **(bottom)** indicate the reduced effective magnetic size due to the FeO$_x$ decoupling cause by the SiO$_2$ support.

a — pure FeO$_x$
b — FeO$_x$ / 45 wt% SiO$_2$
c — FeO$_x$ / 90 wt% SiO$_2$

High Biocompatibility

25 50 100 250 500 1000 µg mL^{-1}

a — PC3
b — HepG2
c — THP-1

control

FeO$_x$ / 95 wt% SiO$_2$ Aerosil 200   ZnO

Excellent MRI performance

r_1 & r_2, s^{-1} mM$_{Fe}^{-1}$ & r_2 / r_1

FeO$_x$ / 95 wt% SiO$_2$ + BSA coating
Dotarem® Gd-complex

r_1 r_2 r_2 / r_1

r_1, s^{-1} mM$_{Fe}^{-1}$

r_2, s^{-1} mM$_{Fe}^{-1}$

wt% SiO$_2$

MRI relaxivites as a function of SiO$_2$ content **(top)** show increased performance due to magnetic decoupling. T_1 MR-images **(bottom)** proof excellent contrast enhancement abilities of FeO$_x$ / 95 wt% SiO$_2$ in tissues.

5 mg mL^{-1} 0.1 mg mL^{-1} 1 mg mL^{-1}

1cm

inversion time   = 700   1000   1200 ms

0.1 mg mL^{-1} 1 mg mL^{-1} 5 mg mL^{-1}
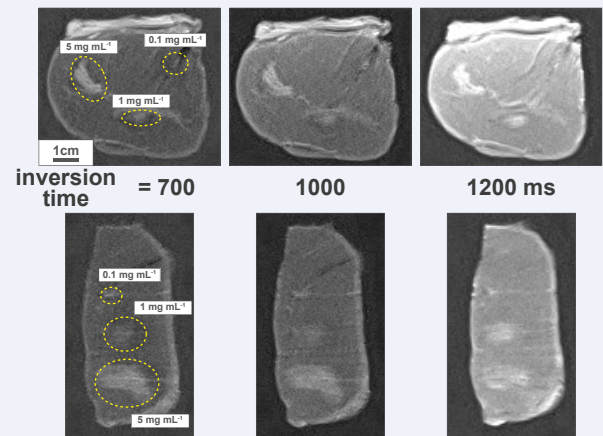
Conclusions

- Scalable (kg h^{-1}) production of biocompatible (Gd-free) T_1 MRI contrast agents with high contrast performance

- SiO$_2$ support reduces magnetic coupling and increases T_1 relaxivity

[1] J.G. Penfield, R.F.Reilly, Nat Clin Pract Nephrol 3 (2007), 654.
[2] F.H.L. Starsich, C. Eberhardt, K. Keevend, A. Boss, A.M. Hirt, I.K. Herrmann, S.E. Pratsinis, ACS Appl Bio Mater 1 (2018), 783-791.

Customizable Immune Modulating Nanogel-platform for Cancer Immunotherapy

Judith Stickdorn[2], Jennifer Hahlbrock[1], Christian Czysch[2], Danielle Arnold-Schild[1], Stephan Grabbe[1], Hansjörg Schild[1], Lutz Nuhn[2]

[1]University Medical Center of JGU and [2]Max-Planck-Institute for Polymer Research

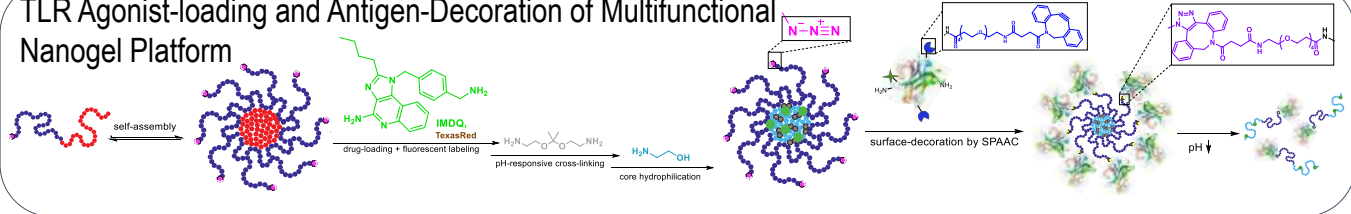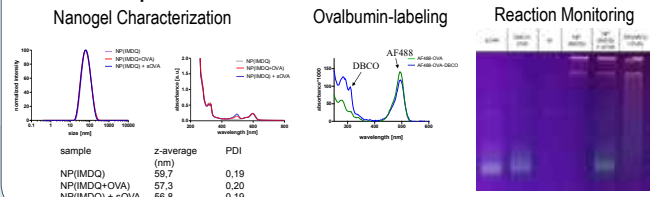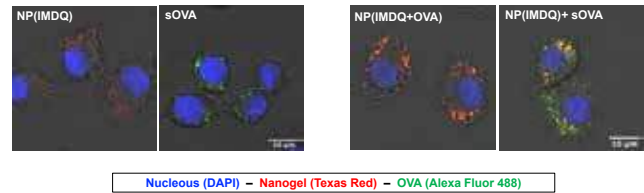**MAX-PLANCK-INSTITUT FÜR POLYMERFORSCHUNG**

TLR Agonist-loading and Antigen-Decoration of Multifunctional Nanogel Platform

self-assembly → drug-loading + fluorescent labeling → pH-responsive cross-linking → core hydrophilication → surface-decoration by SPAAC → pH ↓

IMDQ, TexasRed

Multi-component Vaccine Characterization

Nanogel Characterization

NP(IMDQ)
NP(IMDQ+OVA)
NP(IMDQ) + sOVA

sample	z-average (nm)	PDI
NP(IMDQ)	59,7	0,19
NP(IMDQ+OVA)	57,3	0,20
NP(IMDQ) + sOVA	56,8	0,19

Ovalbumin-labeling

DBCO
AF488
AF488-OVA
AF488-OVA-DBCO

Reaction Monitoring

Co-delivery of Nanogels and Antigens

NP(IMDQ) | sOVA | NP(IMDQ+OVA) | NP(IMDQ)+ sOVA

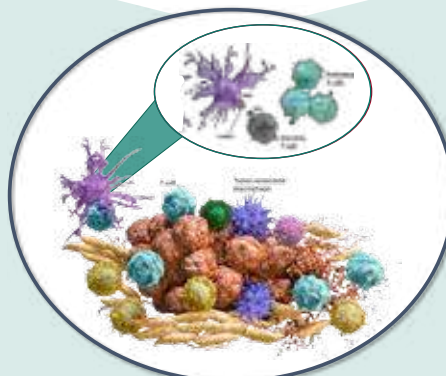**Nucleous (DAPI)** — **Nanogel (Texas Red)** — **OVA (Alexa Fluor 488)**

Chemical Concept

Immune Evasion of Tumor Cells[1]

- down regulation of MHC
- expression of immune suppressive cytokines
- inhibitory ligands (PD-L1)

✓ in-situ Re-activation of Immune Cells by Vaccination Strategies[2]

- activation of antigen-presenting cells (APC)
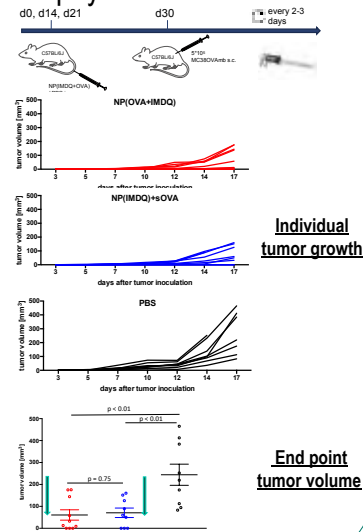- expansion of antigen-specific CD4 and CD8 T cells

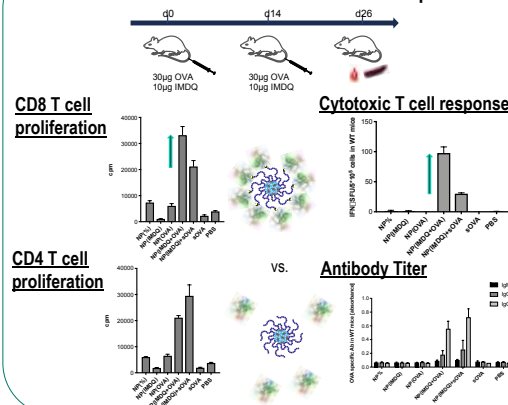### Tumor Immunotherapy by Polymer-based Multi-component nanogels

- Co-delivery of adjuvants and antigens in a hydrophilic nanogel system
- Toll-like receptor agonist IMDQ as potent immune adjuvant[3] and ovalbumin (OVA) as model-antigen covalently bound to nanogel' core and surface
- Multi-component systems show anti-tumor effect on surface neoantigen expressing tumor after systemic i.v. injection

Prophylactic Tumor Model

NP(OVA+IMDQ)
NP(IMDQ)+sOVA
PBS

Individual tumor growth

End point tumor volume

p < 0.01
p < 0.01
p = 0.75

NP(IMDQ+OVA) | NP(IMDQ)+sOVA | PBS

Immunological Outcome

in vitro and ex vivo Immune Response

d0 — d14 — d26

30µg OVA 10µg IMDQ

CD8 T cell proliferation

Cytotoxic T cell response

CD4 T cell proliferation

vs.

Antibody Titer

IgM
IgG1
IgG2a

Therapeutic Tumor Model

NP(OVA+IMDQ)
NP(IMDQ)+sOVA
PBS

Individual tumor growth

End point tumor volume

p < 0.01
p < 0.05
p = 0.25

NP(IMDQ+OVA) | NP(IMDQ)+sOVA | PBS
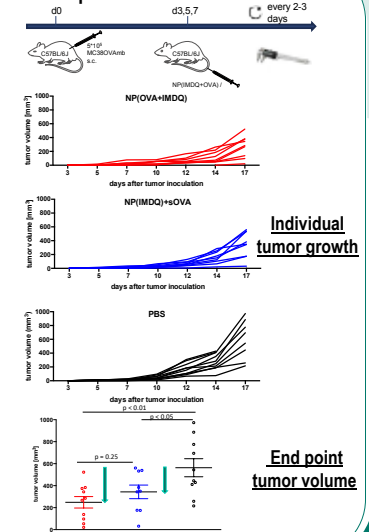
References

[1] D. S. Vinay, E. P. Ryan, G. Pawelec, W. H. Talib, J. Stagg, E. Elkord, T. Lichtor, W. K. Decker, R. L. Whelan, H. M. C. S. Kumara, et al., *Semin. Cancer Biol.* **2015**, *35*, S185–S198.

[2] K. Palucka, J. Banchereau, *Nat. Rev. Cancer* **2012**, *12*, 265–277.

[3] L. Nuhn, N. Vanparijs, A. De Beuckelaer, L. Lybaert, G. Verstraete, K. Deswarte, S. Lienenklaus, N. M. Shukla, A. C. D. Salyer, B. N. Lambrecht, et al., *Proc. Natl. Acad.Sci.* **2016**, *113*, 8098–8103.

[4] central figure modified from: Bristol-Myers Squibb, "Revealing the Potential of the Immune System in Cancer," https://www.immunooncologyhcp.bmsinformation.com/antitumor-immunity, **2017**.

stickdornj@mpip-mainz.mpg.de

Chinese Academy of Sciences
Key Lab for Biomedical Effects of Nanomaterials and Nanosafety

National Center for Nanoscience and Technology of China
11 Beiyitiao, Zhongguancun
Beijing 100190, China

Tel: 0086-13121717399
0098-9122863184
E-mail: taleb@nanoctr.cn.

Normalization of tumor blood vessels, a regulation factor in tumor microenvironment and immune system function

Mohammad Taleb[†,‡], Mona Atabakhshikashi[†], Yazhou Wang[†], Zeinab FarhadiSabet[†,‡], Zhao Ying[*,†], Guangjun Nie[*,†, ‡]

[†]CAS Key Laboratory for Biomedical Effects of Nanomaterials and Nanosafety, CAS Center of Excellence in Nanoscience, National Center for Nanoscience and Technology, Beijing 100190, P. R. China, [‡]University of Chinese Academy of Sciences, Beijing 100049, P. R. China
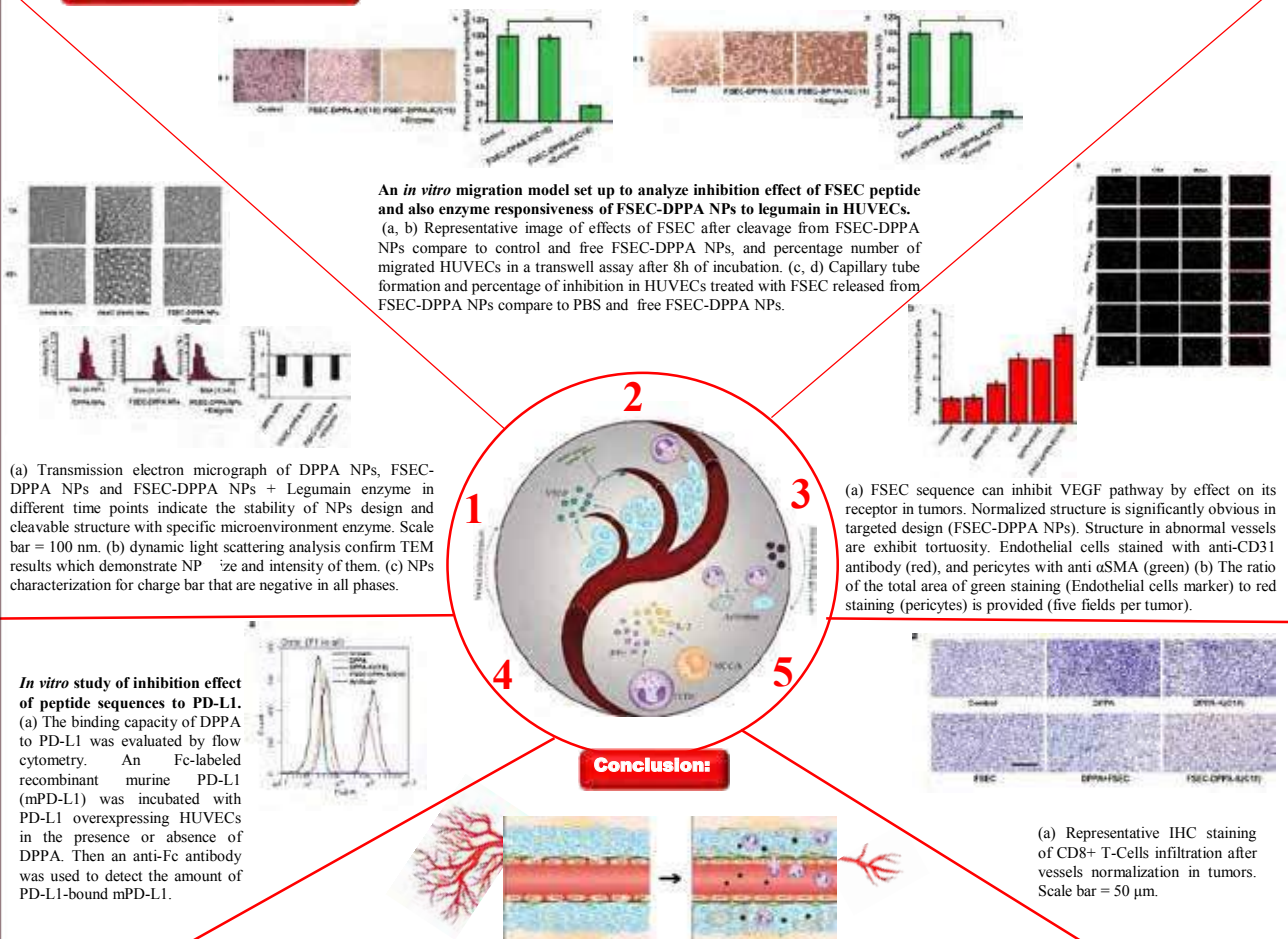
Abstract:

Blood vessels are required for the nutrition and growth of tumors. There are many strategies against tumor vasculature and antiangiogenics to depriving nutrients and oxygen of tumors. Normalization of abnormal tumors vasculature in structure and function to provide vessels for more oxygen efficiency and drug delivery, which result in alleviate the hypoxia. It has been reported that hypoxia zones help the resistance to T cell infiltration. Normalization of vessels increased the number of immune cells in the tumor microenvironment. In this paper, we conjugate the FSEC peptide sequence to another peptide (DPPA) sequences, which designed to make a nanoparticle shape by a carbonic hydrophobic chain. FSEC can significantly normalize vessels. Second part of designed NPs can target PD-L1 (programed death ligand 1) which expressed on tumor cells. Interaction of PD-L1 with programmed death ligand (PD-1) could block the function and act of immune cells against tumor cells. Here we demonstrated that by normalization of tumor vessels, the number of T cells increased, and then by blocking of PD-L1 their function activated. this work introduced a smart peptide nanoparticle with dual targeting.

Objectives:

Vessel normalization, immune cells, peptide, nanoparticle, PD-1, PD-L1

Results and Discussion:

An *in vitro* migration model set up to analyze inhibition effect of FSEC peptide and also enzyme responsiveness of FSEC-DPPA NPs to legumain in HUVECs.
(a, b) Representative image of effects of FSEC after cleavage from FSEC-DPPA NPs compare to control and free FSEC-DPPA NPs, and percentage number of migrated HUVECs in a transwell assay after 8h of incubation. (c, d) Capillary tube formation and percentage of inhibition in HUVECs treated with FSEC released from FSEC-DPPA NPs compare to PBS and free FSEC-DPPA NPs.

(a) Transmission electron micrograph of DPPA NPs, FSEC-DPPA NPs and FSEC-DPPA NPs + Legumain enzyme in different time points indicate the stability of NPs design and cleavable structure with specific microenvironment enzyme. Scale bar = 100 nm. (b) dynamic light scattering analysis confirm TEM results which demonstrate NP size and intensity of them. (c) NPs characterization for charge bar that are negative in all phases.

(a) FSEC sequence can inhibit VEGF pathway by effect on its receptor in tumors. Normalized structure is significantly obvious in targeted design (FSEC-DPPA NPs). Structure in abnormal vessels are exhibit tortuosity. Endothelial cells stained with anti-CD31 antibody (red), and pericytes with anti αSMA (green) (b) The ratio of the total area of green staining (Endothelial cells marker) to red staining (pericytes) is provided (five fields per tumor).

***In vitro* study of inhibition effect of peptide sequences to PD-L1.**
(a) The binding capacity of DPPA to PD-L1 was evaluated by flow cytometry. An Fc-labeled recombinant murine PD-L1 (mPD-L1) was incubated with PD-L1 overexpressing HUVECs in the presence or absence of DPPA. Then an anti-Fc antibody was used to detect the amount of PD-L1-bound mPD-L1.

(a) Representative IHC staining of CD8+ T-Cells infiltration after vessels normalization in tumors. Scale bar = 50 μm.

Conclusion:

Smart dual targeting nanoparticles were used to deliver to tumor microenvironment and target two aim after cleaving by specific tumor microenvironment enzyme (legumain). By proving the biocompatibility and safety of peptide sequences and NPs shape, data presented here show the normalization effect of first sequence which released by legumain and result in increasing the immune cells number. FSEC markedly normalized tumor vessels which released from FSEC-DPPA NPs. In normalized tumor vessels quantity of immune cells contain CD8+ and NK cells increased. Second part of targeting PD-L1 not only in cell treated groups, but also at *in vivo* could activate immune system. Activated immune system by utilizing FSEC-DPPA NPs have been approved by increasing amount of IL2 and IFN-γ. T cells activated by targeting them with DPPA sequence, which remained from FSEC-DPPA NPs.

Supramolecular Platform for The Design of Modular Multifuntional Glycoconjugate Antitumor Vaccines

M. Urschbach[1], R. Attariya[2], D.Straßburger[1], N. Stergiou[2], E.Schmitt[2], P.Besenius[1]

[1]Institute of Organic Chemistry, University of Mainz, Germany; [2]Institute of Immunology, University Medical Center of Mainz, Germany

SFB 1066

Abstract

Classical synthetic vaccine approaches commonly utilize immunogenic carrier proteins of biological origin to immobilize antigens or haptens. These bioconjugation approaches suffer from problems like low reproducibility and poor characterizability of the products. Deviations in the antigen loading are inevitable and may cause issues in biomedical applications. An ideal fully synthetic vaccine should only contain chemically well-defined molecules that are bound in a controlled and multivalent manner onto the carrier.

Supramolecular polymers are a promising scaffold for the presentation of antigenic structures to the immune system due to the dynamic nature of the underlying polymerization process.[1] Each monomer can be individually functionalized and comprise a targeting structure,[2] immunostimulant or antigen. Simple mixing in aqueous solution results in the formation of co-polymers which harbor all desired features on their surface and are able to trigger an antigen-specific humoral immune response.

We present the synthesis and immunological evaluation of a novel modular and fully synthetic antitumor vaccine. The supramolecular platform is employed for versatile multivalent presentation of different epitopes and capable of inducing a strong immune response directed against tumor-associated MUC1, comprising a Tn and 2,3-ST antigen, in C57BL/6 mice.

Nanoplatform For Vaccine Development
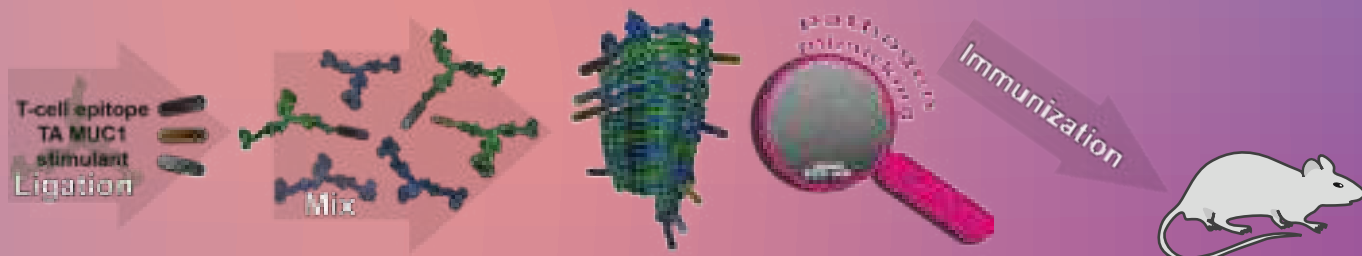
The human immune system is a powerful machinery, evolutionary specialized on recognizing and eliminating nano-scaled pathogens of viral, bacterial or xenobiotic origin. For the design of fully synthetic vaccines, supramolecular polymers can serve as well-defined scaffold to present relevant tumor-associated structures to immune cells on their surface. Bioorthogonality of the conjugation chemistry enables convenient, "last step" attachment of relevant pharmacological structures which was successfully demonstrated for peptidic B-cell and T-cell epitopes as well as heterocyclic immunostimulants. No effects of cytotoxicity or immunogenicity of the self-assembling scaffold were seen in the mouse model. The fact that each monomer bears only one cargo gives the chemists full control on the total amount of active ingredients in the vaccine. Blending diversely loaded monomers with different functional moieties and subsequent copolymerization in physiological media is a promising and modular approach to construct multivalent fully synthetic antitumor vaccines.

Mucin 1 Glycopeptide

Tumor-associated (TA) MUC1 is a glycopeptide and diagnostic marker for different epithelial malignancies like mammary carcinoma, prostate, pancreatic or lung cancer. Besides its overexpression on tumor tissue, aberrant glycosylation due to dysregulation of glycosyltransferases is observed. This leads to truncated short glycan side chains resulting in the collapse of the peptide backbone. As a consequence of the defect glycan-shielding the peptide structure can be accessed and recognized by immunecells.

Immunological Evaluation
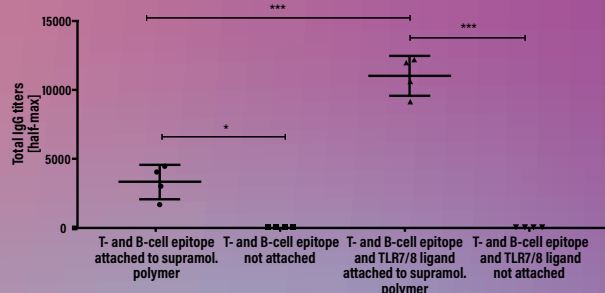
Five C57BL/6 mice were immunized with a vaccine comprising MUC1 B-cell epitope (30)[4], Ttox p30 Th-cell epitope and TLR7/8 ligand decorated FM- together with SM+. After 3 boosts the sera were collected from the tail vein of the mice and analyzed for antibodies directed against TA MUC1. We found robust titers of all antibody classes whereas IgG memory-related type was dominating. Furthermore a significant level IgG2c antibodies was detected. The latter are capable to induce antibody dependent cell-mediated cytotoxicity (ADCC) due to the recruitment of NKs, Mφs and DCs via Fc of the corresponding immunoglobulin. The application of unbound epitopes resulted in significantly lower IgG titers demonstrating the power of the supramolecular approach.

Biomimetic Synthesis Tumor-Associated MUC1
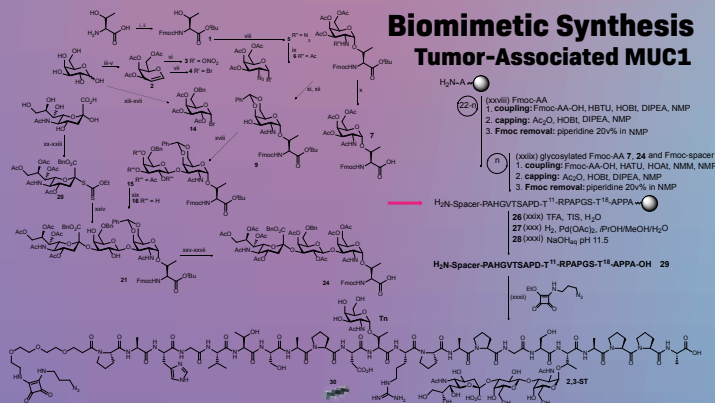
Synthesis of the tumor-associated MUC1 antigen. (i). Fmoc-OSu, NaHCO₃, acetone, 97% (ii). DCC, CuCl, tBuOH, 65% (iii). Ac₂O, HClO₄ (iv). HBr, AcOH, 98% (v). Zn, AcOH, 87% (vi). CAN, NaN₃, MeCN, 40% (vii). LiBr, MeCN, 70% (viii). AgClO₄, Ag₂CO₃, toluene/DCM, 44% (iix). Zn, AcOH, Ac₂O, THF, 55% (ix). NaOMe/MeOH 68%. (x). DCM, TFA, H₂O, 91% (xi). NaOMe, MeOH, 68% (xii). α,α-dimethoxytoluene, p-TosOH, MeCN 82%. (xiii). Hg(CN)₂, MS 3 Å, CH₃NO₂, DCM, 92%. (xix). NaOMe/MeOH 75% (xx). Ac₂O, pyridine, quant. (xxi). 1.Cs₂CO₃, EtOH/H₂O, 2.BnBr, DMF, 67% (xxii). AcCl, H₂O, quant. (xxiii). KEX, EtOH, 82% (xxiv). MeSBr, AgOTf, MS 3 Å, MeCN/DCM, 53% (xxv). AcOH, 70%. (xxvi). Ac₂O, pyridine, DMAP, 97% (xxvii). TFA, anisole, quant. (xxxi). 450 mM Na₂HPO₄(aq), 74%.

Self-Assembling Peptide Motivs
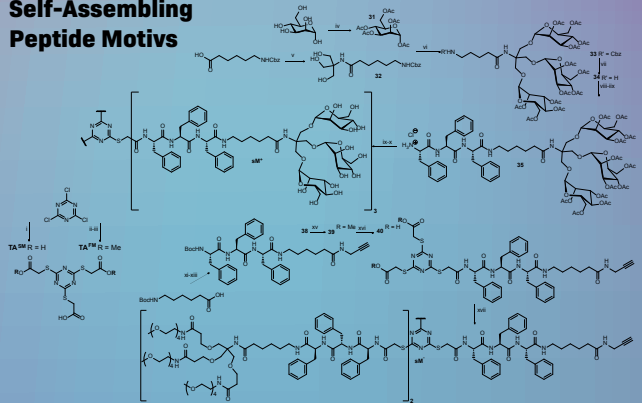
Synthesis of the decorated monomers (i). HSAcOH, DIPEA, MeCN, 60%, (ii). HSAcOMe, K₂CO₃, THF, 58% (iii). HSAcOH, DIPEA, MeCN, 56% (iv). pyridine, Ac₂O, DMAP, quant. (v). TRIS, EEDQ, EtOH, 60% (vi). BF₃×Et₂O, DCM, 40% (vii). dioxane, TFA, Pd/C, H₂, 79% (viii). Boc-Phe₃-OH, PyBOP, HOAt, DIPEA, 66% (iix). TFA/DCM,- TIS, quant. (ix). TASM, PyBOP, DIPEA, DMF, 88% (x). NaOMe, MeOH, quant. (xi). HATU, HOAt, DMF, 56% (xii). DCM/TFA, 97% (xiii). Boc-Phe₃-OH, PyBOP, HOAt, NMM, DMF, 95% (xiv). DCM/TFA, TIS, 96% (xv). TAFM, HATU, HOAt, DIPEA, DMF, quant. (xvi). LiOH 0.1 M, THF 72% (xvii). Dnd-Ahx-Phe₃-OH, PyBOP, HOBt, DIPEA, DMF, 79%.

[1] H. Frisch, Y. Nie, S. Raunser, P. Besenius, *Chem. - A Eur. J.* 2015, 21, 3304–3309.
[2] D. Straßburger, N. Stergiou, M. Urschbach, H. Yurugi, D. Spitzer, D. Schollmeyer, E. Schmitt, P. Besenius, *ChemBioChem* 2018, 19, 912–916.
[3] B. Palitzsch, N. Gaidzik, N. Stergiou, S. Stahn, S. Hartmann, B. Gerlitzki, N. Teusch, P. Flemming, E. Schmitt, H. Kunz, *Angew. Chemie Int. Ed.* 2016, 55, 2894–2898.
[4] D. Straßburger, M. Glaffig, N. Stergiou, S. Bialas, P. Besenius, E. Schmitt, H. Kunz, *ChemBioChem* 2018, 19, 1142–1146.

"Characterization of MDA-MB-231 and Mexican Breast Cancer Cells by Raman Microspectroscopy and Atomic Force Microscopy"

Vazquez Meza F.M. [1], Acosta Elías M.A. [1], Velázquez Contreras C.A. [1], Pieles U. [2], Burgara Estrella A. [1], Silva Campa E. [1], Angulo Molina A. [1]

(1) University of Sonora; Mexico, (2) University of Applied Sciences and Arts Northwestern; Switzerland.

Introduction

Breast cancer is one of the most common cancer in women around the world (American Cancer Society, 2020). In Mexico, the identification and selection of therapeutic targets drugs for breast cancer is made on African American or Caucasian breast cancer cell lines (Holiday, 2011). Differences in prognosis, aggressiveness and mortality have been observed regarding ethnicity, this raises the issue on how representative these few cell lines are of most of the global population (Dai, 2017). Recently, breast cancer cell lines were obtained and partially characterized from tumors removed from Mexican women, by the first time. Raman spectroscopy and atomic force microscopy (AFM) were used to analyze Mexican breast cancers cells to complement the cellular characterization and identify potential biochemical and nanoscale topographic biomarkers.

Aim

To obtain the biochemical fingerprint and nano-topographic surface characterization of MDA-MB-231 and Mexican breast cancer cells by Raman Spectroscopy and AFM.

Importance

The characterization by Raman and AFM will allow us to have for the first time a biochemical and nanoscale reference framework. To the best of our knowledge this is the first work with cell lines obtained from women living in the northwestern of Mexico.

Methodology
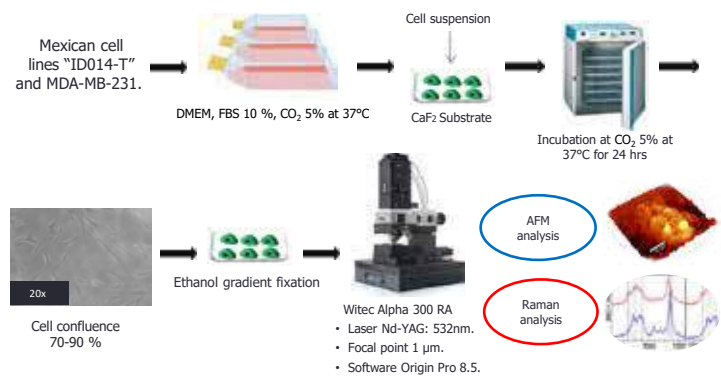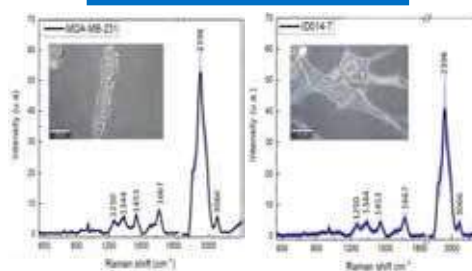

Results

Raman Spectroscopy

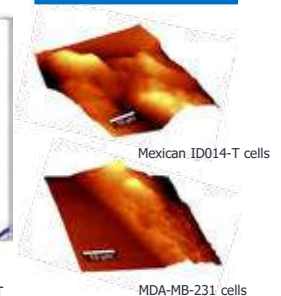Fig 1. Raman spectra fingerprint of MDA-MB-231 and Mexican ID014-T cells. (Preliminary results)

Raman shift (cm⁻¹)	Peak assignment	Component
941	Polysaccharides (amylose amylopectin)	Carbohydrates (skeletal modes)
1007	C-C aromatic ring	Protein (Phenylalanine)
1250	C-N stretch	Protein (Amide III)
1344	Adenine bases	Nucleic acid (nucleobases)
1453	Structural mode	Protein
1667	-C=O- stretch	Protein (Amide I)
2938	C-H stretch	Lipid/Protein
3066	C-H stretch	Lipid (acyl chains)

Table 1. Composition fingerprint with their corresponding functional group or molecule. (Preliminary results)

AFM

Mexican ID014-T cells

MDA-MB-231 cells

Fig 2. 3D Surface topography 50 x 50 µm

Breast cancer cell line	Roughness nucleus (nm)	Roughness Periphery (nm)
MDA-MB-231	41.63 ± 7.94	42.67 ± 7.24
ID014-T	39.07 ± 6.70	37.21 ± 7.53

Table 2. Measurement of cell surface roughness of breast cancer cell lines. (Preliminary results)

Conclusion

It was possible to identified characteristic peaks of biomolecules found in other cancerous and non-cancerous breast cell lines as well as cell surface roughness. These results will allow us to compare similarities and differences between cells at biochemical nanoscale level.

Literature

1. American Cancer Society. 2020
2. Holliday, D.L., Speirs, V. Choosing the right cell line for breast cancer research. *Breast Cancer Res* **13,** 215 (2011). https://doi.org/10.1186/bcr2889
3. Dai, X., Cheng, H., Bai, Z., & Li, J. (2017). Breast Cancer Cell Line Classification and Its Relevance with Breast Tumor Subtyping. *Journal of Cancer*, 8(16), 3131–3141. https://doi.org/10.7150/jca.18457

TGF-β inhibition combined with cytotoxic nanomedicine normalizes triple negative breast cancer microenvironment towards anti-tumor immunity

Chrysovalantis Voutouri[1], Myrofora Panagi[1], Fotios Mpekris[1],
John D Martin[2], Andreas Stylianou[1], Maria Louca[1], Kazunori Kataoka[2,3],
Horacio Cabral[2], Triantafyllos Stylianopoulos[1]

[1]Cancer Biophysics Laboratory, Department of Mechanical Engineering,
University of Cyprus, Cyprus. [2]The University of Tokyo, Bunkyo, Tokyo, Japan.
[3]Innovation Center of NanoMedicine, Kawasaki Institute of Industrial Promotion,
Kawasaki, Kanagawa, Japan

Introduction

➢ Tumor normalization strategies aim to improve tumor blood vessel functionality (i.e., perfusion) by reducing the hyper-permeability of tumor vessels or restoring compressed vessels.

➢ We re-purposed the TGF-β inhibitor tranilast, an approved anti-fibrotic and antihistamine drug, and combined it with Doxil nanomedicine to normalize the tumor microenvironment (TME), increase perfusion and oxygenation, and enhance anti-tumor immunity.
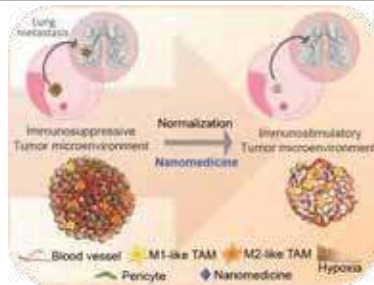
➢ Combination of tranilast with Doxil caused a reduction in extracellular matrix components and an increase in the intratumoral vessel diameter and pericyte coverage, indicators of TME normalization.

➢ Resulted in a significant increase in tumor perfusion and oxygenation and enhanced treatment efficacy as indicated.

➢ Combining tranilast with Doxil nanomedicine, significantly improved the efficacy of the immune checkpoint blocking antibodies anti-PD-1/anti-CTLA-4.
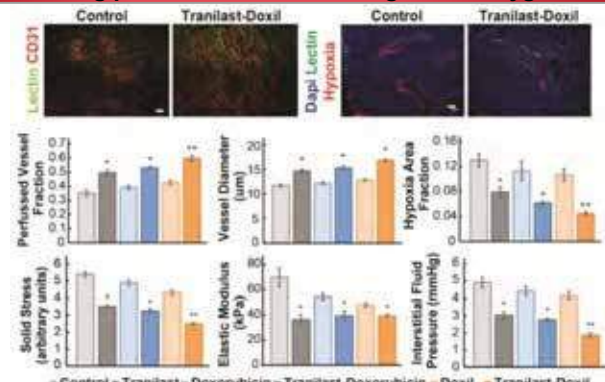
TME normalization improves the efficacy of both chemo- and nanomedicine

➢ Tranilast, doxorubicin or Doxil monotherapy did not induce any significant delay in tumor growth.

➢ Combination of tranilast with doxorubicin caused a 2-fold increase in doubling time of both 4T1 and E0771 tumors, whereas tranilast-Doxil combination produced a more than 3-fold increase in doubling time.

➢ Tranilast and doxorubicin alone had no effect on animal survival.

➢ Overall survival was modestly improved after Doxil monotherapy and tranilast–doxorubicin combinatorial therapy.

➢ The survival benefit was significantly improved following tranilast-Doxil combinatorial treatment compared to the rest of the groups.

➢ The effect of tranilast is necessary for chemotherapy and nanomedicine to exert their anticancer effects and prolong overall survival.

Doxil nanomedicine enhances tranilast mediated normalization effects in the primary tumors

➢ Tranilast-Doxil combination, significantly decreased collagen and hyaluronan levels.

➢ Tranilast-Doxil treated animals exhibited a modest but significant increase in pericyte coverage in tumor vessels, thereby highlighting the ability of tranilast-Doxil combination to promote vascular normalization.
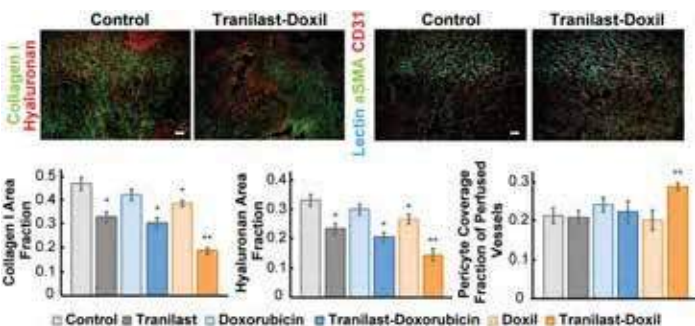
Enhanced tumor normalization by Doxil nanomedicine alleviates intratumoral fluid and solid pressure, increasing perfusion and enhancing tissue oxygenation

➢ Tranilast in combination with doxorubicin or Doxil increased vessel perfusion of tumors by 50% and 66%, respectively, whereas chemotherapy or nanomedicine alone had no effect on tumor perfusion compared to the control group.

➢ The vessel diameter increased in the tranilast-doxorubicin and tranilast-Doxil treated tumors.

➢ Pronounced reduction by 70% of hypoxia within the microenvironment of tranilast-Doxil treated group.

➢ Tranilast-Doxil combination significantly reduced (2-fold) interstitial fluid pressure (IFP) compared to other groups.

➢ Tranilast-Doxil combination, significantly decreased accumulation of solid stresses and stiffness elasticity.

Enhanced tumor normalization by Doxil nanomedicine improves efficacy of immunotherapy

➢ Tranilast-Doxil combinatorial therapy significantly reduced tumor growth by 60%.

➢ The combination of ICBs with tranilast-Doxil treatment led to the most significant reduction in tumor in both mammary tumor models, 4T1 and E0771.
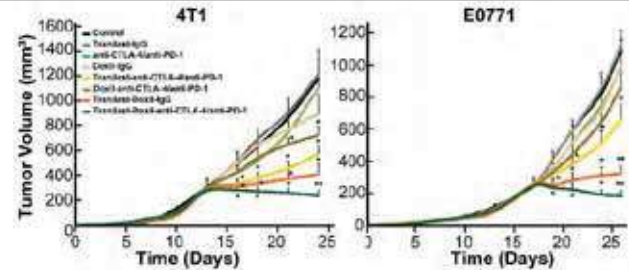
References

1. Panagi M, Voutouri C, Mpekris F, et al., *Theranostics*. 2020;10:1910-1922.
2. Voutouri C, Polydorou C, Papageorgis P, Gkretsi V, Stylianopoulos T. *Neoplasia*. 2016;18:732-41.
3. Polydorou C, Mpekris F, Papageorgis P, Voutouri C, Stylianopoulos T. *Oncotarget*. 2017;8:24506-17.
4. Papageorgis P, Polydorou C, Mpekris F, Voutouri C, et al. *Scientific reports*. 2017; 7: 46140

Acknowledgment

The development of a novel nucleic acid based immunotherapy for treatment of solid tumours

Adam A. Walters, Gemma Santacana-Font, Jin Li, Nadia Rouatbi, Julie Wang and Khuloud T. Al-Jamal

Institute of Pharmaceutical Science, School of Cancer and Pharmaceutical Sciences, Kings College London, Franklin-Wilkins Building, Stamford St, London SE1 9NH
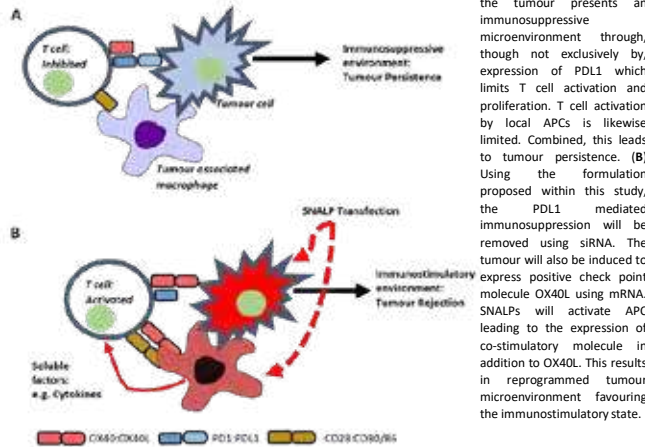
Contact: adam.walters@kcl.ac.uk

Background

1. Immunotherapy is a revolutionary approach in the treatment of cancer that, over the past decades, has transformed the landscape of cancer therapy.

2. Check point molecules may be divided into two categories; inhibitory (such as **PD-L1**) and stimulatory (such as **OX40L**). The former serving to dampen the immune response and the latter serving to amplify the immune response.

3. **Simultaneous blockade of both stimulatory and inhibitory checkpoints maybe advantageous** however the use of the monoclonal antibody platform may result in dose limiting **toxicity** due to off target effects

Aim

To develop a novel rationally formulated '**genetic immunotherapy**' regime based on the **co-delivery of siRNA** to remove inhibitory check point molecules while simultaneously delivering **mRNA** expressing stimulatory checkpoint molecules to the tumour environment in a clinically relevant stable nucleic acid lipid nanoparticle (**SNALP**).

Proposed Mechanism:

(A) Under diseased conditions the tumour presents an immunosuppressive microenvironment through, though not exclusively by, expression of PDL1 which limits T cell activation and proliferation. T cell activation by local APCs is likewise limited. Combined, this leads to tumour persistence. (B) Using the formulation proposed within this study, the PDL1 mediated immunosuppression will be removed using siRNA. The tumour will also be induced to express positive check point molecule OX40L using mRNA. SNALPs will activate APC leading to the expression of co-stimulatory molecule in addition to OX40L. This results in reprogrammed tumour microenvironment favouring the immunostimulatory state.

Stable Nucleic Acid Lipid Particles (SNALPs)

Ionisable Lipid (Dlin-MC3-DMA)
Neutral Lipid (DOPE)
mRNA (mOX40L)
siRNA (siPD-L1)
Ceramide-PEG
Cholesterol

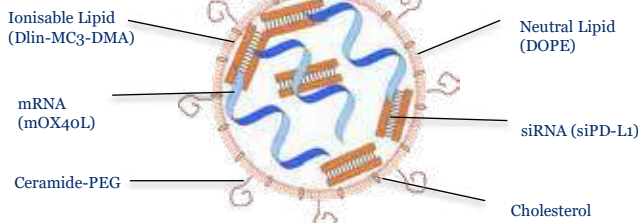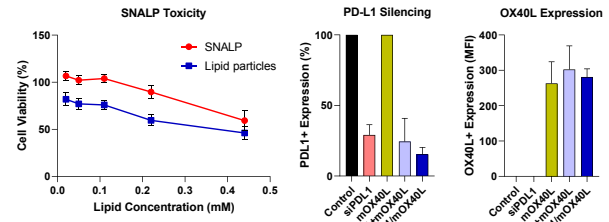**Table 1: Physical characterisation of SNALPS**

Nucleic acid	Size (d.nm)	PDI	Charge (mV)	EE (%)
siRNA	145.05	0.22	16.04	80.90
mRNA	144.87	0.19	17.37	89.58
mRNA-siRNA	153.62	0.23	16.86	93.55

SNALPs produced fall within the desired size and charge range regardless of nucleic acid content with an 80-95% encapsulation efficiency
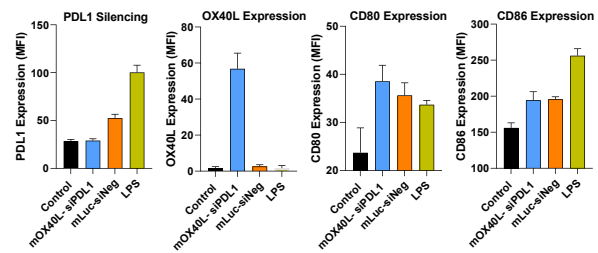
Results

### A. SNALP Transfection of B16F10 cells *in vitro*

Result: SNALPs exhibit a low toxicity profile and are suitable for simultaneously delivery of siRNA and mRNA

B. SNALP can transfect J774 Macrophage

Result: SNALPs successfully transfect macrophage resulting in expression of OX40L and upregulation of maturation markers CD80/86. PDL1 upregulation was inhibited

C. Therapeutic Efficacy of SNALPs in B16F10 model
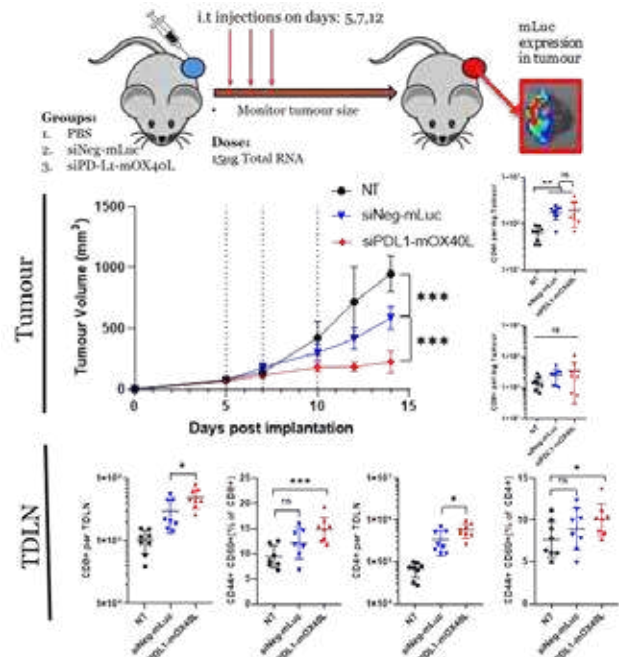
Result: Dual targeting SNALPs significantly inhibit tumour growth and result elevated numbers of activated T cells in the TDLN

Conclusions

SNALPs can successfully deliver both siRNA and mRNA simultaneously and is a therapeutically viable candidate for future immune checkpoint regimes
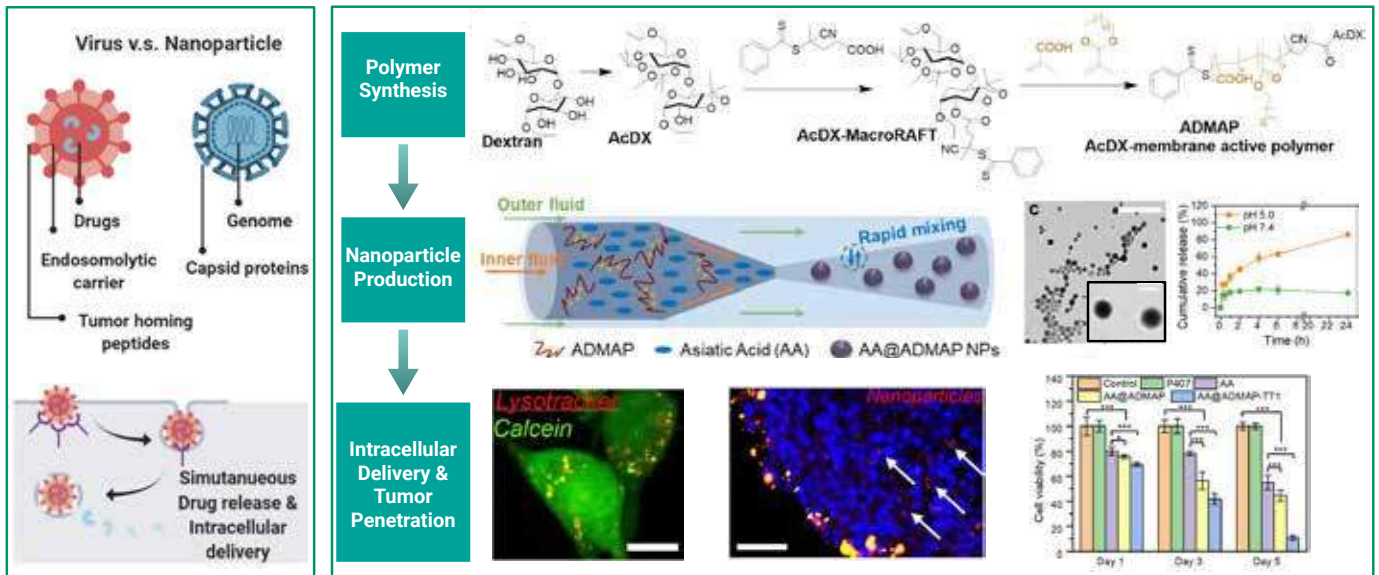
A Virus-Mimicking pH-Responsive Membrane-Active Polymeric Nanoparticle for Intracellular Delivery of Antitumor Therapeutics

Shiqi Wang   shiqi.wang@helsinki.fi

HELSINGIN YLIOPISTO
HELSINGFORS UNIVERSITET
UNIVERSITY OF HELSINKI

Virus v.s. Nanoparticle

Drugs — Endosomolytic carrier — Tumor homing peptides

Genome — Capsid proteins

Simutanueous Drug release & Intracellular delivery

Polymer Synthesis

Dextran → AcDX → AcDX-MacroRAFT → ADMAP AcDX-membrane active polymer

Nanoparticle Production

Outer fluid — Inner fluid — Rapid mixing

ADMAP — Asiatic Acid (AA) — AA@ADMAP NPs

Intracellular Delivery & Tumor Penetration

Lysotracker / Calcein

Nanoparticles

Control — P407 — AA — AA@ADMAP — AA@ADMAP-TT1

Cell viability (%): Day 1, Day 3, Day 5

Cumulative release (%): pH 5.0, pH 7.4 — Time (h)

SANTOSLAB

P-Selectin Targeted Polysaccharide Submicroparticles for Thrombolytic Therapy

Alina Zenych[1], R. Aid-Launais[1], C. Jacqmarcq[2], L. M. Forero Ramirez[1], L. Fournier[1], T. Bonnard[2], D. Letourneur[1], C. Chauvierre[1]

1. Inserm U1148 - LVTS, Université de Paris,[1] Université Paris 13, Paris
2. INSERM U1237 Physiopathology and Imaging of Neurological Disorders, GIP Cyceron, Caen France

Nanomedicine in atherothrombosis

Atherosclerosis is an **asymptomatic disease** which may lead to acute and severe cardiovascular events due to the atherosclerotic plaque rupture [1].

The intravenous injection of **recombinant tissue plasminogen activator** (rtPA), the **gold standard** for thrombolytic therapy, possesses high risks of **intracranial hemorrhages and neurotoxicity** [2]. Hence, there is an unmet medical need for **safe nanomedicine-based** thrombus targeting **solutions**. The objective is to create a **non-toxic, biocompatible, and biodegradable nanocarrier** which is functionalized with a targeting agent and suitable for thrombotic diseases. Fucoidan, a natural anionic polysaccharide, holds thrombus targeting properties due to its strong **affinity for P-selectin**, an inflammatory adhesion molecule [3], [4].
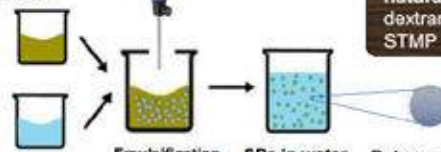
SPs targeting P-Selectin

Overexpression of P-Selectin on the thrombus
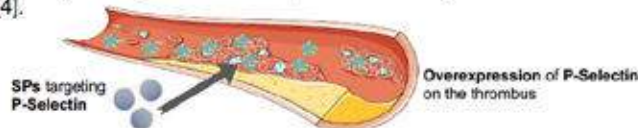
Synthesis of the particles

100% Polysaccharide Submicroparticles (SPs)

Organic phase
· Vegetable oil
· Surfactant

Aqueous phase
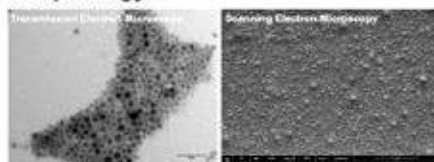· Polysaccharides
· Crosslinking agent
· Water

Emulsification Crosslinking 50°C

SPs in water

Polysaccharide SPs with Fucoidan

Water-in-oil emulsification was combined with a crosslinking process of natural polysaccharides: dextran, fucoidan with STMP

A simple and reproducible **emulsification** based **crosslinking protocol** allows to obtain **100% polysaccharide SPs**
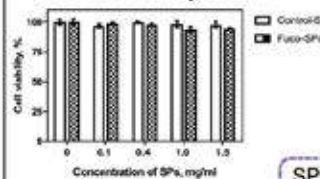
Physico-chemical characterization

Morphology

Transmission Electron Microscopy   Scanning Electron Microscopy

Size (nm)	Zeta Potential (mV)	Fucoidan,% w/w
662.2 ±26.7	-30.30 ±0.14	9

Spherical polysaccharide SPs carry a negative surface charge and possess a **hydrogel** behavior as they swell in water

Biocompatibility

Cytocompatibility
Resazurin assay at 24h

Control-SPs
Fuco-SPs

Cell viability, %
Concentration of SPs, mg/ml

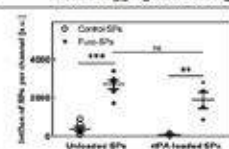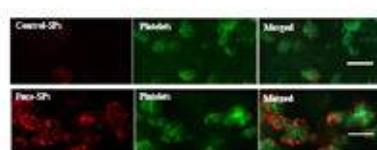### Hemocompatibility

Hemolysis, %
Concentration of Fuco-SPs, mg/ml
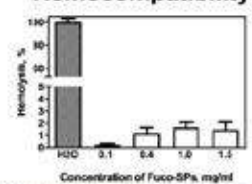
SPs exhibit a favorable biocompatibility profile *in vitro*

Targeting P-Selectin *in vitro*

Method: *In vitro* flow assay

Microfluidic pump
Human arterial flow: 60 µl/min
Biochip
Platelet aggregates coating

SPs with fucoidan

Control-SPs / Platelet / Merged
Fuco-SPs / Platelet / Merged

Control-SPs
Fuco-SPs

Influx of SPs per channel [a.u.]
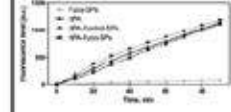Unloaded SPs   rtPA-loaded SPs

Fucoidan increases binding of unloaded or rtPA-loaded SPs to platelet aggregates at arterial shear stress conditions *in vitro*

Thrombolytic activity
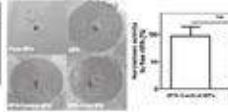
rtPA (Actilyse®) loaded onto Fuco-SPs via adsorption

rtPA
Fucoidan

Amidolytic activity
PefaFluor® assay
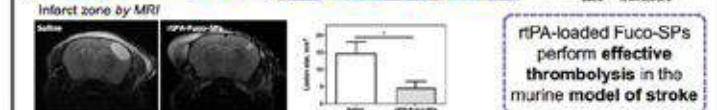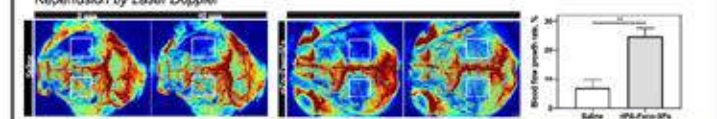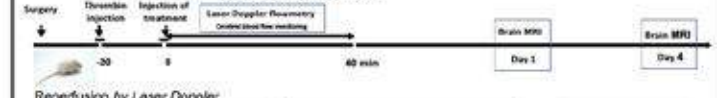
Fuco-SPs

Time, min

Fibrinolytic activity
Fibrin-plate agarose test

rtPA-loaded SPs maintain their **amidolytic** and **fibrinolytic** activity *in vitro* in contact with fibrin

Thrombolytic efficacity *in vivo*
Stroke thrombin model

Surgery   Thrombin injection   Injection of treatment   Laser Doppler Flowmetry Cerebral blood flow monitoring   Brain MRI Day 1   Brain MRI Day 4

-20   0   40 min

Reperfusion by Laser Doppler

Blood flow perfusion, %
Saline   rtPA-Fuco-SPs

Infarct zone by MRI
Saline   rtPA-Fuco-SPs

Lesion size, mm³
Saline   rtPA-Fuco-SPs

rtPA-loaded Fuco-SPs perform **effective thrombolysis** in the murine model of stroke

Conclusion

✓ Biocompatible & biodegradable 100% polysaccharides SPs
✓ Functionalized with fucoidan to target **P-selectin** in thrombus area
✓ rtPA loaded onto SPs via **adsorption**
✓ rtPA-loaded SPs maintain **amidolytic** and **fibrinolytic** activity *in vitro* and perform **effective thrombolysis** *in vivo* stroke model

➢ **Proof of the concept** study for **safe** preclinical thrombolytic therapy

References: [1] P. Libby, Intern. Med. 263 (2008) 517–527. [2] J. Álvarez-Sabin, Lancet Neurol. 12 (2013) 689–705. [3] K.J. Woollard, Inflamm. Allergy Drug Targets. 6 (2007) 69–74. [4] L. Bachelet, Biochim. Biophys. Acta - Gen. Subj. 1790 (2009) 141–146.

CONOTOXIN-DERIVED BIOMIMETIC PEPTIDES FOR ACTIVE TARGETING OF NEUROBLASTOMA CELLS

Hana Zivotska[1], Simona Rex[1,2], Michal Mokry[1,3], Yazan Haddad[1,2], Zbynek Heger[1,2]

[1]Department of Chemistry and Biochemistry, Mendel University in Brno, Zemedelska 1, Brno CZ-613 00, Czechia
[2]Central European Institute of Technology, Brno University of Technology, Purkynova 123, Brno CZ-612 00, Czechia
[3]Department of Biomedical Engineering, Brno University of Technology, Technicka 12, Brno CZ-616 00, Czechia

Introduction

The use of conotoxin-derived peptides as targeting ligands with a natural affinity towards overexpressed human norepinephrine receptors (hNET) on the neuroblastoma cells can lead to reduced cytotoxicity on off-target non-malignant cells and increased efficiency of cancer therapy.

As a means for testing the active targeting of neuroblastoma cells by conotoxin-derived peptides, potential chemotherapeutic drug ellipticine (Elli) was chosen. In order to decrease the negative side effects and also increase the biocompatibility and specificity of this drug in patient's organism, it was encapsulated into a biocompatible nanocarrier apoferritin (EcLHFRT).
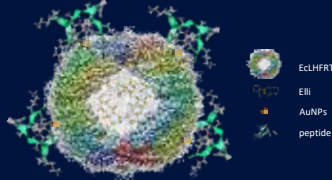

EcLHFRT
Elli
AuNPs
peptide

Fig. 1 Putative structure of targeted EcLHFRT nanocarrier
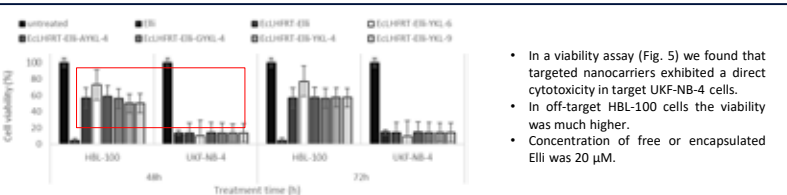

Fig. 5 Comparison of viability of off-target (HBL-100) and target cells (UKF-NB-4) after treatment with free Elli, non-targeted and targeted nanocarrier

- In a viability assay (Fig. 5) we found that targeted nanocarriers exhibited a direct cytotoxicity in target UKF-NB-4 cells.
- In off-target HBL-100 cells the viability was much higher.
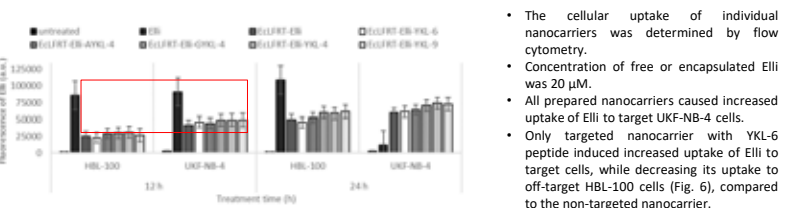- Concentration of free or encapsulated Elli was 20 μM.

Fig. 6 Comparison of uptake of free and encapsulated Elli in off-target and target cells

- The cellular uptake of individual nanocarriers was determined by flow cytometry.
- Concentration of free or encapsulated Elli was 20 μM.
- All prepared nanocarriers caused increased uptake of Elli to target UKF-NB-4 cells.
- Only targeted nanocarrier with YKL-6 peptide induced increased uptake of Elli to target cells, while decreasing its uptake to off-target HBL-100 cells (Fig. 6), compared to the non-targeted nanocarrier.
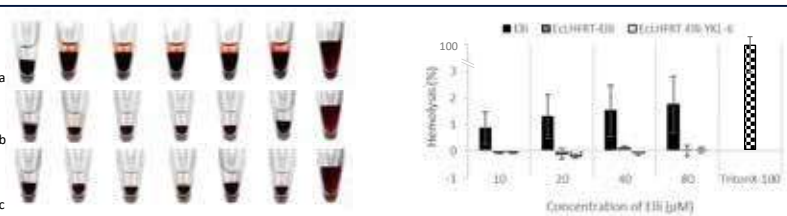

Fig. 7 Hemolytic assay with free Elli, non-targeted and targeted nanocarrier

Fig. 8 Evaluation of hemolysis caused by free and encapsulated Elli

Fig. 7a Hemolytic assay with free Elli; samples from left to right: negative control (PBS); 80, 40, 20, 10, 5 μM Elli; positive control (Triton X-100). Fig. 7b Hemolytic assay with encapsulated Elli in non-targeted nanocarrier; samples from left to right: PBS, 80, 40, 20, 10, 5 μM Elli; Triton X-100. Fig. 7c Hemolytic assay with encapsulated Elli in nanocarrier targeted with YKL-6 peptide; samples from left to right: PBS, 80, 40, 20, 10, 5 μM Elli; Triton X-100.
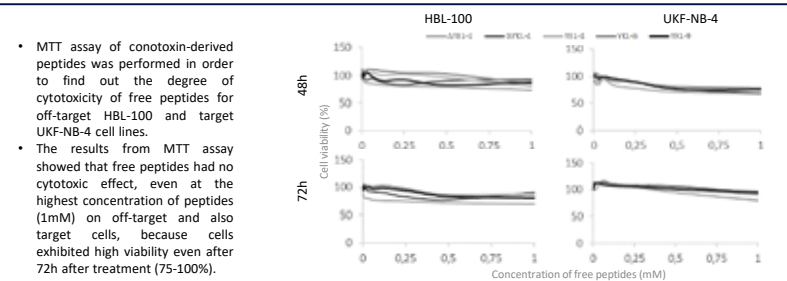
- The process of Elli encapsulation into non-targeted and targeted nanocarriers led to reduction of hemolytic ability of Elli, as shown in Fig. 7 and Fig. 8. Only free Elli had hemolytic effect on fresh human blood.

- MTT assay of conotoxin-derived peptides was performed in order to find out the degree of cytotoxicity of free peptides for off-target HBL-100 and target UKF-NB-4 cell lines.
- The results from MTT assay showed that free peptides had no cytotoxic effect, even at the highest concentration of peptides (1mM) on off-target and also target cells, because cells exhibited high viability even after 72h after treatment (75-100%).

Fig. 9 MTT assay performed on free conotoxin-derived peptides

According to results in Tab. 1 and Fig. 2, it is obvious that the peptide surface modifications did not induce too major structural changes of EcLHFRT.

- Prior the process of encapsulation and surface modification, the size of EcLHFRT was 13.5 nm; after, it was 28.2 nm or 37.8 nm.
- Values of ζ-potential of prepared nanocarriers were very similar.
- Average encapsulation efficiency of Elli in nanocarriers with unmodified or modified surface was 79%.
- The degree of re-association of non-targeted and targeted EcLHFRT was the same as the degree of re-association of empty EcLHFRT (Fig. 2).

Tab. 1 Basic characterization of prepared nanocarriers

Nanocarrier	Size (nm)	ζ-potential (mV)	Encapsulation efficiency of Elli (%)
EcLHFRT	13.5	-28.2	–
EcLHFRT-Elli	37.8	-25.0	75.5
EcLHFRT-Elli-AYKL-4	28.2	-24.9	78.6
EcLHFRT-Elli-GYKL-4	32.7	-25.1	83.1
EcLHFRT-Elli-YKL-4	37.8	-27.6	79.2
EcLHFRT-Elli-YKL-6	28.2	-25.1	77.1
EcLHFRT-Elli-YKL-9	28.2	-26.6	82.7

1 – ladder
2 – EcLHFRT
3 – EcLHFRT-Elli
4 – EcLHFRT-Elli-AYKL-4
5 – EcLHFRT-Elli-GYKL-4
6 – EcLHFRT-Elli-YKL-4
7 – EcLHFRT-Elli-YKL-6
8 – EcLHFRT-Elli-YKL-9

Fig. 2 The size of empty, non-targeted and targeted nanocarrier by native and SDS gel electrophoresis

Fig. 3 Ringer release of Elli from non-targeted and targeted nanocarrier

- The results of release kinetics of encapsulated Elli (Fig. 3) showed only negligible releases of Elli (10-12%) from non-targeted and targeted nanocarrier in Ringer's solution for 72h, showing ideal stability of encapsulated Elli in plasma.
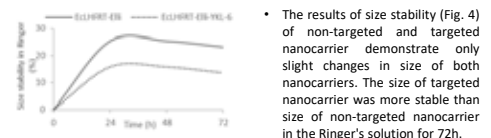

Fig. 4 Size stability of non-targeted and targeted nanocarrier

- The results of size stability (Fig. 4) of non-targeted and targeted nanocarrier demonstrate only slight changes in size of both nanocarriers. The size of targeted nanocarrier was more stable than size of non-targeted nanocarrier in the Ringer's solution for 72h.
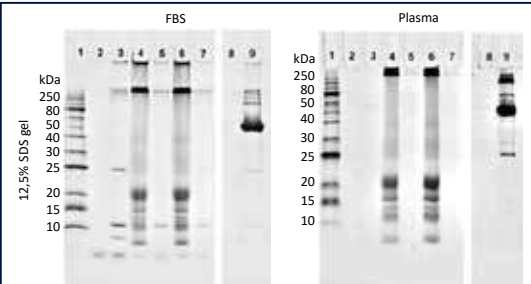

Fig. 10 Evaluation of protein corona formation on the non-targeted and targeted nanocarrier

1 – ladder; 2 – Elli; 3 – Elli + FBS/plasma; 4 – EcLHFRT-Elli; 5 – EcLHFRT-Elli + FBS/plasma; 6 – EcLHFRT-Elli-YKL-6; 7 – EcLHFRT-Elli-YKL-6 + FBS/plasma; 8 – FBS/plasma + PBS (1 : 1); 9 – FBS/plasma + PBS (1 : 100)

- The results from SDS gel electrophoresis revealed no FBS or plasma proteins were found on prepared non-targeted and targeted nanocarriers. Surface modification with conotoxin-derived peptides appeared suitable for further research.

Results

The main aim of this experimental work was to evaluate potential efficiency of conotoxin peptide-based ligands *in vitro* conditions. We prepared 6 types of EcLHFRT nanocarriers with suitable size, high encapsulation efficiency of Elli and exceptional stability properties in plasma. Process of Elli encapsulation into EcLHFRT eliminated cytotoxic effect of Elli for red blood cells and peptide-modified surface of EcLHFRT did not cause protein corona formation. Overall, the results showed that targeted nanocarrier with YKL-6 peptide, in particular favorably influenced the cellular uptake of Elli into target UKF-NB-4 cells, as was also confirmed by viability assay. On the other hand, in off-target cells HBL-100, the viability after treatment with EcLHFRT-Elli-YKL-6 was much higher and cellular uptake of Elli into HBL-100 was much lower, demonstrating successful targeting. The obtained results are crucial for further development of our research regarding targeting biomimetic ligands for neuroblastoma nanomedicine.

References

1. Thole, T. M., et al., *Cell Death Dis.* 2017, *8* (3), e2635.
2. Zhang, X. X., et al., *J. Control. Release* 2012, *159* (1), 2-13.
3. Haddad, Y. et al., *Front. Mol. Neurosci.* 2017, *10*, 7.
4. Kim, M. et al., *Biomacromolecules* 2011, *12* (5), 1629-40.